HARDENING NONLINEAR STIFFNESS BEHAVIOUR OF PIEZOELECTRIC MATERIALS WITH PASSIVE NONLINEAR P-N JUNCTION CAPACITANCE SHUNT CIRCUITS

A THESIS SUBMITTED TO
THE GRADUATE SCHOOL OF NATURAL AND APPLIED SCIENCES
OF
MIDDLE EAST TECHNICAL UNIVERSITY

BY

MUHAMMED ALİ TAŞKIRAN

IN PARTIAL FULFILLMENT OF THE REQUIREMENTS
FOR
THE DEGREE OF MASTER OF SCIENCE
IN
MECHANICAL ENGINEERING

SEPTEMBER 2021

Approval of the thesis:

HARDENING NONLINEAR STIFFNESS BEHAVIOUR OF PIEZOELECTRIC MATERIALS WITH PASSIVE NONLINEAR P-N JUNCTION CAPACITANCE SHUNT CIRCUITS

Submitted by **MUHAMMED ALİ TAŞKIRAN** in partial fulfillment of the requirements for the degree of **Master of Science** i**n Mechanical Engineering, Middle East Technical University** by,

Prof. Dr. Halil Kalıpçılar
Dean, Graduate School of **Natural and Applied Sciences** _____

Prof. Dr. Sahir Arıkan
Head of the Department, **Mechanical Engineering** _____

Assoc. Prof. Dr. Mehmet Bülent Özer
Supervisor, **Mechanical Engineering Dept., METU** _____

Examining Committee Members:

Assoc. Prof. Dr. Yiğit Yazıcıoğlu
Mechanical Engineering, METU _____

Assoc. Prof. Dr. Mehmet Bülent Özer
Mechanical Engineering, METU _____

Assist. Prof. Dr. Gökhan Osman Özgen
Mechanical Engineering, METU _____

Assist. Prof. Dr. Ali Emre Turegut
Mechanical Engineering, METU _____

Assoc. Prof. Dr. Dinçer Gökçen
Electrical-Electronics Engineering, Hacettepe University _____

Date: 06.09.2021

I hereby declare that all information in this document has been obtained and presented in accordance with academic rules and ethical conduct. I also declare that, as required by these rules and conduct, I have fully cited and referenced all material and results that are not original to this work.

Name, Last name: Muhammed Ali Taşkıran

Signature:

ABSTRACT

HARDENING NONLINEAR STIFFNESS BEHAVIOUR OF PIEZOELECTRIC MATERIALS WITH PASSIVE NONLINEAR P-N JUNCTION CAPACITANCE SHUNT CIRCUITS

Taşkıran, Muhammed Ali
Master of Science, Mechanical Engineering
Supervisor: Assoc. Prof. Dr. Mehmet Bülent Özer

September 2021, 131 pages

Piezoelectric materials are electromechanical energy transducers. They can be utilized actively when energized electrically or passively when connected to a passive shunt circuit. Due to this, they have been suggested for several vibrations suppression and energy harvesting applications.

In this thesis, a novel way to attain passive hardening stiffness was suggested by introducing an electrical component for passive nonlinear piezoelectric vibration isolation or energy harvesting. Since piezoelectric materials can be used actively or passively, the introduced component allows it to use of active and passive vibration isolation techniques at the same time. A passive nonlinear component was suggested to be hardening capacitor attained by P-N junction. For the first step of this thesis, conceptual proof that hardening capacitor provides hardening stiffness is demonstrated. The hardening effect in frequency and time domain for single degree of freedom is then studied as the next step. Then the study is extended to piezo attached cantilever beam case. Equations for the beam structure are derived, and they are validated with numerical solutions and tests. It is shown that the test and the numerical simulation results are in agreement with the analytical solutions.

Keywords: Passive Hardening Capacitance, Piezoelectric Vibration Isolation, Passive Vibration Isolation, Nonlinear Passive Shunt Circuit, Varactor.

ÖZ

PASİF DOĞRUSAL OLMAYAN P-N JONKSİYON KAPASİTANSLI ŞÖNT DEVRELERLE PİEZOELEKTRİK MATERYALLERİN DOĞRUSAL OLMAYAN SERTLEŞEN DİRENGENLİĞİ

Taşkıran, Muhammed Ali
Yüksek Lisans, Makina Mühendisliği
Tez Yöneticisi: Doç. Dr. Mehmet Bülent Özer

Eylül 2021, 131sayfa

Piezoelektrik materyaller elektromekanik enerji çevirgeçleridir. Elektriksel olarak enerjilendirildiklerinde aktif olarak olarak kullanılabildikleri gibi pasif şönt devreye bağlandıklarında pasif olarak faydalanılabilirler. Bu sebeple, bu materyaller çeşitli titreşim sönümleme ve enerji hasatı uygulamalarında kullanılabilmektedirler.

Bu tezde sertleşen direngenlik elde edecek pasif doğrusal olmayan piezoelektrik titreşim izolasyonunda veya enerji hasatı uygulamalarında kullanılmak üzere pasif elektriksel komponent çalışılmıştır. Piezoelektrik malzemeler aktif ve pasif olarak kullanılabildikleri için üzerine çalışılan bu elektriksel kavramsal pasif olmasına karşın aktif izolasyon tekniklerinin kullanılabilmesine de olanak sağlamaktadır. Pasif doğrusal olmayan komponent P-N jonksiyonun doğasında olan sertleşen kapasitör özelliğinden elde edilmektedir. Tezin ilk adımında, bu kapasitörün etkisiyle serleşen direngenlik özelliğinin elde edilebilirliği konseptsel olarak gösterilmiştir. Sonraki adımda zaman ve frekans alanında bu etkinin sonuçları tek serbestlik dereceli piezoelektrik yaması için irdelenmiştir. Akabinde bu çalışma piezo entegreli saplama çubuk için genişletilmiş ve denklemler türetilmiştir.

Denklemlerden alınan sonuçların sayısal benzetim ve test sonuçlarıyla uyumlu olduğu gözlenmiştir.

Anahtar Kelimeler: Pasif Sertleşen Kapasitans, Piezoelektrik Titreşim İzolasyonu, Pasif Titreşim İzolasyonu, Doğrusal Olmayan Pasif Paralel Devre, Varaktor.

To My Mother

ACKNOWLEDGMENTS

Firstly, I would like to express my thanks to my thesis supervisor Assoc. Prof. Mehmet Bülent Özer for his great patience and guidance. It is very valuable for me that I have explored so much due to him during this thesis.

Being my former colleague, Görkem Seçer deserves my special thanks for engaging me with power electronics topics. He indirectly guided me to find this thesis subject. I would like to thank my colleague Özgürcan Yıldız, Erem Kutluyuva, and their leader Mümtaz Afşin Esi for their moral support and their works during tests. I also would like to thank my leader Abdül Furkan Kanburoğlu, my former manager Burcu Dönmez, my current manager Özgür Ekinci and my colleague Onur Düzgören for their encouragement and moral support.

Lastly, I would like to express my deepest, heartiest gratitude to my mother. She has always been there to support.

TABLE OF CONTENTS

LIST OF TABLES

TABLES

LIST OF FIGURES

FIGURES

LIST OF ABBREVIATIONS

SDOF: Single Degree of Freedom

NES: Nonlinear Energy Sink

LQR: Linear Quadratic Regulator

LQG: Linear Quadratic Gaussian

CGVF: Constant Gain Velocity Feedback

CAVF: Constant Amplitude Velocity Feedback

MOSFET: Metal Oxide Semiconductor Field Effective Transistor

FEM: Finite Element Method

OC: Open Circuit

SC: Short Circuit

EOM: Equation of Motion

IBP: Integration by Parts

MFC: Micro Fiber Composite

SiC: Silicon Carbide

GaAs: Gallium Arsenide

LIST OF SYMBOLS

S: Mechanical Strain

D: Electrical Displacement

$s^E{}_{33}$: Constant Electric Field Compliance in 3-3 Mode

d_{33}: Piezoelectric Strain Coefficient in 3-3 Mode

d_{31}: Piezoelectric Strain Coefficient in 3-1 Mode

$\varepsilon^T{}_{33}$: Constant Stress Dielectric Permittivity

T: Mechanical Stress

E: Electric Field

$\underline{t}$: Piezoelektric Patch Thickness

V: Voltage

Δx: Mechanical Displacement

C_p: Piezoelectric Capacitance

Q: Electrical Charge

C_c: Cubic Capacitance Including Linear Component

$\underline{m}$: Bulk Mass Attached to Piezoelectric Patch

$\underline{k}$: Additional Spring Attached Between Piezoelectric Patch and Mechanical Ground

L_{ind}: Inductance of Inductor

R: Electrical Resistance

C_l: Capacitance of Linear Capacitor

τ: Normalized Time Variable

t: Time Variable

L_p: Length of Piezoelectric Patch

L_1: Starting Point of Piezoelectric Patch on x Direction

h_{st}: Thickness of Host Structure of Cantilever Beam with Piezo

h_p: Thickness of Piezoelectric Patch on Cantilever Beam with Piezo

h_{kapton}: Kapton layer thickness on one side embodying piezoelectric fibers in an MFC

Y_{33}^{E}: Constant Electric Field Young's Modulus of Piezoelectric Patch on Cantilever Beam with Piezo

Y_{st}: Young's Modulus of Host Structure of Cantilever Beam with Piezo

T_p: Internal Stress Due to Bending on Piezoelectric Patch on Cantilever Beam with Piezo

z: Distance from Neutral Axis of Cantilever Beam under Bending with Piezo

M: External Moment on Bent Element of Cantilever Beam

V_p: Voltage on Piezoelectric Patch Terminals

a: Cubic Coefficient of Nonlinear Capacitance Realized by Diodes

b: Linear Coefficient of Nonlinear Capacitance Realized by Diodes

m: Mass per Length

m_p: Mass per Length of Piezoelectric Material

m_{st}: Mass per Length of Host Structure

$\underline{Q}$: Shear Force on Infinitesimal Element of Cantilever Beam under Transverse Vibration

f: External Forcing per Unit Length on Infinitesimal Element of Cantilever Beam under Transverse Vibration

w: Displacement of Infinitesimal Element of Cantilever Beam under Transverse Vibration

M: Moment on Infinitesimal Element of Cantilever Beam under Transverse Vibration

$\mathcal{L}$: Lagrangian Including External Forcing

$\delta_{kronecker}$: Kronecker Delta Function

c_{31}^{D}: Elastic Stiffness Constant under Constant Electrical Displacement in 3-1 Mode

h_{31}: Piezoelectric Charge Constant in 3-1 Mode

β_{33}^{s}: Impermittivity in 3-3 Mode

X: Step Function

$\bar{X}$: $\left(X(x-L_1)-X\left(x-\left(L_1+L_p\right)\right)\right)$

U_{NL}: Quadratic Softening Strain Energy

U_p: Strain Energy on Piezoelectric Patch

U_{st}: Strain Energy on Host Structure

K_p: Kinetic Energy of the Piezoelectric Patch

K_{st}: Kinetic Energy of the Host Structure

U_{EL}: Electrical Energy

U_{el}: Electrical Energy on the Piezoelectric Patch

W: Work Done by External Forces

U_{SE}: Strain Energy

ω: Angular Frequency

H: Structural Damping Matrix

γ_{st}: Damping portion of the host structure

γ_p: Damping portion of a piezoelectric material

k_q: Quadratic Softening Constant

CHAPTER 1

INTRODUCTION

1.1 Motivation of the Thesis

Vibration and shock isolation is an important subject in many engineering applications. Isolation is important because vibration and shock may cause problems like unpredicted failure of a system, shortened fatigue life of components, decreased comfort in transportation, noisy and ineffective sensing of measurement devices like reconnaissance cameras or accelerometers, and so on.

In active isolation, the system requires power, actuators, controllers, and sensing devices and they introduce complexity in the system. In passive vibration isolation, simple components like spring, mass and damper are enough and they do not require power, controller and sensors.

Piezoelectric materials are electromechanical transducers converting mechanical energy to electrical energy or electrical energy to mechanical energy. These conversions are called direct or reverse piezoelectric effects. This phenomenon allows one to use piezoelectric devices as actuators, sensors and passive structural elements. Compared to bulk, volume requiring mechanical structural elements like spring, damper and mass, piezoelectric devices can be more beneficial when volume is considered since counterparts of mechanical bulk components in electrical domain are resistors, inductors and capacitors which can be much smaller and even can be in micro scales. Moreover, since these devices can be used as structural components and also actuators, active and passive hybrid vibration isolation can be achieved.

Passive vibration isolation can be linear and nonlinear. In mechanical domain, passive nonlinear vibration isolation can commonly be accompanied by geometric nonlinearities resulting in nonlinear stiffness, damping and mass. By introducing

nonlinearities to vibration absorbers, vibration isolation can be improved compared to linear counterparts [1]. It is possible to introduce nonlinear components in electrical domain which can be considered as equivalent nonlinear mechanical mass, damper and spring in the mechanical system with use of piezoelectric transducers.

In this thesis, a passive nonlinear electro-mechanical system (where non-linearity is obtained form an electrical component) will be introduced which can be used in passive, hybrid or active non-linear vibration isolation studies.

1.2 Thesis Outline

This thesis starts with chapter 2 which is the literature review. In this chapter, three main subjects are investigated. The first subject is hardening capacitance used in electrical domain. The second subject is piezoelectric vibration absorber shunt circuits. As subsections, active, passive and semi-active vibration isolation circuits in literature are examined. Lastly, studies on nonlinear softening characteristics of piezoelectric materials near resonance are investigated.

After the literature survey, modelling of simple piezoelectric patch is given in Chapter 3. The chapter starts with conceptual proof of hardening stiffness obtained by a nonlinear hardening capacitor. Then, quasi-static loading of a piezoelectric patch is shown to demonstrate the hardening stiffness effect. Later, time domain response and frequency domain response of the patch are studied.

Following the simple proof of hardening stiffness related to a nonlinear capacitor, the study is extended to a fixed free bimorph cantilever beam with attached piezoelectric patches in Chapter 4. Equations for different modes of operation of the piezoelectric patches are derived and related Matlab simulation results are presented. Matlab simulation results are then validated by Comsol simulations which are performed in frequency domain and time domains. The chapter also includes Matlab simulation results which are to be validated by tests instead of FEM software.

In Chapter 5 experimental study is given. Cantilever beam that is to be tested is given first and then experimental hardware and software are explained. After this, experimental results are shared. The results are then compared with simulation results from chapter 4.

Being the last chapter, chapter 6 is the summary of the thesis. The summary is followed by a discussion of how the method introduced in this thesis can be improved. The chapter finishes with future work suggestions

CHAPTER 2

LITERATURE REVIEW

This chapter consists of four headings:

- Hardening capacitance in electrical domain

  Under this heading nonlinear capacitor use in electrical domain is discussed.
- Piezoelectric vibration absorber shunt circuits

  Under this heading active, passive and semi-active piezoelectric vibration mitigation techniques are discussed.
- Softening characteristics of piezoelectric materials near resonance
- Summary

  A gap in the piezoelectric vibration absorber techniques in the literature is pointed out and the motivating idea of this thesis is explained.

2.1 Hardening Capacitance in Electrical Domain

Under this heading, the use of components named variable capacitors or varactors exhibiting hardening capacitance characteristics in nonlinear electrical circuits literature is investigated. In the literature, variable capacitors are mainly obtained by two components; ferroelectric capacitors and varactor diodes.

It is possible to observe the hardening capacitance components are used in several applications like electromagnetic vibration energy harvesting, electromagnetic wave frequency multiplication, pulse generation and so on [2][3][4][5][6][7][8]. For the applications, two types of variable capacitors are used. They are ferroelectric capacitors and varactors diodes.

Ferroelectric capacitors can be obtained by placing ferroelectric material as a dielectric material in a capacitor and due to the ferroelectric layer, the capacitor

possesses hysteresis [4][9][10]. Typical charge-voltage characteristic of a ferroelectric capacitor is given in Figure 2-1. Gluskin [4] reported ferroelectric capacitors could be used as nonlinear capacitors in electrical applications. In the article, it is mentioned that ferroelectric capacitors show hysteretic characteristics and the condition for the degree of the hysteresis is discussed. He also reported that if the nonlinearity is not very strong and hysteresis is neglected, relation between voltage and charge accumulated on the capacitor can be approximated as follows:

$$V = a_1 q + a_3 q^3 \tag{2.1}$$

It is obvious from equation (2.1) that ferroelectric capacitors can have cubic nonlinearity however, the conditions mentioned above should be satisfied for accurate modeling. Apparently, the conditions introduce extra limitations in designing process of the components.

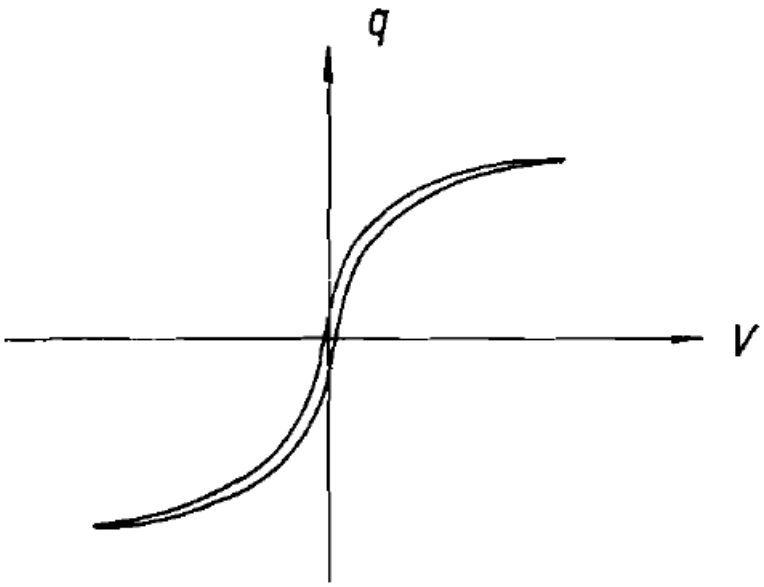

Figure 2-1 Typical Charge-Voltage Characteristic of a Ferroelectric Capacitor [4]

Varactor diode, which is another type of nonlinear capacitor, is used in nonlinear electrical circuits. Its nonlinear behavior stems from P-N junction [11] which is used in solid state devices like diodes and transistors. P-N junction reaction under voltage load is demonstrated in Figure 2-2. As can be seen from Figure 2-2 at the equilibrium,

distance between p doped and n doped region is moderate. When the junction is forward biased, the distance decreases and when reverse biased, the distance increases. As the distance increase, capacitance of the structure decrease and oppositely, as the distance decrease, capacitance increase. Considering equation (2.2), this phenomenon can be imagined as two imaginary capacitor electrodes come closer in forward bias condition resulting in increased capacitance, whereas the electrodes move away in reverse bias condition resulting in decreased capacitance. In (2.2), C, ε, A, d stand for capacitance, dielectric permittivity, area of the electrodes and distance between the electrodes, respectively. Connecting two P-N junctions back to back in series, which is, in fact, connecting two diodes such that no conduction occurs, gives a variable capacitor in both directions. It is because one of the junctions will be reverse biased in any direction.

$$C = \varepsilon \times \frac{A}{d} \tag{2.2}$$

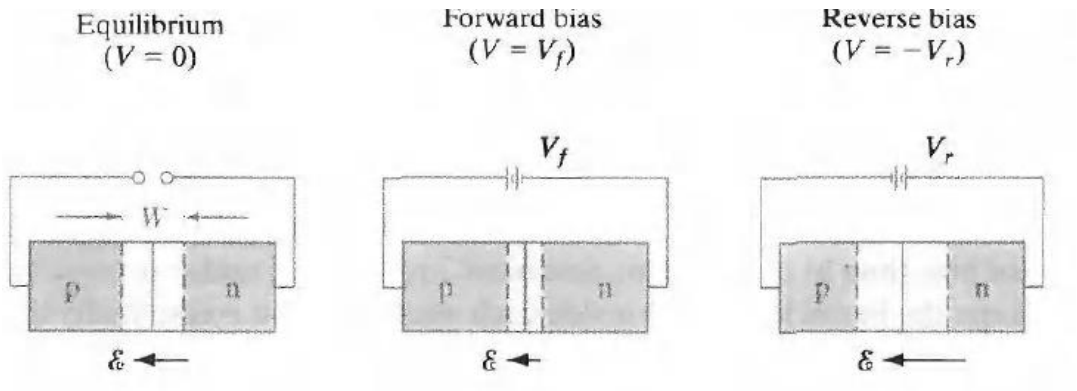

Figure 2-2 P-N Junction Biasing and Junction Reaction [12]

Nonlinear capacitance versus voltage model of P-N junction under reverse voltage load can be found in the literature [13][11]. The function of the capacitance versus voltage is given in equation (2.3)

$$C = \frac{K}{(\varphi + V)^n} \tag{2.3}$$

In (2.3), C, K, φ, V, n denote capacitance, built-in potential, reverse voltage, power law exponent, respectively.

Similar to the ferroelectric capacitor approximation mentioned above, voltage versus charge of a P-N junction can be approximated as linear and cubic capacitances in series [5][2][8], which is given in (2.1). Krishnamurthi et al. [8] studied a frequency tripler with approximation formulized in (2.1). Li et al. [5] studied frequency multiplier with cubic capacitance approximation and 20^{th} degree polynomial Taylor series expansion approximation. In the work, it is possible to observe that the approximations are close. Wang et al. [2][14] studied electromagnetic nonlinear energy harvester to widen the useful bandwidth employing varactor diodes. In the work, cubic nonlinear approximation is used in calculations. Calculations are validated with experiments.

2.2 Piezoelectric Vibration Absorber Shunt Circuits

In the literature, it is possible to find numerous piezoelectric vibration absorber shunt circuits. They can be classified as passive, semi-passive and active shunt circuits [15]. The shunt circuits can be linear and nonlinear. Review articles [15] and [16] include several different studies on shunt circuits.

2.2.1 Passive Shunt Circuits

Passive shunt circuits require no power and controller to suppress vibration. They are constructed with use of passive, linear or nonlinear electrical components. Therefore, they are also cheaper and easy to implement. Passive circuits can be linear or nonlinear.

2.2.1.1 Passive Linear Shunt Circuits

Hagood et al. [17] studied passive R and RL shunt circuits. The authors derived piezoelectric models and conducted experiments. They reported that the model and the experiments are in good agreement. The experiments are conducted using specific R or RL parameters which are tuned by techniques they discussed in their study. It was pointed that a large inductor is required for low frequency isolation. In reference [18], tuning of the parameters was also discussed, and the tuning technique introduced was experimentally validated. The authors, different from [17], discussed not only serially connected RL circuit but also parallel connected RL circuits and compared their advantages and disadvantages. In [19] additional strategied on tuning is discussed.

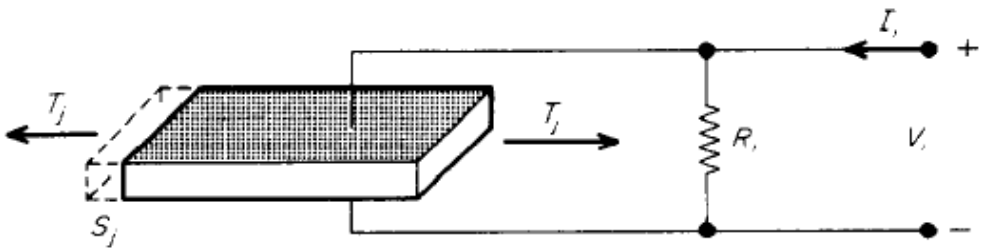

Figure 2-3 R Shunt Circuit [17]

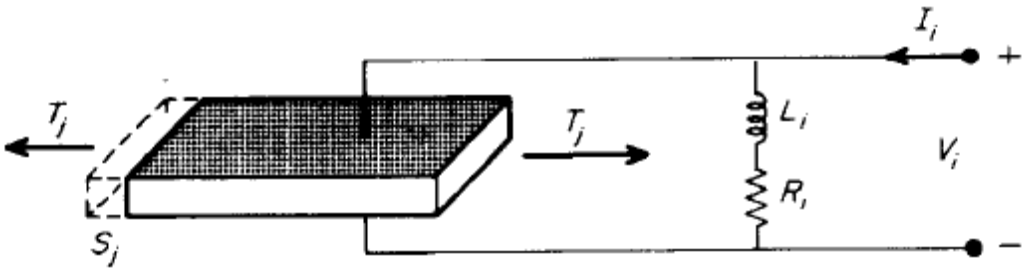

Figure 2-4 RL Shunt Circuit [17]

Park et al. [20] suggested a shunt decreasing inductance requirement which is mentioned in [17]. In the article, synthetic active inductor replacing bulky physical

inductor. The authors conducted experiments and showed that using their approach, the value of required inductance dropped by 50%.

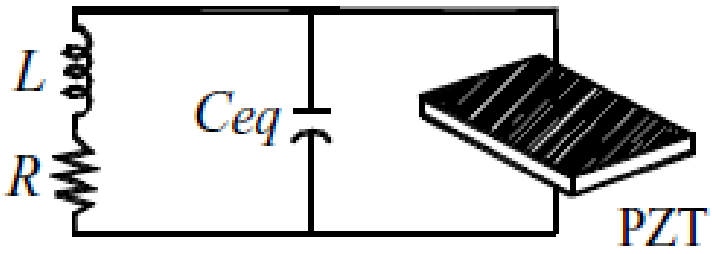

Figure 2-5 Enhanced Piezoelectric Shunt Circuit [20]

Studies mentioned so far can mitigate vibration only for a specified structural mode. [21] and [22] offered a remedy for this deficiency (Figure 2-6 and Figure 2-7). The main idea in their shunts is that multiple shunt circuits which are tuned to suppress desired structural mode are parallel connected. Each shunt has its own filter, which is composed of passive electrical components like capacitor, inductor, and resistor, filtering frequency for vibration suppressing shunt circuit tuned for certain frequency range. In [21] and [22] experiments are also performed to verify their analytic derivations.

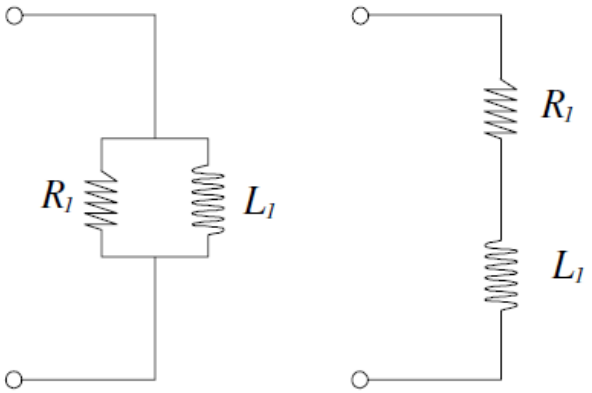

Figure 2-6 Single Mode Vibration Isolation Shunt Circuit [21]

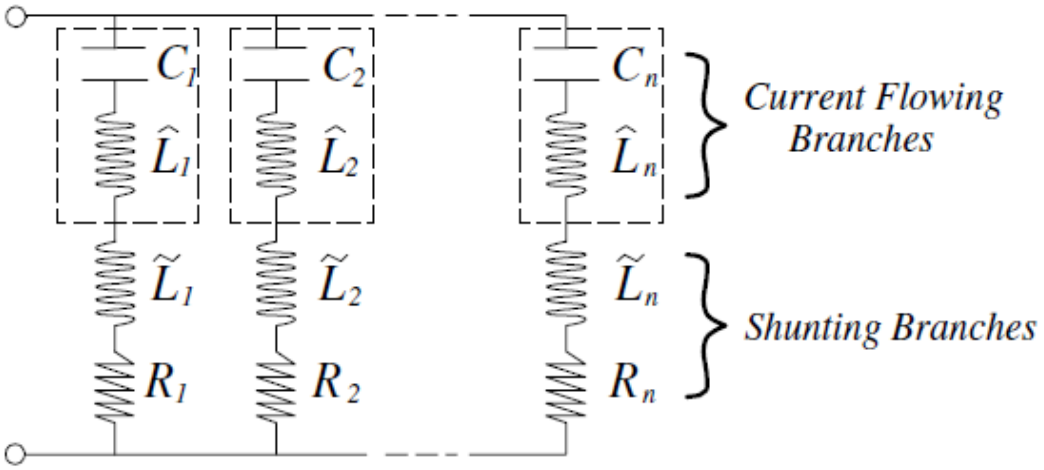

Figure 2-7 An Example of Multi Mode Vibration Absorber Shunt Circuit Mentioned in [22]

2.2.1.2 Passive Nonlinear Shunt Circuits

Inman [23] analyzed a fictitious nonlinear shunt whose capacitors' voltage related to 1st, 2nd, and 3rd polynomial order of the electrical charge on the fictitious electrical component. Inman reported that higher bandwidth is obtained by using a nonlinear shunt circuit; however, a resonant response is also introduced. The author did not mention what kind of electrical circuit component could be used to obtain the nonlinearity, and therefore, the work cannot be experimentally validated.

Zhou et al. [24] studied a nonlinear energy sink consisting of piezoelectric material and a nonlinear shunt circuit to lessen the vibration of mistuned bladed disks. The authors suggested ferroelectric capacitors to obtain nonlinearity they examined in their work. They investigated SDOF nonlinear shunt circuit first (Figure 2-8), and they showed that the inductance required for the vibration absorption is decreased, and higher bandwidth is obtained. After the SDOF model, a nonlinear shunt is theoretically applied to bladed disks, and the system is reported as successful for mitigating vibration caused by mistuned blades. Even though they offered an electrical component which is ferroelectric capacitor, to obtain nonlinearity in the circuit, unlike Inman [23], they only mentioned the characteristics of the component

and did not mention the component's cost, size, etc. their work includes only theoretical calculations. Similarly, Soltani et al. [25] offered a piezoelectric shunt circuit whose nonlinearity is suggested to be obtained by a ferroelectric capacitor. They investigated a nonlinear tuned vibration absorber. They reported better vibration mitigation compared to linear shunt made by Den Hartog's tuning method.

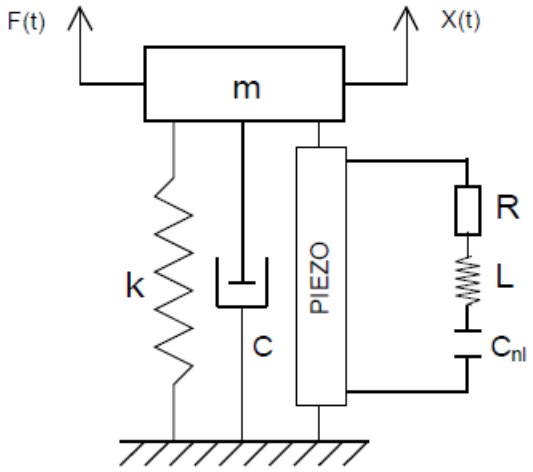

Figure 2-8 SDOF Nonlinear Shunt Circuit Introduced by Zhou et al. [24]

Lossouarn et al. [26] studied a nonlinear tuned piezoelectric vibration absorber. Unlike nonlinearities studies by Soltani et al. [25] and Zhou et al. [24], nonlinearity is introduced by saturating inductance (Figure 2-9). Saturating inductance is reported to have a good performance on vibration isolation. Their theoretical work was experimentally supported.

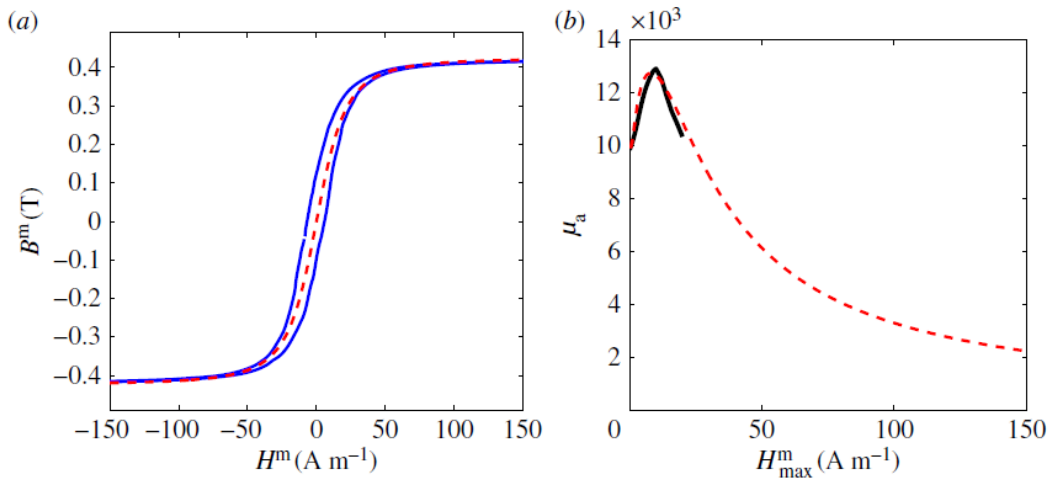

Figure 2-9 Saturating Inductor Material Data Used in [26]: (a) Magnetic Field vs. Magnetic Field Intensity of the Material (blue line) Polynomial Approximation (red line) (b) Relative Magnetic Permeability vs. Magnetic Field Intensity of the Material (black line) Polynomial Approximation (red line)

Another passive or self-powered shunt circuit is introduced by Niederberger et al. [27]. The circuit is shown in Figure 2-10. Their shunt circuit includes two piezoelectric structures. One of the piezoelectric material is used as a sensor, and the other one is used for vibration absorption. The main idea behind their shunt circuit is to create an electromagnetic shock on the inductor by switching the circuit from open to RL circuit with use of MOSFETs, and this switching action is to increase the effectiveness of the inductor used in the system. The experiments conducted in their article demonstrated that better performance was obtained when compared to passive R circuit. It is important to point out that this circuit can suppress only one frequency value.

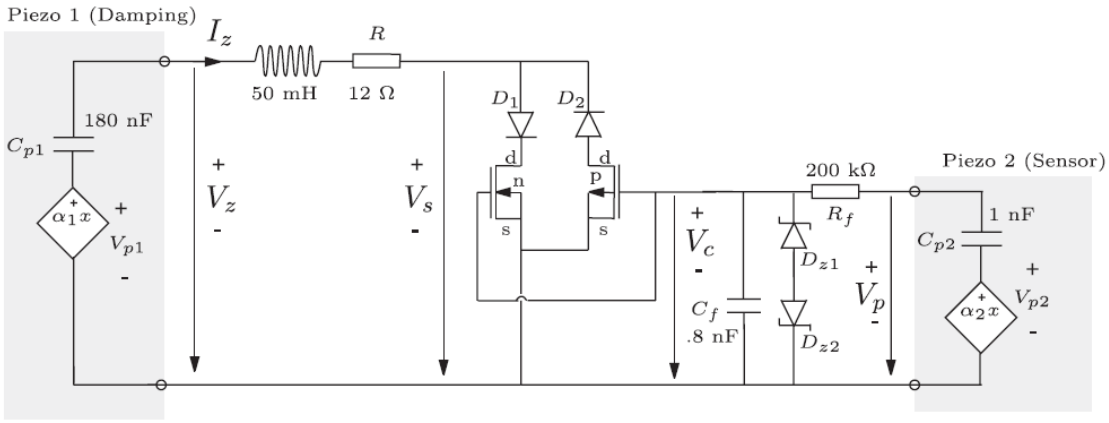

Figure 2-10 Nonlinear Shunt Circuit Introduced by Niederberger et al. [27]

Similar to [27], switching based damping was studied in [28]. Switching controller is realized by an analog circuit. The system has a vibration energy harvester that is to switch the circuit and supply energy to the controller. As a result, the system is not only a vibration absorber but also an energy harvester. [28] also includes experimental results.

2.2.2 Semi-passive Shunt Circuits

Semi-passive shunt circuits, as described in [15], do not exert energy into the system; rather, they use the energy to tune or switch the parameters in the circuit. Even though they do not input energy into a system, they require power to operate. In order to tune or switch the parameters, a control system and an algorithm are required. This further complicates the system, but still, power is not an issue.

Switching shunts can be found in the literature as smart switch or state switch damping. Switching of the shunt can be done on one or more parallel/series combinations of electrical circuit elements, which are R, L, and C. Here it is important to note that infinite or zero values of the components can result in open or short circuits. For example, infinite R value between two nodes results in open circuit, whereas zero R value results in short circuit. In Figure 2-11, some switching

shunts are shown. From a to c in the figure, passive electrical components are switched, and from d to f, active components are switched. Active electrical component switches will be mentioned in the next section due to the fact that they intend to exert energy into the system.

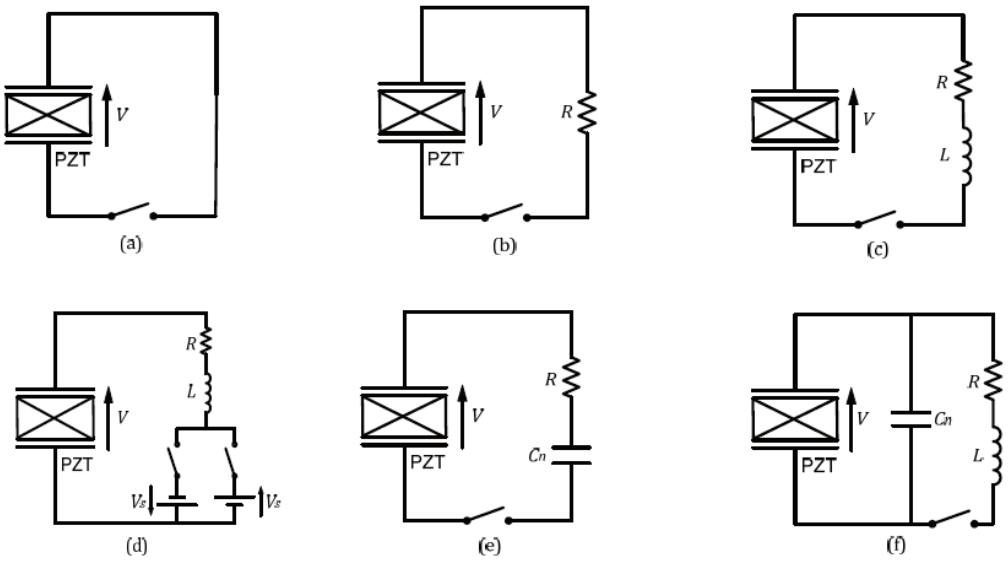

Figure 2-11 Switching Shunt Circuits [15]; (a) State Switch (b) Switch on Resistor (c) Switch on Inductor (d) Switch on Voltage (e) Switch on Negative Capacitor (f) Switch on Negative Capacitance and Inductor

Clark [29] studied switching on a resistor. He explained state switch as stiffness control of the system, and he proposed resistor switch can improve vibration absorption performance. His intention on switching was said to be capturing vibration energy while the piezoelectric element has high stiffness and dissipating it through the resistor. His theoretical work resulted in better free vibration decay compared to state switch and resistive shunt. He used a specific state switch control law and an optimal resistance for switching regarding the cost function constructed by regarding the tip displacement over time. Experimental work is not shared in his study. Similar to Clark's approach on state switch [29], Ramaratnam et al. [30] studied stiffness control on a piezoelectric vibration absorber. He carried out stability

analysis and presented experimental results for verification of theoretical claims. He reported good damping performance of free vibration decay.

Richard et al. [31] suggested that instead of switching the shunt from open circuit to a short circuit, switching can be done between open circuit and a small inductor. The authors reported better harmonic and free vibration performance with the experimental data. Similarly, Corr et al. [32] investigated switching on an inductor and named it as pulse switching. In the article, it was observed that switching circuit with much smaller inductance than passive RL shunt outperformed state switch circuit. In [31] and [32], it is commonly noted that mistuning of the parameters is not an issue. Two articles utilize different switching strategies. Reference [33] is another inductor switch circuit with a different switching logic and optimization.

Davis [34] offered a method of capacitance tuning of the shunt circuit using a capacitor bank. Similar to [31] and [32], his motivation was to adjust the stiffness in the system. He mentioned that tuned piezoelectric shunt is sensitive to parameters and in case of using resistance affects the absorber's performance in high frequency range negatively in his paper. His work includes an experimental study.

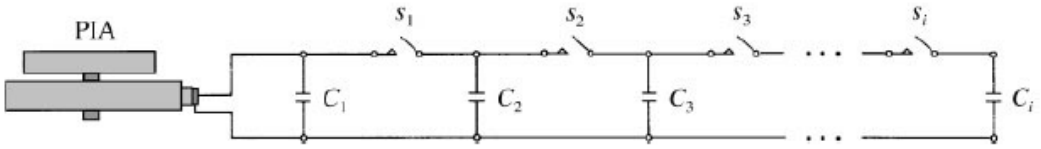

Figure 2-12 Capacitor Bank Offered by Davis [34]

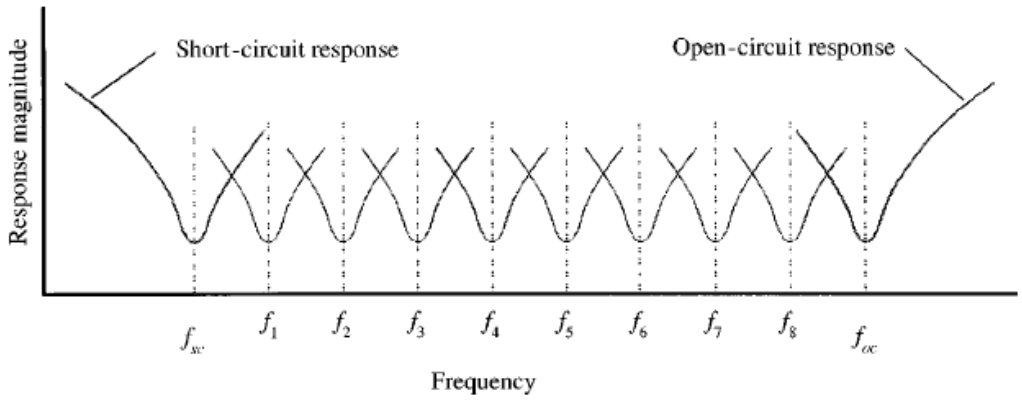

Figure 2-13 Response of the Piezoelectric Shunt System for Open Circuit and Short Circuit and Intermediate Tuned Capacitive Shunt [34]

Lallart et. al. [35] offered blind switching technique to suppress vibration. The basic theory of the technique is that in a period of vibration, switching is done several times different from the above techniques, whose switching signals were mainly maximum voltage. The work includes semi passive and active versions. In semi passive part of the paper, blind switching is done on short circuit. In the active part, switching is done on a voltage source. The authors stated that blind switching on voltage a source resulted in better vibration attenuation regarding the experiments they have conducted.

2.2.3 Active Shunt Circuits

In the previous section, smart switching circuits are mentioned mainly, and active smart switching can also be found in the literature among numerous active shunt techniques. As shown in Figure 2-11 (d), switching can be done on a voltage source. Petit et al. [36] studied smart switching on a voltage source as well as switching on short circuit and inductance. In the paper performance of the techniques is demonstrated. Switching on voltage was shown to have the best performance than switching on inductance. The least effective shunt was observed as switching on short circuit. The authors modified the switch detector circuit by adding parallel RLC

shunts, which filter each resonant frequency to feed the detector circuit. Therefore, multi mode of a vibrating structure was claimed to be influenced. Badel et. al. [37] offered an adaptive voltage source to widen the frequency range of the vibration absorber shunt. Makihara et al. [38] offered a passive R-L shunt circuit which is serially connected to overcome the chattering problem of the switching. More than that, they improved switching by enriching the switching voltage source for opposite terminals with excluding a voltage source. As a result, three switching positions were created.

Han et. al.[39] studied switching on negative capacitance, which is depicted in Figure 2-11 (f). The authors showed their technique performed better than switching on inductor. They supported their investigation with experiments. In [40], also negative switch on a capacitor is examined, which is given in Figure 2-11 (e). It was reported that the shunt offered in the paper performed better than switching on inductor shunt relying on the experimental work.

Before continuing with more complex active shunts, it would be better to mention synthetic electrical circuit components. Previously synthetic inductor and synthetic capacitor were mentioned. In Figure 2-14, negative capacitance is shown. In [41] pure negative capacitance shunt circuit is studied. The authors concluded the study by stating that the system they proposed was able to suppress vibration with several harmonic components. In Figure 2-15, a synthetic inductor is shown. In reference [20], it was reported that instead of a bulky physical inductor, a more compact synthetic inductor was more flexible and simpler.

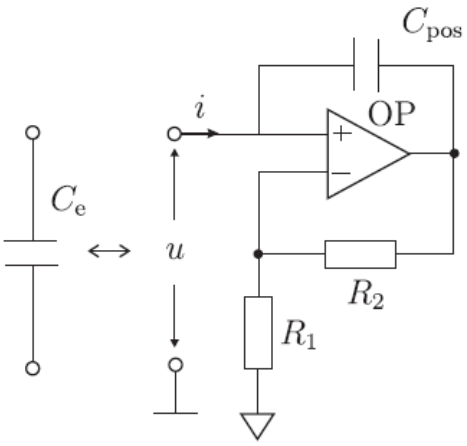

Figure 2-14 Negative Capacitance Offered by Han et al. [39]

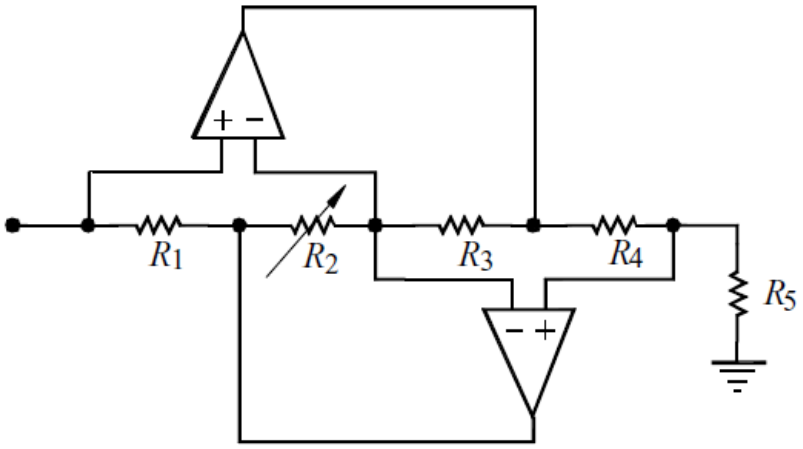

Figure 2-15 Synthetic Inductor in [20]

Morgan et al. [42] offered a control law that alters the inductance and resistance parameters in the circuits. The circuit has a passive R-L circuit cascaded with a controlled voltage source. The voltage source is driven such that it gives an output voltage that is the same as the actively tuned inductance and resistance. In the paper, the technique was reported to perform better than short circuit and semi active piezoelectric shunt techniques. Experimental results of the compared systems are presented in the study. Reference [43] includes more information on the

experimental study whose results are given in [42]. The system offered is depicted in Figure 2-16

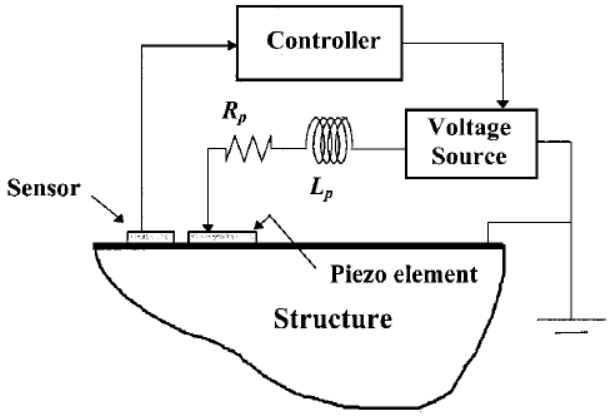

Figure 2-16 Piezoelectric Vibration absorber Suggested in [42]

Similar to [42], Niederberger et al. [44] studied active impedance tuning. The difference between [42] and [44] is that synthetic inductance (called virtual inductance in the paper) is used instead of a voltage source in [44]. The suggested absorber is shown in Figure 2-17.

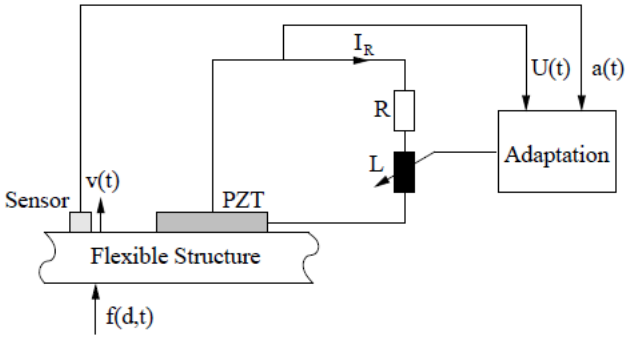

Figure 2-17 Piezoelectric Vibration absorber Suggested in [44]

In [45], active and passive vibration absorber shunt circuits are used at the same time. A collocated piezoelectric element was used as a sensor with a passive R-L shunt circuit. In other words, one of the piezoelectric elements was used to serve as a

passive vibration absorber as well as a sensor whose input is used in an active vibration control system. The second piezoelectric element was supposed to suppress vibration actively with the use of a voltage source. The authors declared that the absorber they suggested was able to perform better for a tuned frequency; however, active absorption is sensitive to the R-L parameters used in the sensori-passive piezoelectric shunt.

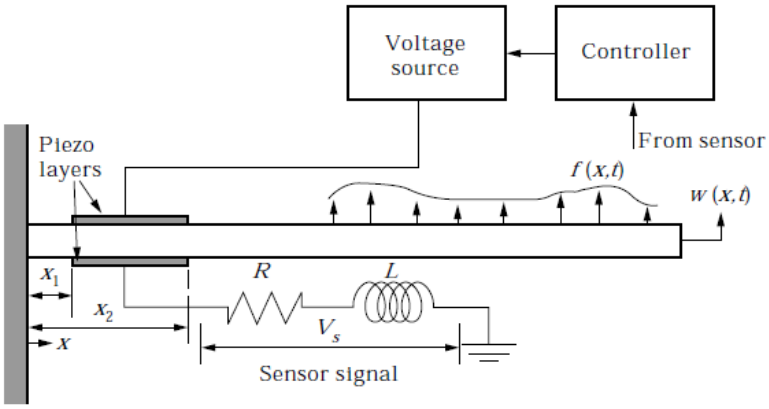

Figure 2-18 Active Passive Piezoelectric Vibration Absorber System in [45]

In [42] and [44], a piezoelectric element is used as a sensor. In [45], the piezoelectric sensor element is used as a sensor and isolator at the same time. However, the active vibration absorber piezoelectric element can be used as an active isolator and sensor at the same time. In [46] self sensing actuator concept is studied. Self sensing concept is realized by the use of opamps. Analog circuits for rate sensing feedback and self sensing strain feedback systems are given in Figure 2-19 and Figure 2-20, respectively. The systems suggested in the article were experimentally validated for free vibration case. A significant vibration reduction is reported in the study considering the experimental results. The authors also stated that performance of the offered systems is comparable to the systems, which are realized by two distinct piezoelectric elements as a sensor and an actuator.

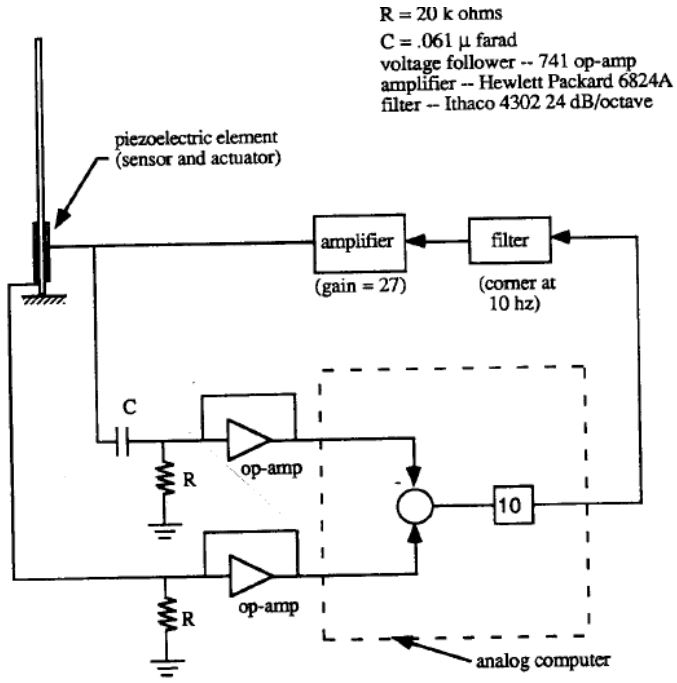

Figure 2-19 Self Sensing Rate Feedback Sensori Actuator System in [46]

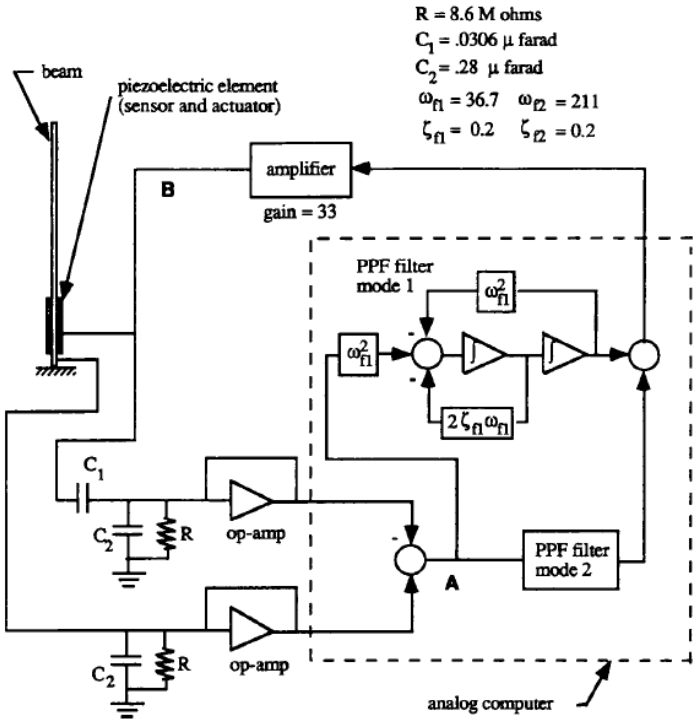

Figure 2-20 Self Sensing Positon Feedback Sensori Actuator System in [46]

The positive position feedback concept mentioned in [46] is improved in [47] with the name of modified positive position feedback. The main idea of the improved concept is to use two parallel compensators. This method was reported to be more effective for harmonic disturbance and equally effective for transient vibration. The study was supported by experimental work.

In [48], constant gain and constant amplitude velocity feedback controls (CGVF and CAVF) are presented. Constant gain control, as obvious from the name, is linear and continuous; however, constant amplitude controller was said to be continuous but nonlinear. As can be understood from the name itself, constant amplitude controller is supposed to feed a constant voltage amplitude back. The results given in the study reveals that constant amplitude controller suppressed transient free vibration faster compared to constant gain feedback controller.

In addition to CGVF and CAVF control strategies, LQR and LQG controller strategies are presented their performances presented in [49]. In the study, it was found that for free vibration with initial displacement, CAVF and LQG performed better. However, CAVF could not suppress multi mode vibration, whereas LQR could. It was reported that quadratic cost function increase flexibility easily when compared to classical control methods.

Up to now, several active vibration elimination techniques in the literature presented. Some of them require a proper controller design, and some of them are simple system energizing circuits. Nonetheless, another technique that stands as a bridge between passive and active piezoelectric vibration isolation is studied in [50]. The main idea of the study is to use cubic capacitance mentioned in section 2.2.1.2. The nonlinear capacitor with cubic capacitance is realized by active linear electrical circuit components. Furthermore, to increase the effectiveness of the piezoelectric vibration absorber, a negative capacitance was added in series to the system. The system suggested in the paper was reported to be useful for aeroelastic control to reduce flutter. Their work was validated by only simulations. In [51], the concept was experimentally validated.

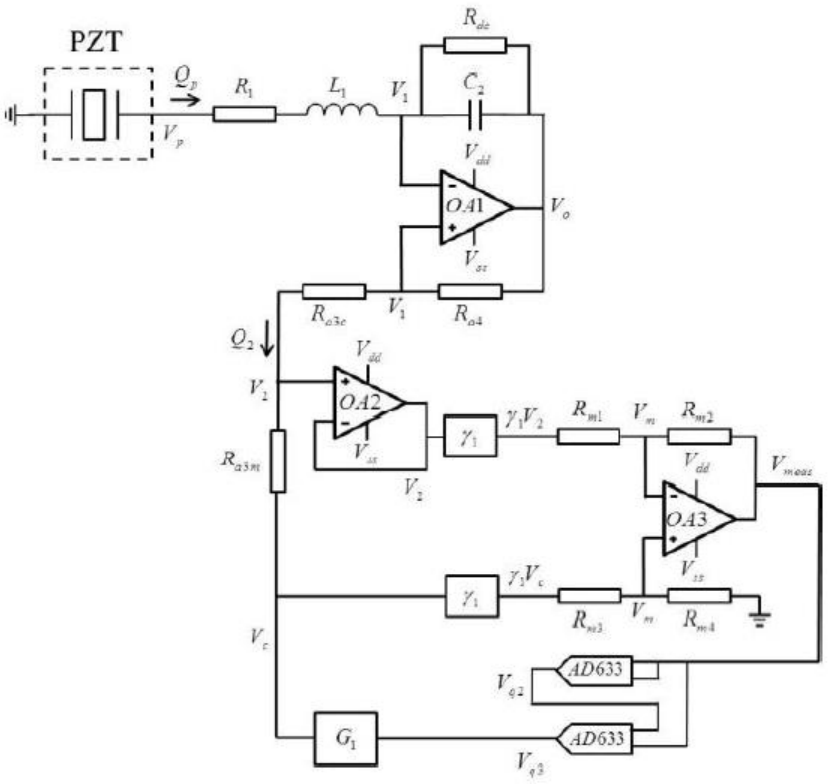

Figure 2-21 Nonlinear Piezoelectric Shunt Circuit Studied in [50]

2.3 Softening Effects of Piezoelectric Materials under Harmonic Excitation

Piezoelectric materials are commonly modelled as linear components ([52]). For cantilever beam applications, linear model can be used for small excitation amplitudes ([53]). For the case when amplitudes increase, piezoelectric materials such as PZT-5A and PZT-5H exhibit softening characteristics near resonance. This softening nonlinearity was reported in many publications such as references [54][55][56][57][58][59]. In [58] and [57], 3-3 mode piezoelectric patches interdigitated electrodes called MFC are studied, and the rest studied well-known 3-1 mode piezoelectric patches.

The softening effect can be considered as ferroelastic material softening, as stated in [58][55][57] and [59]. In [55], softening effect is claimed to be stemmed from

ferroelastic hysteresis, and for steady state applications, this hysteresis can be observed as softening spring effect. The nonlinear model introduced in the publication was confirmed with experiments.

In [59], Leadenham and Ertürk summarized several nonlinear elasticity approximations. Among the approximations, the ferroelastic softening approach is employed, and the cantilever system is modelled accordingly. The cantilever is tested, and test results are shown to be in agreement with the mathematical modelling. Moreover, quadratic softening parameter is given in the paper, and it was reported to be found experimentally.

2.4 Summary

In the literature, several vibration isolation techniques are present. The isolation can be done actively, passively, and semi actively. Nonlinear vibration absorbers are reported to have some advantages. As mentioned in 2.2.1.2, cubic nonlinear capacitors are suggested for the isolation. However, most of the studies did not offer a way to achieve nonlinearity. In some papers in 2.1, it was suggested that the cubic capacitance could be achieved by ferroelectric capacitors due to their voltage-charge characteristics, but the practical implementation and feasibility were not mentioned. Cubic capacitance is only realized and implemented in [50] and [51], but the realization of the nonlinear component was obtained actively. Therefore, passive cubic capacitance in vibration isolation can be considered valuable.

In the literature, practical considerations of implementation of a passive cubic capacitance for piezoelectric vibration isolation and validating experiments are absent. For this reason, in this thesis implementation of diodes for cubic capacitance capacitors for piezoelectric vibration isolation will be studied. Quadratic ferroelastic softening model of the piezoelectric materials mentioned in 2.3 is considered in the study.

CHAPTER 3

SDOF MODELING OF A PIEZOELECTRIC PATCH OPERATING IN d_{33} MODE

This chapter starts with conceptual proof of hardening stiffness obtained by hardening capacitance. After verification of the applicability of a mechanical hardening through hardening capacitance, quasi-static loading of a piezoelectric patch with linear shunt and nonlinear shunt, which is realized by diodes, and their comparison will be examined. Later, time domain response under harmonic forcing of the piezoelectric patches with linear and nonlinear shunts are simulated with Comsol 5.4 and Simulink. The study ends with frequency analysis of linear and nonlinear shunts. The chapter closes with a summary.

3.1 Conceptual Proof of Hardening Stiffness via Hardening Capacitance

Constitutive relations of a piezoelectric patch shown in Figure 3-1 operating in d_{33} mode can be expressed as below,

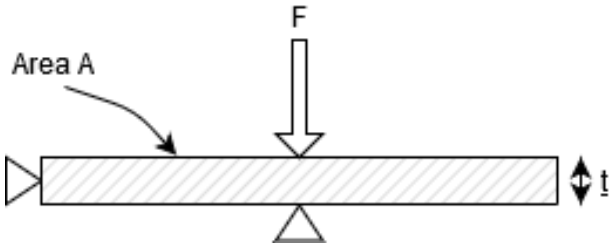

Figure 3-1 Simply Supported 2D Piezoelectric patch

$$\begin{Bmatrix} S \\ D \end{Bmatrix} = \begin{bmatrix} {s^E}_{33} & d_{33} \\ d_{33} & {\varepsilon^T}_{33} \end{bmatrix} \begin{Bmatrix} T \\ E \end{Bmatrix} \tag{3.1}$$

Writing the first equation obtained by matrix multiplication in (3.1) gives;

$$S = T{s^E}_{33} + d_{33}E \tag{3.2}$$

Multiplying with the thickness of piezoelectric patch both sides of (3.2) results;

$$S\tilde{t} = Ts^{E}{}_{33}\underline{t} + d_{33}E\underline{t} \tag{3.3}$$

Since multiplication of strain and the thickness gives mechanical displacement, the equation can be rewritten as follows;

$$\Delta x = Ts^{E}{}_{33}\underline{t} + d_{33}V \tag{3.4}$$

Writing the second equation of (3.1) gives;

$$D = d_{33}T + \varepsilon^{T}{}_{33}E \tag{3.5}$$

Multiplying both sides of (3.5) with the area of piezoelectric patch;

$$DA = d_{33}TA + \varepsilon^{T}{}_{33}EA \tag{3.6}$$

Surface integral of the electrical displacement gives electrical charge, and electric field is voltage per thickness. Thus, (3.6) can be rewritten as;

$$Q = d_{33}TA + \frac{\varepsilon^{T}{}_{33}A}{\underline{t}}V \tag{3.7}$$

It can be realized that the coefficient of voltage in (3.7) is the capacitance of the piezoeletric patch, and therefore, the equation becomes;

$$Q = d_{33}TA + C_p V \tag{3.8}$$

In Figure 3-2, circuit diagram of an external capacitor connected to the terminals of a piezoelectric patch is shown. Relation between charge and voltage can be written as follows considering the figure;

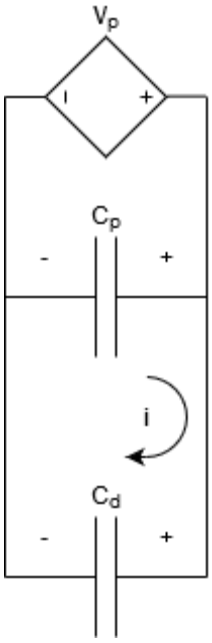

Figure 3-2 Circuit Diagram of Capacitance C_d Connected to Terminals of Piezoelectric Patch

$$Q = -VC_d \tag{3.9}$$

Using (3.8) and (3.9);

$$-VC_d = d_{33}TA + C_pV \tag{3.10}$$

Can be obtained. Rearranging (3.10) yields;

$$-V = \frac{d_{33}TA}{C_d + C_p} \tag{3.11}$$

Combining (3.11) and (3.4) and noting that force per area is equal to stress gives;

$$\Delta x = Ts^E{}_{33}\underline{t} - d_{33}\frac{d_{33}TA}{C_d + C_p} = F\left(\frac{s^E{}_{33}\underline{t}}{A} - \frac{{d_{33}}^2}{C_d + C_p}\right) \tag{3.12}$$

For a linear spring, spring constant is defined as force per unit deflection. Assuming that the piezoelectric patch in Figure 3-1 to be linear spring, the spring constant can be obtained;

$$k = \frac{F}{\Delta x} = \frac{1}{\left(\frac{{s^E}_{33}\underline{t}}{A} - \frac{{d_{33}}^2}{C_d + C_p}\right)} \tag{3.13}$$

Perturbing C_d in (3.13), it is possible to observe as C_d decreases $\frac{{d_{33}}^2}{C_d+C_p}$ value increases. This decreases the denominator value, and the total expression, which is spring constant, increases. Therefore, hardening capacitor, the capacitor with decreasing capacitance with increasing voltage, results in a hardening stiffness. Even though the above expression does not include voltage variable directly, one can deduce as forcing and hence displacement increase since voltage builds up on the piezoelectric patch terminals.

3.2 Quasi Static Loading of a Piezoelectric Patch

Constitutive equations for piezoelectric material can also be expressed as;

$$\begin{Bmatrix} T \\ E \end{Bmatrix} = \frac{1}{{s^E}_{33}{\varepsilon^T}_{33} - {d_{33}}^2} \begin{bmatrix} {\varepsilon^T}_{33} & -d_{33} \\ -d_{33} & {s^E}_{33} \end{bmatrix} \begin{Bmatrix} S \\ D \end{Bmatrix} \tag{3.14}$$

The first equation of (3.14) can be expanded as follows;

$$T = \frac{1}{{s^E}_{33}{\varepsilon^T}_{33} - {d_{33}}^2} (S{\varepsilon^T}_{33} - d_{33}D) \tag{3.15}$$

Multiplying both sides with area yields;

$$F = \frac{A}{{s^E}_{33}{\varepsilon^T}_{33} - {d_{33}}^2} (S{\varepsilon^T}_{33} - d_{33}D) \tag{3.16}$$

(3.16) can be rewritten to give the equation below;

$$F\left({s^E}_{33}{\varepsilon^T}_{33} - {d_{33}}^2\right) = (AS{\varepsilon^T}_{33} - d_{33}Q) \tag{3.17}$$

The second equation of (3.14) yields;

$$E = \frac{1}{{s^E}_{33}{\varepsilon^T}_{33} - {d_{33}}^2}(-d_{33}S + D{s^E}_{33}) \tag{3.18}$$

Multiplying both sides of (3.18) with the area and denominator of the right hand side and noting that electric field is voltage per distance (in this case thickness) gives;

$$\frac{VA}{\underline{t}}\left({s^E}_{33}{\varepsilon^T}_{33} - {d_{33}}^2\right) = (-d_{33}AS + Q{s^E}_{33}) \tag{3.19}$$

Dielectric constant ${\varepsilon^S}_{33}$ can be written as

$${\varepsilon^S}_{33} = {\varepsilon^T}_{33}\left(1 - \frac{d_{33}^2}{{s^E}_{33}{\varepsilon^T}_{33}}\right) = \frac{\left({s^E}_{33}{\varepsilon^T}_{33} - {d_{33}}^2\right)}{{s^E}_{33}}$$

Since capacitance formula is defined as dielectric constant times area per thickness, it can be written as;

$$C_p = \frac{{\varepsilon^S}_{33}A}{\underline{t}} \tag{3.20}$$

Dielectric constant ${\varepsilon^S}_{33}$ can be written as

$${\varepsilon^S}_{33} = {\varepsilon^T}_{33}\left(1 - \frac{d_{33}^2}{{s^E}_{33}{\varepsilon^T}_{33}}\right) = \frac{\left({s^E}_{33}{\varepsilon^T}_{33} - {d_{33}}^2\right)}{{s^E}_{33}} \tag{3.21}$$

Inserting the above expression into (3.19) gives;

$$C_pV{s^E}_{33} = (-d_{33}AS + Q{s^E}_{33}) \tag{3.22}$$

In [8] back to back connected diodes are approximated as;

$$\alpha V = \frac{Q}{Q_0} + \beta\left(\frac{Q}{Q_0}\right)^3 \tag{3.23}$$

Where α and β are constants for nonlinear capacitance realized by the diodes. Substituting voltage expression in (3.23) into (3.20) gives;

$$\frac{-C_p}{\alpha}{s^E}_{33}\left(\frac{Q}{Q_0} + \beta\left(\frac{Q}{Q_0}\right)^3\right) = (-d_{33}AS + Q{s^E}_{33}) \tag{3.24}$$

The expression can be reduced to;

$$Q^3 + c_1 Q + c_2{}'S = Q^3 + c_1 Q + c_2{}'\frac{\Delta x}{\underline{t}} = Q^3 + c_1 Q + c_2 = 0 \qquad (3.25)$$

The solution of a cubic equation similar to (3.25) is given in [60]. The details of the solution are given below;

Let the solution of Q be $u + v$ then

$$(u+v)^3 = u^3 + 3u^2 v + 3uv^2 + v^3 = 3uv(u+v) + u^3 + v^3 \qquad (3.26)$$

Since $Q = u + v$ and letting $c_1 = -3uv$ and $c_2 = -(u^3 + v^3)$ results in the original equation. Let $r = u^3$ and $s = v^3$ and therefore, $r + s = u^3 + v^3$and $rs = u^3 v^3$. If rs and $r + s$ are the multiplication of the roots and addition of a quadratic equation respectively then, the equation can be written as with dummy variable z as $z^2 + c_2 z - (c_2/3)^3 = 0$. One solution to the equation can then be determined as;

$$u^3 = -\frac{c_2}{2} + \sqrt{\left(\frac{c_2}{2}\right)^2 + \left(\frac{c_1}{3}\right)^3} \qquad (3.27)$$

Then,

$$u_0 = \sqrt[3]{-\frac{c_2}{2} + \sqrt{\left(\frac{c_2}{2}\right)^2 + \left(\frac{c_1}{3}\right)^3}} \qquad (3.28)$$

u_0 is the first root of (3.27). 2nd and 3rd roots are multiplication of u_0 with 1st and 2nd powers of $\left(-1 + \sqrt{-3}\right)/2$. As obvious, other roots are not real, and they are not applicable solutions for the physical system.

Because $c_1 = -3uv$ then other root can directly be calculated as;

$$-\frac{c_1}{3u} = v \qquad (3.29)$$

Finally, the solution of (3.25) becomes;

$$Q = u + v = \sqrt[3]{-\frac{c_2{}'\Delta x}{2\underline{t}} + \sqrt{\left(\frac{c_2{}'\Delta x}{2\underline{t}}\right)^2 + \left(\frac{c_1}{3}\right)^3}} - \frac{c_1}{3u} \tag{3.30}$$

The constants c_1 and c_2 can be expressed when necessary manipulation is done as;

$$c_1 = \frac{\frac{-C_p}{\alpha Q_0} s^E{}_{33} - s^E{}_{33}}{\frac{-C_p \beta}{\alpha Q_0{}^3} s^E{}_{33}} \tag{3.31}$$

$$c_2{}' = \frac{d_{33} A}{\frac{-C_p \beta}{\alpha Q_0{}^3} s^E{}_{33}} \tag{3.32}$$

(3.31) describes the behavior of charge depending on the displacement of the piezoelectric element. Consequently, force can be expressed as a function of displacement using (3.17). Substituting relation between strain and displacement into (3.17) equation below can be written;

$$F(x) = \frac{\left(\frac{\Delta x A \varepsilon^T{}_{33}}{\underline{t}} - d_{33} Q(x)\right)}{\left(s^E{}_{33} \varepsilon^T{}_{33} - d_{33}{}^2\right)} \tag{3.33}$$

In order to observe displacement vs. forcing characteristics of a piezoelectric system with nonlinear shunt, material and diode parameter values could be inserted into the equation above.

For PZT-5H piezoelectric patch material parameters and 10^4 parallel connected Toko KV1471 diode parameters are given in Table 3.1, and results obtained using the table are given in Figure 3-3 are obtained.

Table 3.1 Parameters Used for Simulating Quasi-Static Response of Piezoelectric Patch

Parameter	Value
$\underline{t}\ (m)$	200x10^{-6}
$d_{33}\ (C/N)$	400x10^{-12}
${\varepsilon^T}_{33}(F/m)$	1.549x10^{-8}
$A(m^2)$	20.8x10^{-4}
${s^E}_{33}(1/Pa)$	20.7 x10^{-12}
$Q_0(C)$	(9 x10^{-11}) x10^4
$\alpha(1/V)$	1.8
$\beta(C^2)$	2

Parameters for diodes can be obtained by using the approach mentioned in [8]. Values in certain ranges substituted for the constants a_1 and a_2 in (2.1) and then for each value error is calculated by comparing analytical expression given in (2.3) and then square is taken for each value. Parameters giving the least squared value are chosen as approximation diode model parameters a_1 and a_2. This approximation requires high resolution of sweep range of the parameters a_1 and a_2.

The same calculations can be done with PMN-PT single crystal piezoelectric patch. Parameters for the patch are as follows; $d_{33} = 1620 \times 10^{-12}\ (C/N)$, ${\varepsilon^T}_{33} = 6.198 \times 10^{-8}\ (F/m)$, ${s^E}_{33} = 49.18 \times 10^{-12}\ (1/Pa)$ and geometrical parameters are the same. The results are shown in Figure 3-4.

Considering Figure 3-3 and Figure 3-4 force of the piezoelectric patches is bounded between open and short circuit conditions. It can be observed that PMN-PT piezoelectric material has a broader force range when compared to PZT-5H material. The Metric for comparing performance of piezoelectric material is the coupling

coefficient. The coupling coefficient is a metric defined by the ratio of energy conversion ratio of mechanical domain to electrical domain.

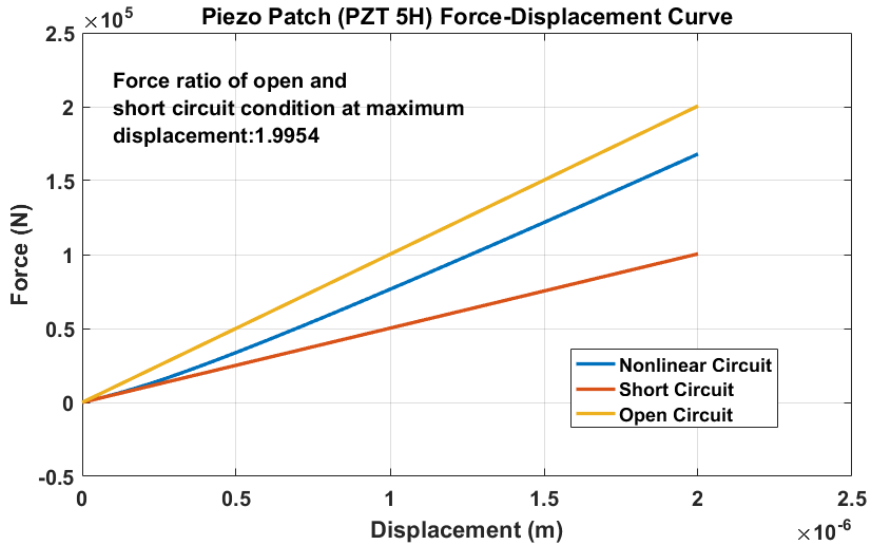

Figure 3-3 Force vs. Displacement Curve for PZT-5H piezoelectric patch with cubic curve fit to 10000 number of parallel connected Toko KV1471

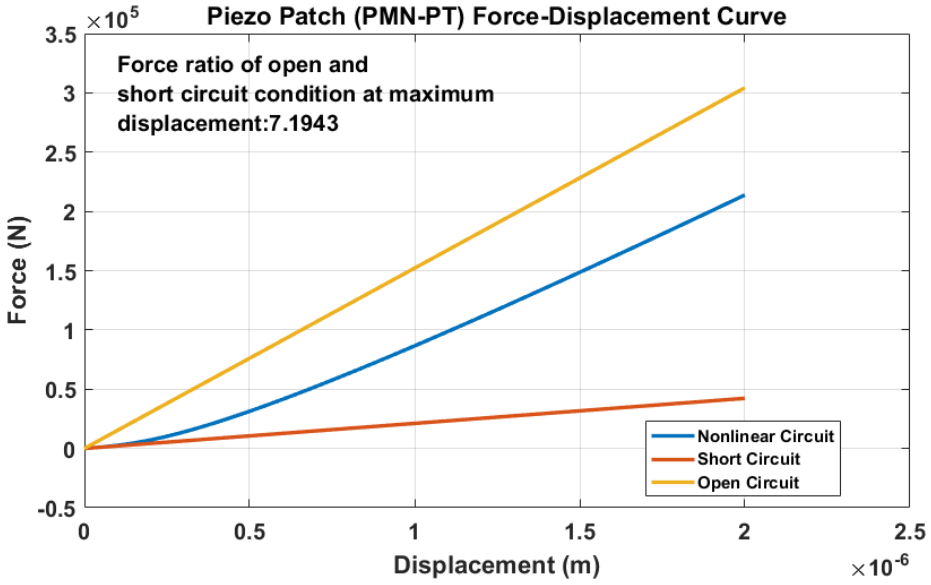

Figure 3-4 Force vs. Displacement Curve for PMN-PT single crystal piezoelectric patch with cubic curve fit to 10000 number of parallel connected Toko KV1471

Coupling coefficient is defined as below:

$$k = \frac{d_{33}}{\sqrt{{s^E}_{33}{\varepsilon^T}_{33}}} \tag{3.34}$$

Substituting the values from Table 3.1 for PZT-5H and values of $d_{33} = 1620 \times 10^{-12}\ (C/N)$, ${\varepsilon^T}_{33} = 6.198 \times 10^{-8}\ (F/m)$, ${s^E}_{33} = 49.18 \times 10^{-12}\ (1/Pa)$ for PMN-PT in to (3.34) results are found as 0.706 and 0.928 respectively. Consequently, Figure 3-3 and Figure 3-4 indicate that stiffness change is bounded, and a higher coupling coefficient gives a broader stiffness range.

Hardening stiffness of the piezoelectric system with diode shunt can also be demonstrated with the use of FEA software Comsol 5.4. FEA analysis is made for a 2D piezoelectric patch with a size of 30x20x1 and material of PZT-5H. Roller boundary regions are shown in Figure 3-5. Load is applied on the upper surface of the patch, as shown in Figure 3-6. Diode parameter values are given in Table 3.2. The analysis is done for five different shunt circuits. They are open circuit, short circuit, diode realized nonlinear capacitor, -100nF capacitance negative capacitor, and -200nF capacitance negative capacitor. It is important to note that Comsol can model a diode with the model given in equation (2.3). The results for five different shunts are given in Figure 3-7. Effect of negative capacitance, which is also mentioned in [51], on stiffness can be comprehended by observing the results. Similar to the effect of high coupling coefficient, negative capacitance also widens the stiffness range.

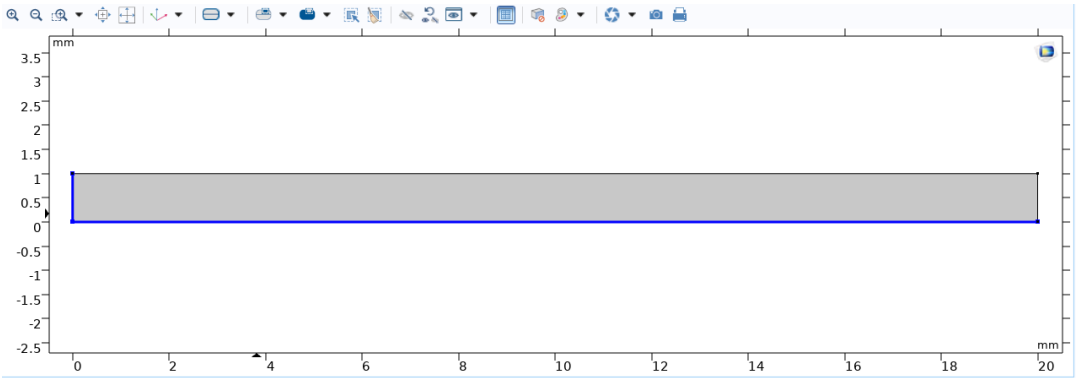

Figure 3-5 Roller Boundary Regions in Comsol For Quasi Static Loaded Piezoelectric Patch Analysis

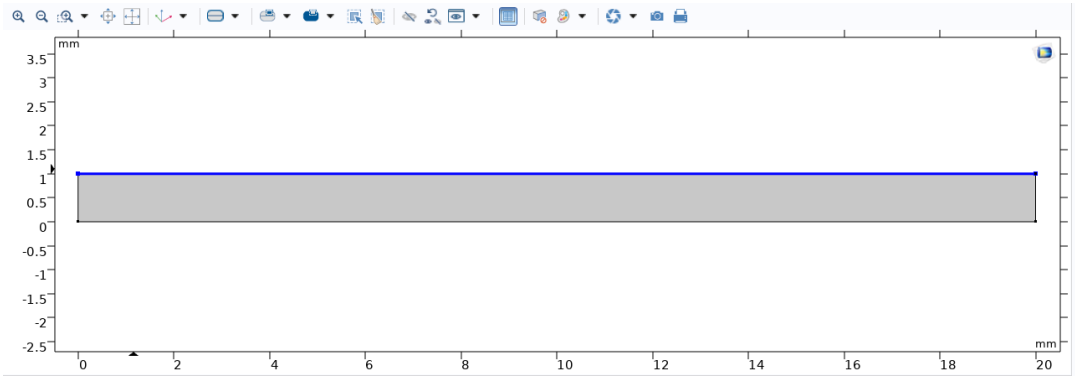

Figure 3-6 Loading Regions in Comsol For Quasi Static Loaded Piezoelectric Patch Analysis

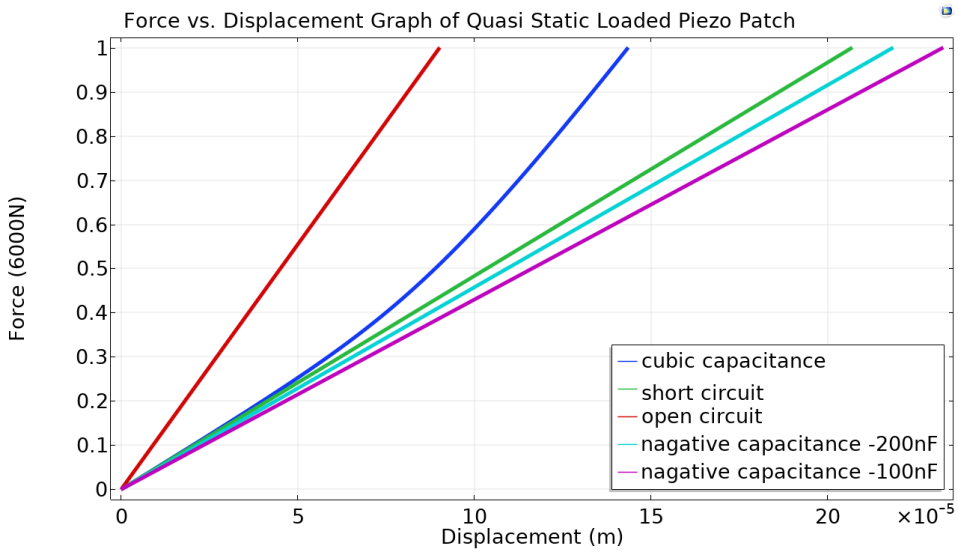

Figure 3-7 Force vs. Displacement Graph of Quasi Static Loaded Piezoelectric Patch with 5 Different Shunt Circuits; Open Circuit, Short Circuit, Nonlinear Capacitor, and Two Negative Capacitance Capacitors

Table 3.2 Diode Parameter Values Used for Comsol to Simulate Quasi Static Loading of a Piezoelectric Patch

Diode parameters	**Value**
Zero-bias junction capacitance (F)	10^{-7}
Current at breakdown voltage (A)	10^{-9}
Saturation current (A)	10^{-13}
Reverse saturation current (A)	10^{-13}
Grading coefficient	1.2
Junction potential (V)	0.5

3.3 Time Domain Response of Piezoelectric Patch with Nonlinear Capacitor under Harmonic Forcing Neglecting Softening Effect

In the previous section, proof of concept of hardening stiffness achieved with use of diodes for quasi static loading was mentioned. Taking one step further, this section presents response of the same piezoelectric under harmonic excitation. To do this, Matlab Simulink and Comsol software programs are utilized. The Simulink model is shown in Figure 3-8. In the model, sine forcing is fed into nonlinear and linear systems. The response or outputs of the systems, which are position, current, and voltage, are observed. Parameters used in the simulations are taken from Table 3.2. Results are given from Figure 3-11 to Figure 3-13.

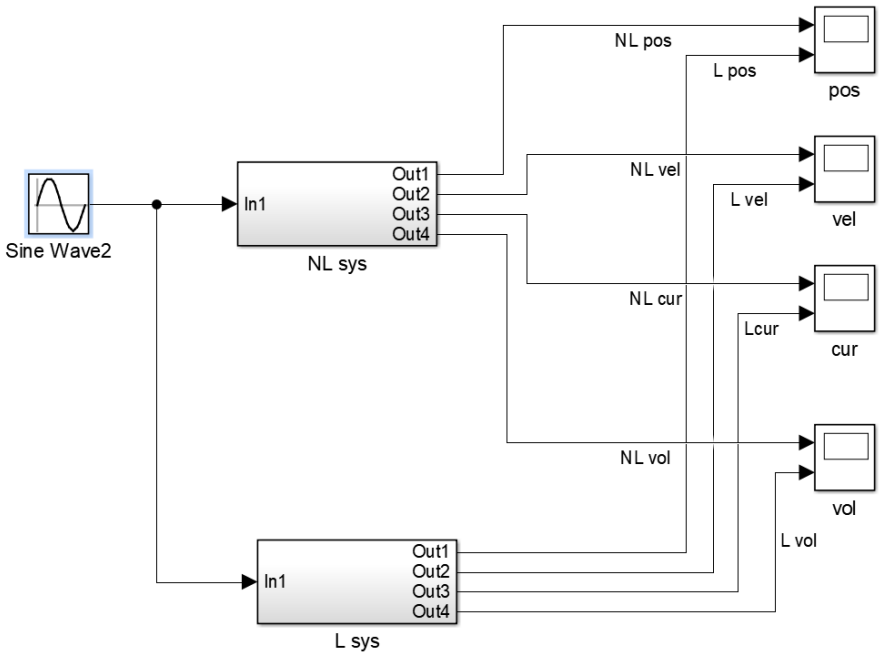

Figure 3-8 Simulink Model of SDOF Piezoelectric Patch under Harmonic Forcing

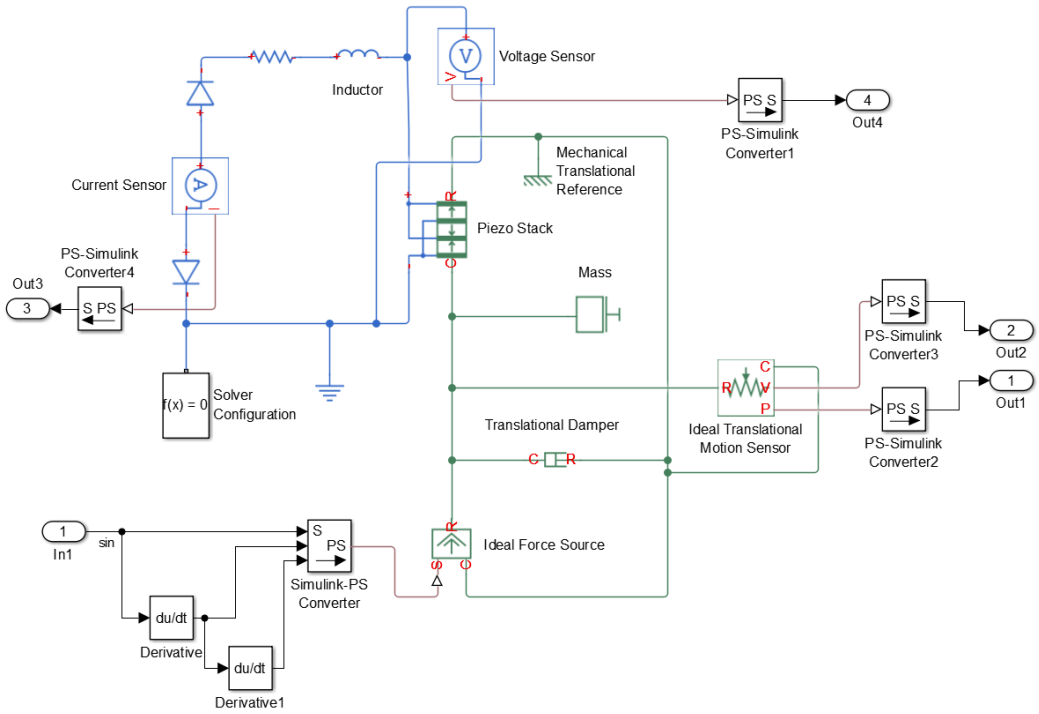

Figure 3-9 Nonlinear System Block in Figure 3-8

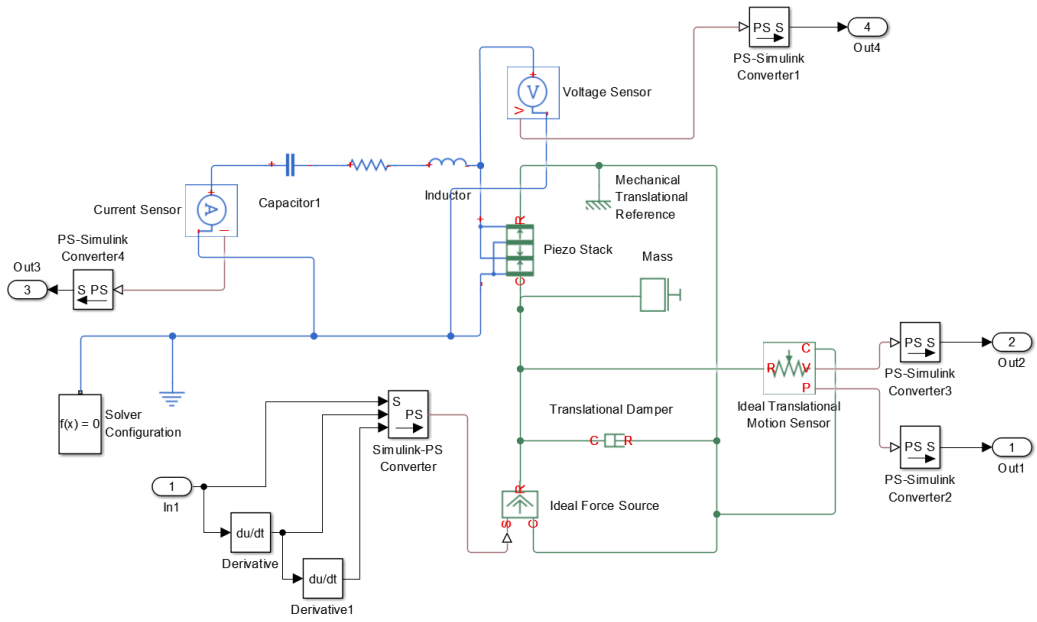

Figure 3-10 Linear System Block in Figure 3-8

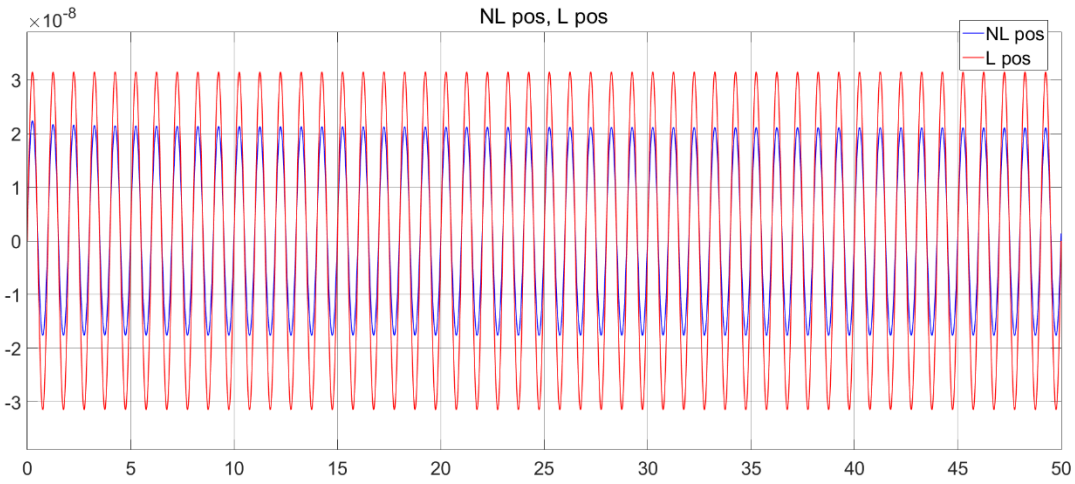

Figure 3-11 Displacement of SDOF Piezoelectric Patch under Harmonic Forcing in Simulink; Nonlinear Shunt (Blue), Linear Shunt (Red)

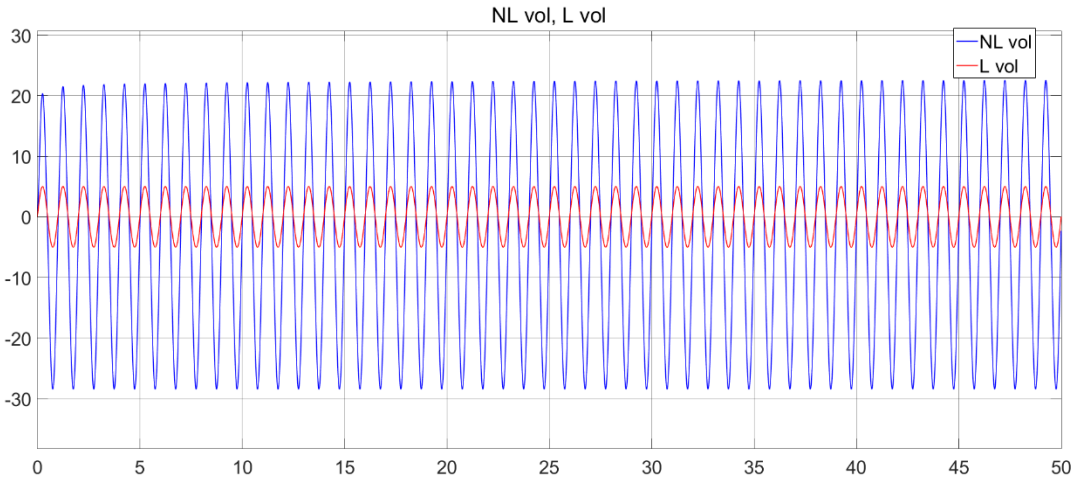

Figure 3-12 Terminal Voltage of SDOF Piezoelectric Patch under Harmonic Forcing in Simulink; Nonlinear Shunt (Blue), Linear Shunt (Red)

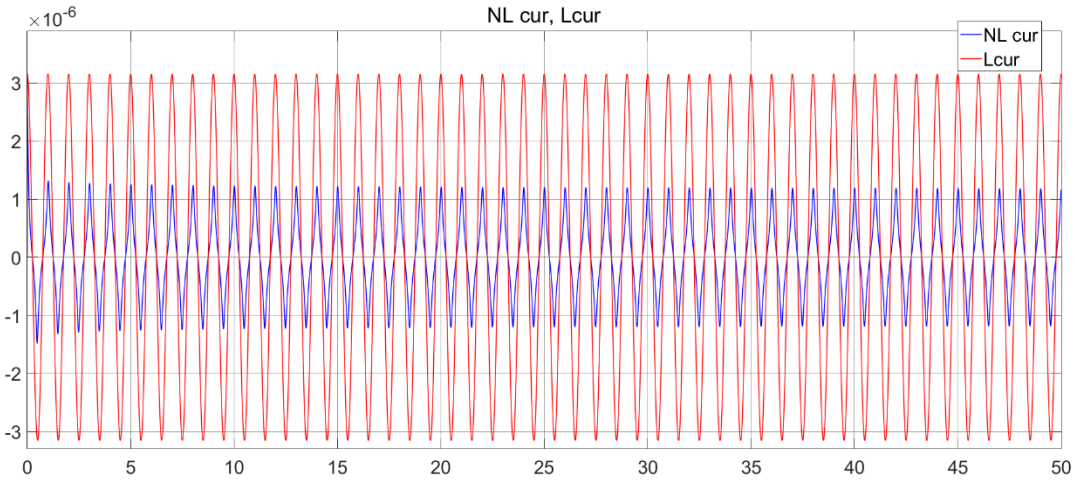

Figure 3-13 Current of SDOF Piezoelectric Patch under Harmonic Forcing in Simulink; Nonlinear Shunt (Blue), Linear Shunt (Red)

The parameters used for the system presented in Figure 3-8 are given in Table 3.3. Parameters not presented in the table are taken as default. Further, auto solver configuration is used.

Table 3.3 Parameter Values of the System Shown in Figure 3-8

Parameter	Value
Sine forcing amplitude	1000
Angular frequency (rad/s)	2π
Inductance of inductor (H)	10^{-9}
Resistance of resistor (ohm)	10^{4}
Diode device area (m^2)	1
Diode number of parallel devices	1
Diode saturation current, IS (A/m^2)	10^{-13}
Diode ohmic resistance, RS (m^2Ohm)	10^{-13}
Diode emission coefficient, ND	1
Diode zero-bias junction capacitance, CJO (F/m^2)	10^{-7}
Diode junction potential, VJ (V)	0.5
Diode grading coefficient, MG	1.2
Diode capacitance coefficient, FC	0.5
Diode reverse breakdown current, IBV (A/m^2)	10^{-13}
Piezo stack area (mm^2)	600
Piezo layer thickness (mm)	1
Piezo number of layers	1
Piezoelectric charge constant (m/V)	$593x10^{-12}$
Piezo dielectric constant (F/m)	$3400x(8.854x10^{-12})$
Piezo elastic compliance (m^2/N)	$2.07x10^{-11}$
Damping coefficient (Ns/m)	10^{-3}
Mass (kg)	10^{-3}
Capacitance of capacitor (F)	10^{-7}

The same simulation can be done using Comsol. The model given in section 3.2 is used with sinusoidal forcing input; however, this time plane stress is used instead of plain strain in 2D approximation. The parameters used are the same as those given

in Table 3.3 except for mass and damper. Results are given from Figure 3-14 to Figure 3-16.

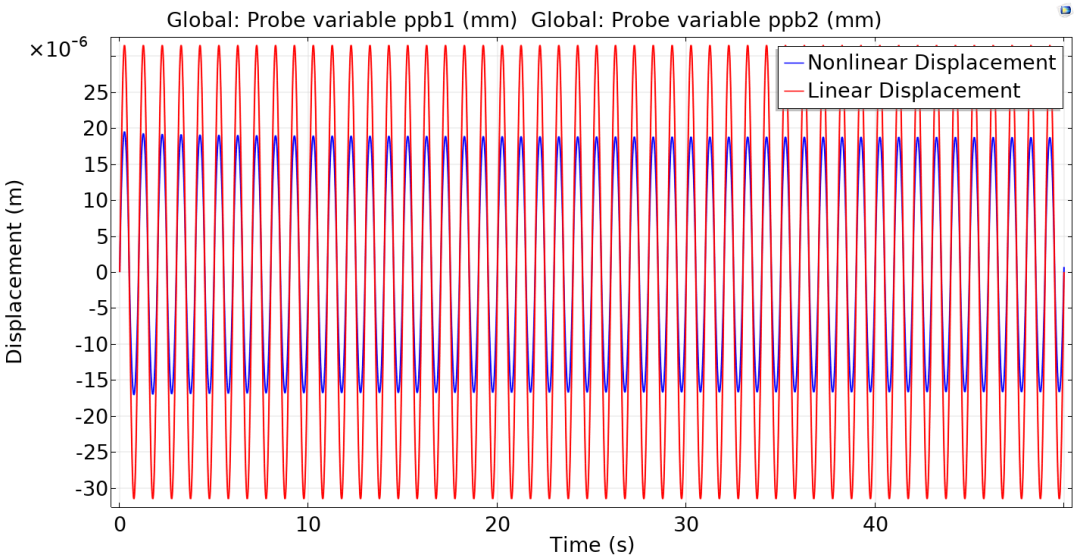

Figure 3-14 Displacement of SDOF Piezoelectric Patch under Harmonic Forcing in Comsol 5.4; Nonlinear Shunt (Blue), Linear Shunt (Red)

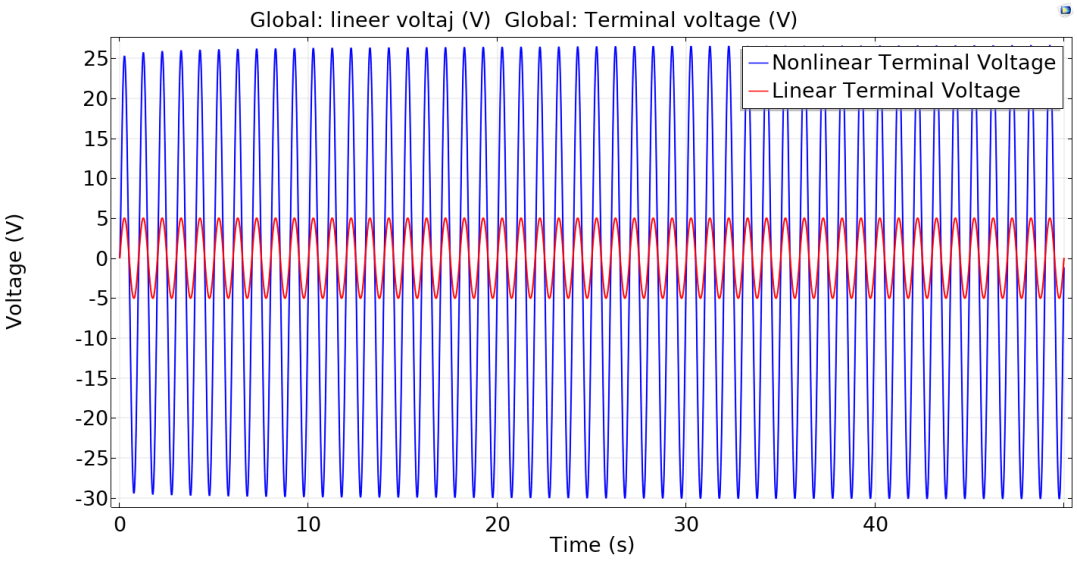

Figure 3-15 Terminal Voltage of SDOF Piezoelectric Patch under Harmonic Forcing in Comsol 5.4; Nonlinear Shunt (Blue), Linear Shunt (Red)

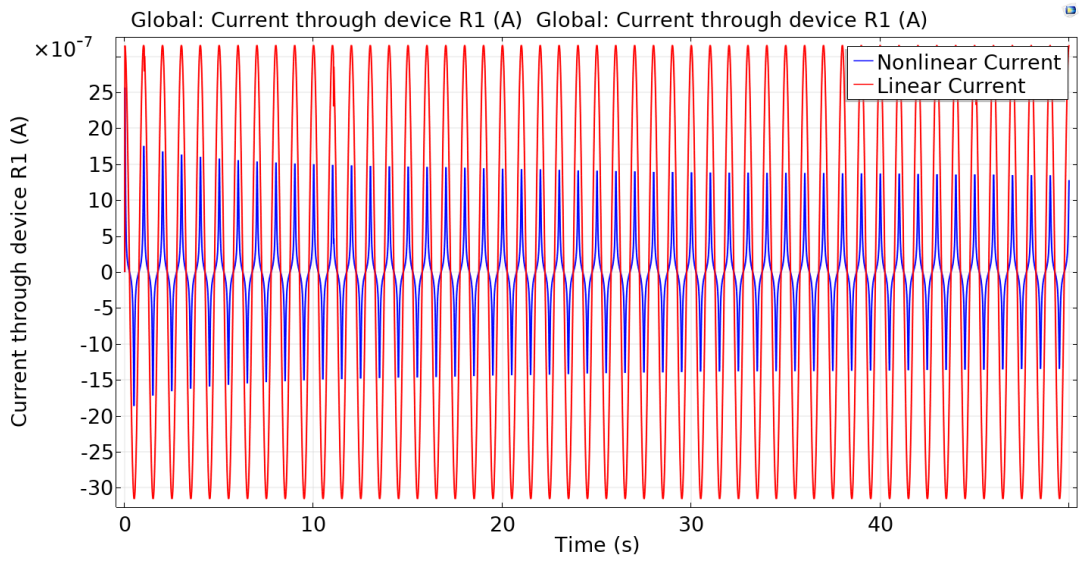

Figure 3-16 Current of SDOF Piezoelectric Patch under Harmonic Forcing in Comsol 5.4; Nonlinear Shunt (Blue), Linear Shunt (Red)

Comparing results from Comsol 5.4 and Simulink, it can be noticed that differences in linear system responses cannot be distinguished. Nevertheless, amplitudes of nonlinear system displacements of Comsol 5.4 results differ about 11% that of Simulink for steady state condition.

3.4 Frequency Response of Piezoelectric Patch under Harmonic Forcing without Softening Effect

Piezoelectric patch is a continuous body with multi modes; however, for frequencies much lower than the first mode, it can be modelled as a spring whose spring constant can be calculated regarding quasi static loading. Therefore, the system can be modelled as spring, mass, and damper as shown in Figure 3-17. By doing so, only the first mode is considered. Even though this is not a precise way to approximate the system, it builds insight into how a nonlinear system behaves. Also, assuming that the system is forced by a frequency much lower than first resonance frequency excitation, mechanical damping effect can be neglected.

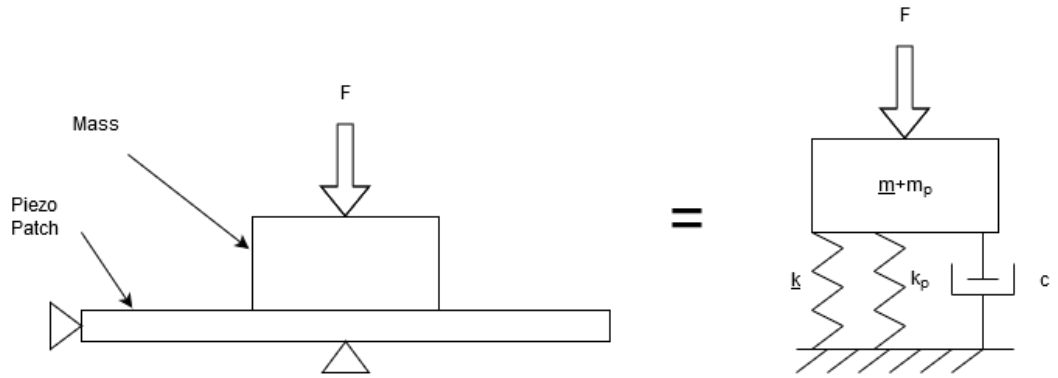

Figure 3-17 Equivalent Model of Piezoelectric Patch system with Mass under Harmonic Loading

(3.17) describes the relation between exerted external force on a piezoelectric patch, and electrical and mechanical force response of the piezoelectric material. If additional mass, spring, and damper added to the system, the force equation could be updated as below;

$$F = \frac{(AS\varepsilon^{T}{}_{33} - d_{33}Q)}{\left(s^{E}{}_{33}\varepsilon^{T}{}_{33} - d_{33}{}^{2}\right)} + \underline{m}\ddot{S}\underline{t} + c\dot{S}\underline{t} + \underline{k}S\underline{t} \tag{3.35}$$

Just as mentioned earlier, strain times thickness gives the displacement. Thus, it is evident that, $\ddot{S}\underline{t} = \ddot{\Delta x}$, $\dot{S}\underline{t} = \dot{\Delta x}$ and $S\underline{t} = \Delta x$ in (3.35).

Rearranging (3.35) results in;

$$\begin{aligned} F &= \left(k_{pzt} + \underline{k}\right)\Delta x + c\dot{\Delta x} + \underline{m}\ddot{\Delta x} - \theta Q \\ &= \overline{k}\Delta x + c\dot{\Delta x} + \underline{m}\ddot{\Delta x} - \theta Q \end{aligned} \tag{3.36}$$

where $k_{pzt} = \frac{(A\varepsilon^{T}{}_{33})}{(s^{E}{}_{33}\varepsilon^{T}{}_{33} - d_{33}{}^{2})\underline{t}}$ and $\theta = \frac{(d_{33}Q)}{(s^{E}{}_{33}\varepsilon^{T}{}_{33} - d_{33}{}^{2})}$ and $\left(k_{pzt} + \underline{k}\right) = \overline{k}$.

As (3.20) describes the relation between an external voltage applied on a piezoelectric material and electrical and mechanical voltage response of the piezoelectric material, adding RLC components in parallel into electrical circuit result in a modified version of (3.20) which is given below;

$$V = \frac{(-d_{33}AS + Qs^{E}{}_{33})}{C_p s^{E}{}_{33}} + L_{ind}\ddot{Q} + R\dot{Q} + \frac{Q}{C_l} \tag{3.37}$$

(3.37) can be rewritten as below;

$$V = -\theta\Delta x + \left(C_{pzt} + \frac{1}{C_l}\right)Q + R\dot{Q} + L_{ind}\ddot{Q} \tag{3.38}$$

Where, $C_{pzt} = \frac{1}{C_p}$.

Using the same notation, (3.36) and (3.38) are the same as the 2nd equation in [25], considering no voltage is applied on the piezoelectric patch.

In order not to deal with specific Hertz values, the equations normalized. In order to do this, it is required to define normalized time variable as below;

$$\tau = \omega t, d\tau = \omega dt \tag{3.39}$$

Where ω is the angular frequency. For a dummy variable x, differentiation with respect to normalized time variable can be written as below;

$$\frac{dx}{d\tau} = \frac{dx}{dt}\frac{dt}{d\tau} \tag{3.40}$$

Rearranging (3.40) yields;

$$\frac{dx}{dt} = \frac{dx}{d\tau}\omega \tag{3.41}$$

Second time derivative of the x with respect to time can then be calculated as follows;

$$\frac{d}{dt}\left(\frac{dx}{dt}\right) = \frac{d}{dt}\left(\frac{dx}{d\tau}\omega\right) = \frac{d}{d\tau}\left(\frac{dx}{d\tau}\omega\right)\frac{d\tau}{dt} = \frac{d^2x}{d\tau^2}\omega^2 \tag{3.42}$$

Equation (3.36) then can be expressed in terms of normalized time variable as below;

$$\Delta x''\omega^2\underline{m} + c\Delta x'\omega + \overline{k}\Delta x - \theta Q = F \tag{3.43}$$

In (3.43), $'$ denotes derivative of a variable wrt. τ. Defining $\omega = \omega_r = \sqrt{\frac{k}{m}}$, neglecting damping coefficient and considering no additional mechanical spring is attached, (3.43) can be converted as follows;

$$\Delta x'' + \Delta x - \frac{\theta}{k_{pzt}} Q = \frac{F}{k_{pzt}} \tag{3.44}$$

Similarly, (3.38) without additional capacitor can be written as;

$$V = L_{ind} Q'' \omega_r^2 + R Q' \omega_r + C_{pzt} Q - \theta \Delta x \tag{3.45}$$

Let electrical resonant frequency be defined as $\omega_e = \frac{C_{pzt}}{L_{ind}}$ and rearranging (3.45) yields;

$$V = Q'' + \frac{R}{L_{ind}\omega_r} Q' + \frac{\omega_e^2}{\omega_r^2} Q - \theta^* \Delta x \tag{3.46}$$

Where $\theta^* = \frac{\theta}{L_{ind}\omega_r^2}$. Noting that if no voltage will be applied $V = 0$ and adding cubic capacitor realized by diodes terms in to (3.46), the equation becomes;

$$0 = Q'' + \frac{R}{L_{ind}\omega_r} Q' + \frac{\omega_e^2}{\omega_r^2} Q + \frac{a}{L_{ind}\omega_r^2} Q^3 + \frac{b}{L_{ind}\omega_r^2} Q - \theta^* \Delta x \tag{3.47}$$

Assuming mechanical and electrical response of the piezoelectric patch to harmonic forcing $Fsin(\gamma\tau)$ considering single harmonic for harmonic balance method;

$$\Delta x = x_s sin(\gamma\tau) + x_c cos(\gamma\tau) \tag{3.48}$$

$$Q = Q_s sin(\gamma\tau) + Q_c cos(\gamma\tau) \tag{3.49}$$

In the above equations, γ denotes normalized angular frequency. Substituting (3.48) and (3.49) into (3.44) and (3.47) respectively;

$$\begin{aligned} -\gamma^2\big(x_s sin(\gamma\tau) + x_c cos(\gamma\tau)\big) + x_s sin(\gamma\tau) + x_c cos(\gamma\tau) \\ - \frac{\theta}{k_{pzt}}\big(Q_s sin(\gamma\tau) + Q_c cos(\gamma\tau)\big) = \frac{F}{k_{pzt}} sin(\gamma\tau) \end{aligned} \tag{3.50}$$

$$
\begin{aligned}
&-\gamma^2\left(Q_s sin(\gamma\tau) + Q_c cos(\gamma\tau)\right) \\
&+\frac{R\gamma}{L_{ind}\omega_r}\left(Q_s cos(\gamma\tau) - Q_c sin(\gamma\tau)\right) \\
&+\frac{\omega_e^2}{\omega_r^2}\left(Q_s sin(\gamma\tau) + Q_c cos(\gamma\tau)\right) \\
&+\frac{\theta}{L_{ind}\omega_r^2}\left(x_s sin(\gamma\tau) + x_c cos(\gamma\tau)\right) \\
&+\frac{a}{L_{ind}\omega_r^2}\left(Q_s sin(\gamma\tau) + Q_c cos(\gamma\tau)\right)^3 \\
&+\frac{b}{L_{ind}\omega_r^2}\left(Q_s sin(\gamma\tau) + Q_c cos(\gamma\tau)\right) = 0
\end{aligned}
\tag{3.51}
$$

Rewriting $\left(Q_s sin(\gamma\tau) + Q_c cos(\gamma\tau)\right)^3$ gives;

$$Q_s^3 sin(\gamma\tau)^3 + 3Q_s^2 sin(\gamma\tau)^2 Q_c cos(\gamma\tau) + 3Q_s sin(\gamma\tau) Q_c^2 cos(\gamma\tau)^2 + Q_c^3 cos(\gamma\tau)^3$$

Using trigonometric relations above expression can be expressed as;

$$\frac{3}{4}(Q_c^2 Q_s + Q_s^3) sin(\gamma\tau) + \frac{3}{4}(Q_s^2 Q_c + Q_c^3) cos\,(\gamma\tau) + \frac{1}{4}(Q_c^3 - 3Q_s^2 Q_c) cos\,(3\gamma\tau) + \frac{1}{4}(3Q_c^2 Q_s - Q_s^3) sin(3\gamma\tau)$$

Considering only first harmonics and neglecting higher ones in the above equation, the equation below can be written;

$$\left(Q_s sin(\gamma\tau) + Q_c cos(\gamma\tau)\right)^3 = \frac{3}{4}(Q_s^2 + Q_c^2)\left(Q_s sin(\gamma\tau) + Q_c cos(\gamma\tau)\right)$$

Substituting the above expression into Equation (3.51) and parsing coefficients of the sin and cos terms, four equations can be built as follows;

$$-x_s\gamma^2 + x_s - \frac{\theta}{k_{pzt}} Q_s = \frac{F}{k_{pzt}} \tag{3.52}$$

$$-x_c\gamma^2 + x_c - \frac{\theta}{k_{pzt}} Q_c = 0 \tag{3.53}$$

$$-\gamma^2 Q_s - \frac{R\gamma}{L_{ind}\omega_r} Q_c + \frac{\omega_e^2}{\omega_r^2} Q_s - \frac{\theta}{L_{ind}\omega_r^2} x_s + \frac{a}{L_{ind}\omega_r^2} \frac{3}{4} (Q_s^2 + Q_c^2) Q_s = 0 \tag{3.54}$$

$$-\gamma^2 Q_c + \frac{R\gamma}{L_{ind}\omega_r} Q_s + \frac{\omega_e^2}{\omega_r^2} Q_c - \frac{\theta}{L_{ind}\omega_r^2} x_c + \frac{a}{L_{ind}\omega_r^2} \frac{3}{4} (Q_s^2 + Q_c^2) Q_c = 0 \tag{3.55}$$

Before investigation of nonlinear shunt circuit, it would be better to inspect effect of the coupling coefficient for linear open and short circuit frequency response. Parameter values in Table 3.4 are used for analyzing linear and nonlinear piezoelectric patch systems. In Figure 3-18, open and short circuit conditions for original PMN-PT and weakened piezoelectric charge constant resulting in weakened coupling coefficient are given. By looking at the figure, it can be deduced that as coupling coefficient decrease, frequency range between open and short circuit condition also decreases.

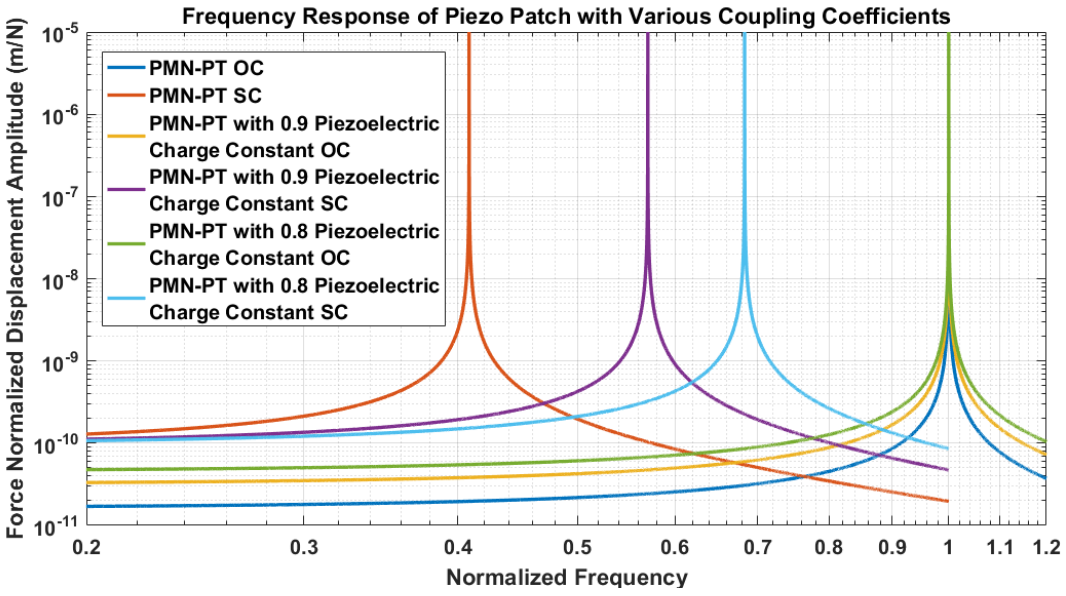

Figure 3-18 Displacement Frequency Response of Original and Weakened Charge Constant Piezoelectric Patches for Open and Short Circuit Conditions Only

By introducing the nonlinear shunt circuit, it can be observed that range decrease also holds for the nonlinear system, which is shown in Figure 3-19. The figure reveals that when coupling coefficient decrease, nonlinear effect increase, and region that for the nonlinear curve gets narrower. Nonetheless, as the band gets narrower and narrower and the damping in the system is not at a considerable level, nonlinear curve may not turn and converge to open circuit system.

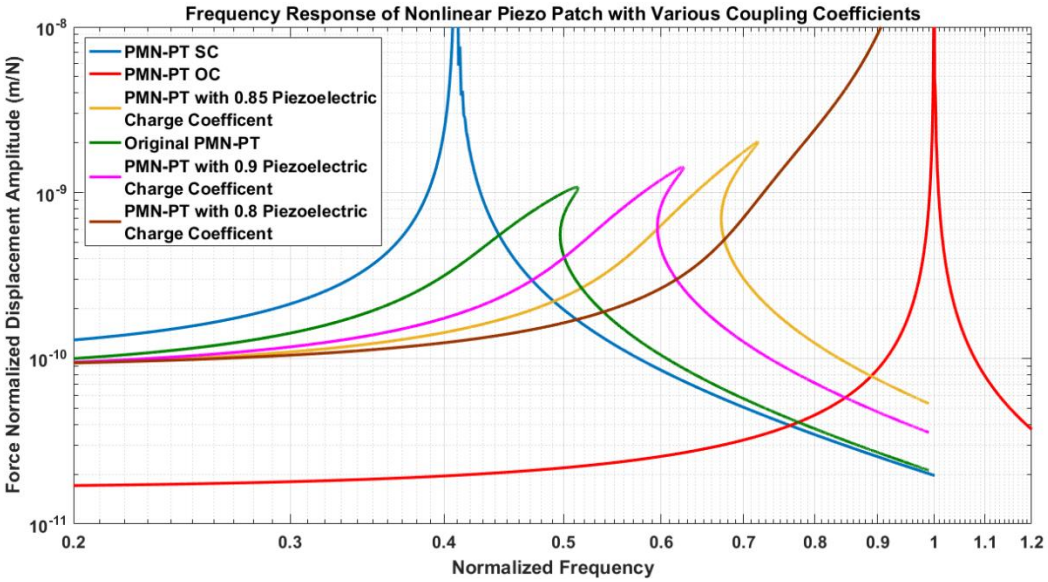

Figure 3-19 Displacement Frequency Response of Original and Weakened Piezoelectric Patches with Open Circuit, Short Circuit, and Nonlinear Circuit

Table 3.4 Parameters and Their Values Used to Calculate Frequency Response of Piezoelectric Patch with Nonlinear shunt circuit

Parameter	**Value**
Forcing amplitude (N)	0.5
Mass (kg)	10^2
Inductance (H)	$3x10^{-2}$
Resistance (ohm)	10^2
Piezoelectric material thickness (m)	$968x10^{-6}$
Piezoelectric charge constant (m/V)	$1500x10^{-12}$

Table 3.4 Cont'd

Piezoelectric dielectric constant (F/m)	$5017\times(8.854\text{x}10^{-12})$
Piezoelectric patch area (mm^2)	30×20
Piezoelectric material elastic compliance (m^2/N)	$60.8\text{x}10^{-12}$
Q_0	$2.7548\text{x}10^{-8}$
α	3.63
β	0.35

3.5 Summary of the Chapter

The chapter started with conceptually proving that hardening capacitance results in hardening stiffness. Then hardening stiffness effect is shown by hand calculations whose nonlinear parameter values are obtained by curve fitting stemming from [8] and by Comsol 5.4 simulations which can model diodes as they are. In addition to hardening stiffness, how negative capacitance concept induces stiffness was briefly mentioned.

By observing hardening stiffness effect of the nonlinear shunt, time domain response of harmonically forced simply supported piezoelectric patch systems are studied. Time domain analyses are conducted with use of Comsol 5.4 and Simulink with a single low frequency value. In the software's diodes in shunt circuits, which introduce nonlinearity, are modelled, and the results are given with linear shunt circuit case. For time domain analysis, it was found that results from Comsol 5.4 are in agreement with results from that of Simulink by around 10% error.

Lastly, frequency response of the piezoelectric patches is studied in the chapter. The study basically revealed the nonlinear trend and the importance of the coupling coefficient in observation of the nonlinear effects. It was found that stiffness value of the piezoelectric patch system is bounded by open and short circuit stiffness values. Moreover, the fact that frequency range between open and short circuit

conditions is related to coupling coefficient of the piezoelectric material was demonstrated with several different simulations throughout this chapter.

CHAPTER 4

MODELING OF PIEZOELECTRIC PATCH INTEGRATED COMPOSITE CANTILEVER BEAM

In the previous chapter cubic capacitance shunt circuit was investigated using a piezoelectric patch. Nonlinear effect was observed for fictitious cubic capacitance values and piezoelectric element by itself. The proposed shunt circuit can be modelled for a realizable practical system that is a piezoelectric patch attached cantilever beam.

This chapter starts with analytical modelling of bimorph piezoelectric material attached composite cantilever beam with linear piezoelectric material assumption. Since the analytical model of the composite structure can be reduced to plain cantilever beam by equating some parameters to zero, frequency responses of the analytical and FEM model plain cantilever beam are compared for verification. Then, analytical model is used to describe plain discontinuous cantilever beam, and frequency responses of the model and FEM model are compared. The chapter proceeds by introducing piezoelectric effect to the discontinuous cantilever structures, and again, frequency responses of FEM and derived model are compared for linear shunt circuit. Since FEM software employs linear piezoelectric model, the aforementioned assumption is utilized. After this, analytical method is used to determine frequency response of the proposed nonlinear shunt circuit with theoretical piezoelectric material and electrical component, and time domain analysis is made to observe jumps in frequency responses. Finally, frequency response plots are generated for a commercially available piezoelectric patch with interdigitated electrodes and a commercially available diode. However, this time softening stiffness of the piezoelectric material, which is discussed in 2.3, is included since the method will be compared with tests instead of FEM software.

The analyses mentioned above include theoretical elements as well as commercially available elements. Theoretical elements make it possible to pass beyond the available limits and observe the exaggerated effects of parameters. Using commercially available elements in models paves the way for experimental studies. Also, it demonstrates if the proposed system is realizable or not with off the shelf components.

4.1 Derivation of Equation of Motion for Piezoelectric Patch Integrated Composite Cantilever Beam with Linear Piezoelectric Material Assumption

Modelling of the beam structure shown in Figure 4-1 can be done in two ways; using Newton's second law and using Hamilton's principle. In this section, both of the derivations are presented, and for further analysis, Hamilton's principle is implemented.

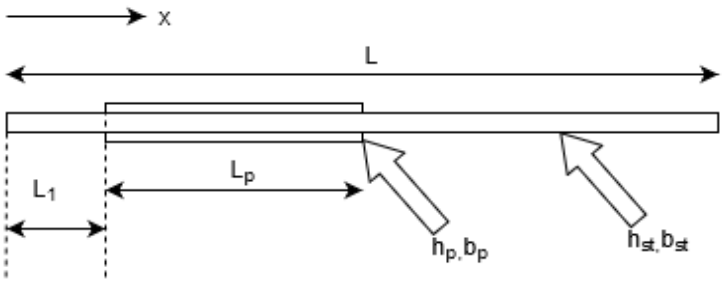

Figure 4-1 Schematic of Bimorph Composite Piezoelectric Integrated Cantilever Beam

4.1.1 Derivation of Equation of Motion with Newton's Second Law

Cantilever beam structure is a continuous body and Euler-Bernoulli beam theory can be employed to define motion of the system if slender beam requirement is met. A beam having low thickness/length ratio is considered as slender. Since in this thesis,

slender beams having slenderness ratio of not more than 5% are presented, Euler-Bernoulli beam theory is used. The theory neglects shear deformations in the beam, and therefore results may include small discrepancies due to shear effects. However, the approximation is employed in the literature [61][62][63], and the results of theoretical calculations are found to be close to that of experiments [51].

Considering that the cantilever beam element experiences only pure bending and neglecting shear deflections, the element takes the form shown in Figure 4-2. In the figure neutral axis is the line where no strain occurs, ρ is the radius of the curve, θ is the angle which caused by bending action, w is transverse displacement, z is the distance from the neutral axis, and h and b are thicknesses and width of the piezoelectric material and host structure.

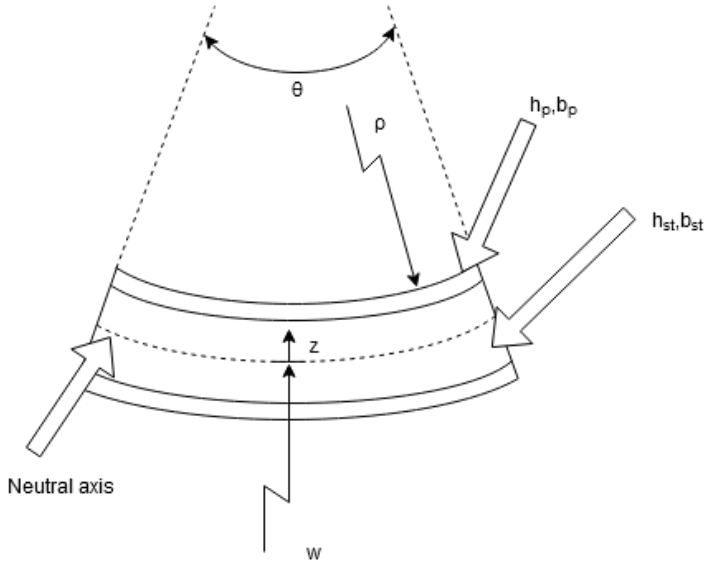

Figure 4-2 Bent Composite Beam Element

Let L_0 be the length of the element before bending. After bending, the length of each layer of the element can be calculated as

$$L' = (\rho - z)\theta$$

Then strain becomes

$$S = \frac{L' - L_0}{L_0} = -\frac{z\theta}{\rho\theta} = \frac{z}{\rho}$$

Curvature of the beam is defined as;

$$\kappa = \frac{1}{\rho} = \frac{w''}{\left(1 + w'^2\right)^{\frac{3}{2}}}$$

Assuming relatively small angle θ, which is a reasonable approximation for a beam made of steel or aluminum, $w' \ll 1$. Then above expression reduces to;

$$\kappa = \frac{1}{\rho} = w''$$

Thus, strain can be determined as below;

$$S = -w''z \tag{4.1}$$

Recalling (3.2) and substituting $Y_{33}^E = (s^E{}_{33})^{-1}$ internal stress on the piezoelectric element is defined as;

$$SY_{33}^E - d_{31}EY_{33}^E = T_p \tag{4.2}$$

Internal stress on the host structure can be expressed as;

$$T = Y_{st}S \tag{4.3}$$

Hence, internal mechanical moment on the element can be calculated as follows;

$$\begin{aligned} M_{mech} = &\iint_{-\left(\frac{h_{st}}{2}+h_p\right)}^{-\frac{h_{st}}{2}} SY_{33}^E z dz dy + \iint_{\frac{h_{st}}{2}}^{\left(\frac{h_{st}}{2}+h_p\right)} SY_{33}^E z dz dy \\ &+ \iint_{-\frac{h_{st}}{2}}^{\frac{h_{st}}{2}} SY_{st} z dz dy \end{aligned} \tag{4.4}$$

The other term of the internal moment being electrical moment can be calculated as below;

$$M_{elec} = \iint_{-\left(\frac{h_{st}}{2}+h_p\right)}^{-\frac{h_{st}}{2}} d_{31}EY_{33}^{E}zdzdy + \iint_{\frac{h_{st}}{2}}^{\left(\frac{h_{st}}{2}+h_p\right)} d_{31}EY_{33}^{E}zdzdy \qquad (4.5)$$

Substituting strain into equations (4.4) and (4.5) and evaluating the integrals total external moment becomes;

$$\begin{aligned} M &= M_{mech} + M_{elec} \\ &= \frac{Y_{33}^{E}w''z^3}{3}b_p\Big|_{-\left(\frac{h_{st}}{2}+h_p\right)}^{-\frac{h_{st}}{2}} + \frac{Y_{33}^{E}w''z^3}{3}b_p\Big|_{\frac{h_{st}}{2}}^{\left(\frac{h_{st}}{2}+h_p\right)} \\ &+ \frac{d_{31}EY_{33}^{E}z^2}{2}b_p\Big|_{-\left(\frac{h_{st}}{2}+h_p\right)}^{-\frac{h_{st}}{2}} \\ &+ \frac{d_{31}EY_{33}^{E}z^2}{2}b_p\Big|_{\frac{h_{st}}{2}}^{\left(\frac{h_{st}}{2}+h_p\right)} + \frac{Y_{st}w''z^3}{3}b_{st}\Big|_{-\frac{h_{st}}{2}}^{\frac{h_{st}}{2}} \end{aligned} \qquad (4.6)$$

Using equation (3.5) electrical part of the system can be written as below;

$$\begin{aligned} D &= d_{31}T + \varepsilon^{T}{}_{33}E = d_{31}(SY_{33}^{E} - d_{31}EY_{33}^{E}) + \varepsilon^{T}{}_{33}E \\ &= d_{31}SY_{33}^{E} + E(\varepsilon^{T}{}_{33} - d_{31}^{2}Y_{33}^{E}) \end{aligned} \qquad (4.7)$$

In order to obtain electrical charge from electrical displacement, area integral of the above equation should be taken;

$$\iint Ddxdy = \int_{L_1}^{L_1+L_p}\left(-w''zd_{31}Y_{33}^{E} + E(\varepsilon^{T}{}_{33} - d_{31}^{2}Y_{33}^{E})\right)b_p dx \qquad (4.8)$$

Since the strain along z-direction varies linearly, taking the middle point of the piezoelectric element gives average strain along with the piezoelectric material thickness. Regarding this and expressing electric field in terms of voltage electrical charge can be written as;

$$Q = \left(-w'\overline{z}d_{31}Y_{33}^{E}\Big|_{L_1}^{L_1+L_p} + \frac{V}{h_p}(\varepsilon^{T}{}_{33} - d_{31}^{2}Y_{33}^{E})L_p\right)b_p \qquad (4.9)$$

where,

$$\overline{z} = \frac{h_{st}}{2} + \frac{h_p}{2}$$

When two piezoelectric patches are connected in parallel, the width of the connected piezoelectric structure can be considered as doubled for the electrical equations. Hence, inserting $2b_p$ instead of b_p in the above equation changes noting in it.

When piezoelectric patches are connected in series, piezoelectric structure can be considered as stack, and for this reason, piezoelectric patches can be considered as one piezoelectric patch with doubled thickness. As a result, electrical equation for serially connected piezoelectric patches can be written as below;

$$Q = \left(-w'\overline{z}d_{31}Y_{33}^{E} \Big|_{L_1}^{L_1+L_p} + \frac{V}{2h_p}(\varepsilon^{T}{}_{33} - d_{31}^{2}Y_{33}^{E})L_p \right) b_p \qquad (4.10)$$

By taking parallel connected piezoelectric patch configuration into account, circuit equation of the shunt circuit given in Figure 4-3 can be written as below;

$$V_p = -\left(L\ddot{Q} + R\dot{Q} + aQ^3 + bQ\right) \qquad (4.11)$$

Substituting (4.11) into (4.10) gives;

$$Q = \left(-w'\overline{z}d_{31}Y_{33}^{E} \Big|_{L_1}^{L_1+L_p} - \frac{\left(L\ddot{Q} + R\dot{Q} + aQ^3 + bQ\right)}{2h_p}(\varepsilon^{T}{}_{33} - d_{31}^{2}Y_{33}^{E})L_p \right) b_p \qquad (4.12)$$

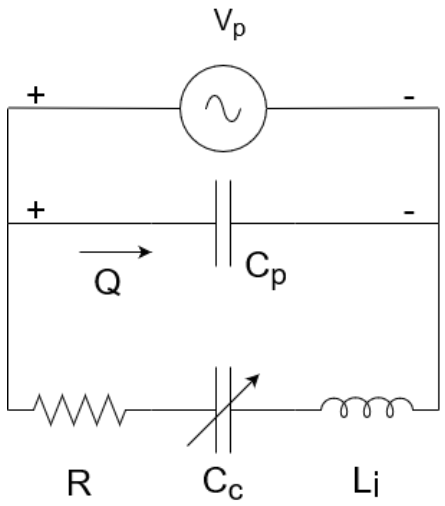

Figure 4-3 Piezoelectric Shunt circuit

Continuing from (4.6) equation of motion of the beam can be determined by considering Figure 4-4.

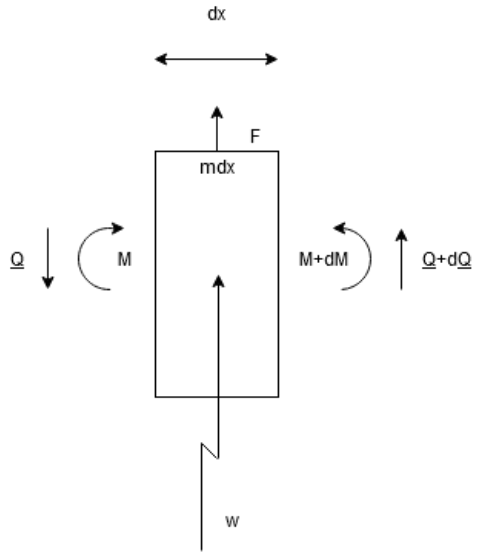

Figure 4-4 Free Body Diagram of Infinitesimal Element of Cantilever Beam Experiencing Transverse Vibration

Applying Newton's second gives;

$$-d\underline{Q} + fdx = mdx\ddot{w} \tag{4.13}$$

Noting that

$$\frac{dQ}{dx} = \frac{d^2M}{dx^2}$$

(4.13) can be written as;

$$f - \frac{d^2M}{dx^2} = m\ddot{w} \tag{4.14}$$

Piezoelectric material and host structures' material constitutes m; thus, it can be expressed as;

$$m = m_p\left(X(x - L_1) - X\left(x - \left(L_1 + L_p\right)\right)\right) + m_{st} = m_p\bar{X} + m_{st} \tag{4.15}$$

Where X denotes step function. Substituting (4.6) and (4.15) into (4.14) gives the EOM below;

$$\begin{aligned} f = \Bigg(& \frac{Y_{33}^E w^{(4)} z^3}{3} b_p \Big|_{-\left(\frac{h_{st}}{2}+h_p\right)}^{-\frac{h_{st}}{2}} + \frac{Y_{33}^E w^{(4)} z^3}{3} b_p \Big|_{\frac{h_{st}}{2}}^{\left(\frac{h_{st}}{2}+h_p\right)} \\ & + \frac{d_{31} E Y_{33}^E z^2}{2} b_p \Big|_{-\left(\frac{h_{st}}{2}+h_p\right)}^{-\frac{h_{st}}{2}} \\ & + \frac{d_{31} E Y_{33}^E z^2}{2} b_p \Big|_{\frac{h_{st}}{2}}^{\left(\frac{h_{st}}{2}+h_p\right)} \Bigg)\Big(X(x - L_1) \\ & - X\left(x - \left(L_1 + L_p\right)\right)\Big) + \frac{Y_{st} w^{(4)} z^3}{3} b_{st} \Big|_{-\frac{h_{st}}{2}}^{\frac{h_{st}}{2}} \\ & + \left(m_p\left(X(x - L_1) - X\left(x - \left(L_1 + L_p\right)\right)\right)\right. \\ & \left. + m_{st}\right)\ddot{w} \end{aligned} \tag{4.16}$$

In the equation above, forcing can be exerted as base excitation, tip forcing, and so on. In addition to that, the tip mass can be introduced to the system by adding a term given below in (4.15).

$$M_{tip}\delta_{kronecker}(x - L)$$

Where $\delta_{kronecker}$ denotes Kronecker delta function.

4.1.2 Derivation of Equation of Motion with Hamilton's Principle

EOM can be derived using Hamilton's principle considering the assumptions mentioned in 4.1.1 for the cantilever beam structure. Using the principle equation below can be written;

$$\int_{t_1}^{t_2} \delta(\mathcal{L})dt = 0 \tag{4.17}$$

In order to express Lagrangian $\mathcal{L}$, its components giving total energy in the system need to be calculated. Strain energy can be calculated as;

$$U_{SE} = \frac{1}{2}ST \tag{4.18}$$

For 3-1 mode operating piezoelectric patch equations (3.15) and (3.18) can be modified as below;

$$T = \frac{1}{s^E{}_{31}\varepsilon^T{}_{33} - d_{31}{}^2}(S\varepsilon^T{}_{33} - d_{31}D) = c_{31}^D S - h_{31}D \tag{4.19}$$

$$E = \frac{1}{s^E{}_{31}\varepsilon^T{}_{33} - d_{31}{}^2}(-d_{31}S + Ds^E{}_{31}) = -h_{31}S + \beta_{33}^S D \tag{4.20}$$

Using (4.18), (4.19), (4.20), and (4.1), strain energy in the piezoelectric patch can be expressed as below;

$$U_p = \frac{1}{2}\Bigg(\int_0^L \int_{-\left(\frac{h_{st}}{2}+h_p\right)}^{-\frac{h_{st}}{2}} \int_0^{b_p} \left(c_{31}^D z^2 w''^2 + h_{31} z w'' D\right) dy dz dx + \int_0^L \int_{\frac{h_{st}}{2}}^{\left(\frac{h_{st}}{2}+h_p\right)} \int_0^{b_p} \left(c_{31}^D z^2 w''^2 + h_{31} z w'' D\right) dy dz dx \Bigg) \bar{X} \tag{4.21}$$

(4.21) can be evaluated as;

$$U_p = \frac{1}{2}\int_0^L \bar{X} b_p \left(2c_{31}^D \frac{\left(\left(\frac{h_{st}}{2}+h_p\right)^3 - \left(\frac{h_{st}}{2}\right)^3\right)}{3} w''^2 + h_{31}\left(\left(\frac{h_{st}}{2}+h_p\right)^2 - \left(\frac{h_{st}}{2}\right)^2\right) w'' D \right) dx$$

Above equation can be simplified to give;

$$U_p = \frac{1}{2}\int_0^L \bar{X}\left(c_{31}^D J_{3p} w''^2 + h_{31} J_{2p} w'' D\right) dx \tag{4.22}$$

Similarly, strain energy of the host structure can be calculated as;

$$U_{st} = \frac{1}{2}\int_0^L \int_{-\frac{h_{st}}{2}}^{\frac{h_{st}}{2}} \int_0^{b_{st}} Y_{st} z^2 w''^2 dy dz dx = \int_0^L \frac{Y_{st} b_{st} h_{st}^3}{24} w''^2 dx = \int_0^L \frac{Y_{st} J_{3st} w''^2}{2} dx \tag{4.23}$$

Kinetic energy of the piezoelectric patch can be calculated as below;

$$K_p = \frac{1}{2}\int_0^L m_p \bar{X} \dot{w}^2 dx \tag{4.24}$$

Likewise, kinetic energy of the host structure can be written as;

$$K_{st} = \frac{1}{2}\int_0^L m_{st}\dot{w}^2 dx \tag{4.25}$$

Considering electrical equation as;

$$U_{EL} = \frac{ED}{2}$$

Electrical energy stored in the piezoelectric element can be expressed as below;

$$\begin{aligned} U_{el} = \frac{1}{2}\Bigg(& \int_0^L \int_{-\left(\frac{h_{st}}{2}+h_p\right)}^{-\frac{h_{st}}{2}} \int_0^{b_p} (h_{31} z w'' + \beta_{33}^s D)\bar{X}\, dy\, dz\, dx \\ & + \int_0^L \int_{\frac{h_{st}}{2}}^{\left(\frac{h_{st}}{2}+h_p\right)} \int_0^{b_p} (h_{31} z w'' + \beta_{33}^s D)\bar{X}\, dy\, dz\, dx \Bigg) \\ & = \frac{1}{2}\left(\int_0^L b_p \bar{X}\left(h_{31} J_{2p} D w'' + \beta_{33}^s D^2\right) dx \right) \end{aligned} \tag{4.26}$$

Finally, work done by external forces on the system can be expressed as follows;

$$W = fw \tag{4.27}$$

Although the system suggested in this thesis is suitable for controlling by external electrical power application, work done by electric domain is omitted to observe passive components' effects.

Regarding equations from (4.21) to (4.27), Lagrangian becomes;

$$\mathcal{L} = K_p + K_{st} - U_p - U_{st} - U_{el} + W \tag{4.28}$$

To evaluate (4.17), variation of each term in (4.28) must be evaluated.

Time integral of variation of K_p yields;

$$\int_{t_1}^{t_2} \delta K_p dt = \int_0^L \int_{t_1}^{t_2} m_p \bar{X} \dot{w} \delta \dot{w} dt dx \tag{4.29}$$

Applying integration by parts (IBP) to (4.29) gives;

$$\int_0^L m_p \bar{X} \dot{w} \delta w \Big|_{t_1}^{t_2} dx - \int_0^L \int_{t_1}^{t_2} m_p \bar{X} \ddot{w} \delta w dt\, dx \tag{4.30}$$

The first term in (4.30) is zero since variation from t_1 to t_2 is zero. Thus;

$$\int_0^L \int_{t_1}^{t_2} \delta K_p dt dx = \int_0^L - \int_{t_1}^{t_2} m_p \bar{X} \ddot{w} \delta w dt\, dx \tag{4.31}$$

Using the same procedure for K_{st} which is the second term in (4.28), its time integral of variation can be expressed as below;

$$\int_{t_1}^{t_2} \delta K_{st} dt = \int_0^L - \int_{t_1}^{t_2} m_{st} \ddot{w} \delta w dt\, dx \tag{4.32}$$

Time integral of variation of the third term's first term in (4.28) U_p yields;

$$\int_{t_1}^{t_2} \delta \left(\frac{1}{2} \int_0^L \bar{X} c_{31}^D J_{3p} w''^2 dx\, dt \right) = \int_{t_1}^{t_2} \int_0^L c_{31}^D J_{3p} w'' \bar{X} \delta w'' dx dt \tag{4.33}$$

Applying IBP to (4.33) considering $u = w''\bar{X}$ and $dV = w''$ gives;

$$\begin{aligned} &\int_{t_1}^{t_2} \delta \left(\frac{1}{2} \int_0^L \bar{X} c_{31}^D J_{3p} w''^2 dx\, dt \right) \\ &= \int_{t_1}^{t_2} c_{31}^D J_{3p} (w'' \bar{X}) \delta w' \Big|_0^L dt \\ &- \int_{t_1}^{t_2} \int_0^L c_{31}^D J_{3p} (w'' \bar{X}) \delta w' dx dt \end{aligned} \tag{4.34}$$

In the above equation $\bar{X}$ is zero at the boundaries 0 and L and applying IBP on the second term yields,

$$\int_{t_1}^{t_2} \delta\left(\frac{1}{2}\int_0^L \bar{X} c_{31}^D J_{3p} w''^2 dx\, dt\right)$$
$$= -\left(\int_{t_1}^{t_2} c_{31}^D J_{3p}(w''\bar{X})'\delta w \Big|_0^L dt \right. \tag{4.35}$$
$$\left. - \int_{t_1}^{t_2}\int_0^L c_{31}^D J_{3p}(w''\bar{X})''\delta w dx dt\right)$$

The first term on the right hand side in (4.35) is zero because variation of w is zero from t_1 to t_2. Rewriting the equation, one can obtain the relation below;

$$\int_{t_1}^{t_2} \delta\left(\frac{1}{2}\int_0^L \bar{X} c_{31}^D J_{3p} w''^2 dx\, dt\right)$$
$$= \int_{t_1}^{t_2}\int_0^L c_{31}^D J_{3p}\big(w^{(4)}\bar{X} + 2w^{(3)}\bar{X}' \tag{4.36}$$
$$+ w''\bar{X}''\big)\delta w dx dt$$

To complete time integration of variation of U_p's the second term should be calculated.

$$\int_{t_1}^{t_2} \frac{1}{2}\int_0^L \delta\big(\bar{X} b_p h_{31} J_{2p} w'' D dx\big)\, dt$$
$$= \int_{t_1}^{t_2} \frac{1}{2}\int_0^L \bar{X} b_p h_{31} J_{2p}\delta(w'') D dx\, dt \tag{4.37}$$

Applying IBP to the above equation gives;

$$\int_{t_1}^{t_2} \frac{1}{2}\int_0^L \delta\big(\bar{X} b_p h_{31} J_{2p} w'' D dx\big)\, dt$$
$$= \int_{t_1}^{t_2} \frac{1}{2} J_{2p} h_{31} D\left(\bar{X}\delta w' \Big|_0^L - \int_0^L \bar{X}'\delta w' dx\right) dt \tag{4.38}$$

Since $\bar{X}$ is zero at the boundaries, the first term in the parenthesis above is zero. One more IBP gives;

$$\int_{t_1}^{t_2} \frac{1}{2} \int_0^L \delta\left(\bar{X} b_p h_{31} J_{2p} w'' D dx\right) dt$$
$$= \int_{t_1}^{t_2} -\frac{1}{2} J_{2p} h_{31} D \left(\bar{X}' \delta w \Big|_0^L - \int_0^L \bar{X}'' \delta w dx \right) dt \tag{4.39}$$

Again, due to that $\bar{X}$ is zero at the boundaries and therefore $\bar{X}'$ is also zero above equation reduces to following;

$$\int_{t_1}^{t_2} \frac{1}{2} \int_0^L \delta\left(\bar{X} b_p h_{31} J_{2p} w'' D dx\right) dt = \int_{t_1}^{t_2} \frac{1}{2} J_{2p} h_{31} D \int_0^L \bar{X}'' \delta w dx \, dt \tag{4.40}$$

To continue with the 3rd term (U_{st}) in (4.28), the time integral can be written as;

$$\int_{t_1}^{t_2} \delta U_{st} dt = \int_{t_1}^{t_2} \delta \left(\int_0^L \frac{Y_{st} J_{3st}}{2} w''^2 dx \right) dt$$
$$= \int_{t_1}^{t_2} \int_0^L Y_{st} J_{3st} w'' \delta w'' dx \, dt \tag{4.41}$$

Applying IBP above equation can be written as;

$$\int_{t_1}^{t_2} \int_0^L Y_{st} J_{3st} w'' \delta w'' dx \, dt$$
$$= \int_{t_1}^{t_2} Y_{st} J_{3st} \left(w'' \frac{d}{dx} \delta w \Big|_0^L - \int_0^L w^{(3)} \delta w' dx \right) dt \tag{4.42}$$

Since either moment or slope is zero first term in the parenthesis above goes to zero. Applying one more IBP gives;

$$\int_{t_1}^{t_2} \int_0^L Y_{st} J_{3st} w'' \delta w'' dx \, dt$$
$$= \int_{t_1}^{t_2} -Y_{st} J_{3st} \left(w^{(3)} \delta w \Big|_0^L - \int_0^L w^{(4)} \delta w dx \right) dt \tag{4.43}$$

The first term above goes to zero since either moment or slope is zero at the boundaries. Hence,

$$\int_{t_1}^{t_2} \delta U_{st} dt = \int_{t_1}^{t_2} Y_{st} J_{3st} \int_0^L w^{(4)} \delta w dx \, dt \tag{4.44}$$

Time integral of variation calculation of U_{el} is similar to U_p's second term's;

$$\begin{aligned} \int_{t_1}^{t_2} \delta U_{el} dt &= \int_{t_1}^{t_2} \delta \left(\frac{1}{2} \left(\int_0^L b_p \bar{X} \left(h_{31} J_{2p} D w'' + \beta_{33}^S D^2 \right) dx \right) \right) dt \\ &= \int_{t_1}^{t_2} \frac{1}{2} \left(\int_0^L b_p \bar{X} \left(h_{31} J_{2p} D \delta w'' \right. \right. \\ &\quad \left. \left. + \delta (\beta_{33}^S D^2) \right) dx \right) dt \end{aligned} \tag{4.45}$$

The term including electrical displacement in the above equation is independent of any path, and the remaining term is the same with (4.37). Hence, the equation can be written as;

$$\int_{t_1}^{t_2} \delta U_{el} dt = \int_{t_1}^{t_2} \frac{1}{2} J_{2p} h_{31} D \int_0^L \bar{X}'' \delta w dx \, dt \tag{4.46}$$

Calculation for W is trivial; however, it can be written as below;

$$\int_{t_1}^{t_2} \delta W dt = \int_{t_1}^{t_2} \int_0^L f \delta w dx dt \tag{4.47}$$

Evaluating the time integral of variations, EOM can be now expressed as below;

$$\begin{aligned} m_p \bar{X} \ddot{w} + m_{st} \ddot{w} + c_{31}^D J_{3p} \left(w^{(4)} \bar{X} + 2 w^{(3)} \bar{X}' + w'' \bar{X}'' \right) \\ + Y_{st} J_{3st} w^{(4)} + J_{2p} h_{31} D \bar{X} = f \end{aligned} \tag{4.48}$$

4.2 Deriving Equations for Response of Bimorph Composite Piezoelectric Integrated Cantilever Beam in 3-1 Mode with Linear Piezoelectric Material Assumption

Response of the system whose EOM is derived in 4.1 can be expressed using expansion theorem [64][65][66][61] as below;

$$w = \sum_{r} \phi_r q_r \tag{4.49}$$

In the equation above ϕ_r denotes r[th] eigenfunction and q_r denotes r[th] modal coordinate. Multiplying equation (4.48) with ϕ_r and taking integral along the length of the beam gives;

$$\begin{aligned}\int_0^L \big(m_p \bar{X}\ddot{w} + m_{st}\ddot{w} + c_{31}^D J_{3p}\big(w^{(4)}\bar{X} + 2w^{(3)}\bar{X}' + w''\bar{X}''\big) \\ + Y_{st}J_{3st}w^{(4)} + J_{2p}h_{31}D\bar{X}\big)\phi_r dx = \int_0^L f\phi_r dx\end{aligned} \tag{4.50}$$

Substituting (4.49) in (4.50) equation below can be written;

$$[M]\ddot{q} + [K]q + \{C\}Q = F \tag{4.51}$$

Where,

$$M_{i,j} = \big(m_{st} + m_p\bar{X}\big)\int_0^L \phi_i\phi_j dx \tag{4.52}$$

$$\begin{aligned}K_{i,j} = c_{31}^D J_{3p}\int_0^L \Big(\phi_i^{(4)}\bar{X} + 2\phi_i{}^{(3)}\bar{X}' + \phi_i{}''\bar{X}''\Big)\phi_j dx \\ + Y_{st}J_{3st}\int_0^L \phi_i^{(4)}\phi_j dx\end{aligned} \tag{4.53}$$

$$C_i = J_{2p}h_{31}D\int_0^L (\bar{X}'')\phi_i dx = \frac{J_{2p}h_{31}Q}{2b_pL_p}\int_0^L (\bar{X}'')\phi_i dx \tag{4.54}$$

$$F_i = \int_0^L f\phi_i dx \tag{4.55}$$

Integral equation in (4.53) can be divided into three sub integrals;

$$\begin{aligned}&\int_0^L \left(\phi_i^{(4)}\bar{X} + 2\phi_i{}^{(3)}\bar{X}' + \phi_i{}''\bar{X}''\right)\phi_j dx \\ &= \int_0^L \left(\phi_i^{(4)}\bar{X}\right)\phi_j dx + \int_0^L \left(2\phi_i{}^{(3)}\bar{X}'\right)\phi_j dx \\ &+ \int_0^L (\phi_i{}''\bar{X}'')\phi_j dx = I_1 + I_2 + I_3\end{aligned} \tag{4.56}$$

I_2 can be rewritten as below after applying IBP;

$$\begin{aligned}I_2 &= \int_0^L \left(2\phi_i{}^{(3)}\bar{X}'\right)\phi_j dx \\ &= 2\left(\phi_i{}^{(3)}\phi_j\bar{X}\Big|_0^L - \int_0^L \bar{X}'\left(\phi_i{}^{(4)}\phi_j + \phi_i{}^{(3)}\phi_j'\right)dx\right)\end{aligned} \tag{4.57}$$

Since the $\bar{X}$ is zero at the given boundaries, the first term in the parenthesis becomes zero and can be expressed as below;

$$I_2 = 2\left(-\int_0^L \bar{X}'\left(\phi_i{}^{(4)}\phi_j + \phi_i{}^{(3)}\phi_j'\right)dx\right) \tag{4.58}$$

IBP can be applied to I_3 also and gives;

$$I_3 = \phi_i{}''\phi_j\bar{X}'\Big|_0^L - \int_0^L \bar{X}'\left(\phi_i{}^{(3)}\phi_j + \phi_i{}''\phi_j'\right)dx \tag{4.59}$$

As stated above, $\bar{X}'$ is the derivative of the zero value. Hence, the first term goes to zero, and IBP can be applied to the remaining integral;

$$I_3 = -\left(\bar{X}\left(\phi_i{}^{(3)}\phi_j + \phi_i{}''\phi_j'\right)\Big|_0^L - \int_0^L \bar{X}\left(\phi_i{}^{(3)}\phi_j + \phi_i{}''\phi_j'\right)'dx\right) \tag{4.60}$$

Nonzero element of the I_3 is only the integral appearing in (4.60), and it rewriting the equation gives;

$$I_3 = \int_0^L \bar{X}\left(\phi_i{}^{(4)}\phi_j + 2\phi_i{}^{(3)}\phi_j' + \phi_i{}''\phi_j''\right)dx \tag{4.61}$$

$K_{i,j}$ in (4.53) can be reduced to the equation below;

$$K_{i,j} = c_{31}^D J_{3p}\int_0^L \bar{X}\phi_i''\phi_j''dx + Y_{st}J_{3st}\int_0^L \phi_i^{(4)}\phi_j dx \tag{4.62}$$

Similar to $K_{i,j}$, the integral part of C_i can be rearranged by applying IBP;

$$\int_0^L (\bar{X}'')\phi_i dx = \bar{X}'\phi_i \Big|_0^L - \int_0^L \bar{X}'\phi_i' dx \tag{4.63}$$

The first term above integral is zero because of the same reason mentioned between (4.57) and (4.58). The second term can be integrated by parts one more time to give;

$$\int_0^L (\bar{X}'')\phi_i dx = -\left(\bar{X}\phi_i'' - \int_0^L \bar{X}\phi_i'' dx\right) \tag{4.64}$$

The first term in the above equation is zero, and the evaluated integral can be substituted into (4.54) and C_i becomes;

$$C_i = \frac{J_{2p}h_{31}Q}{2b_pL_p}\left(\phi_i'(L_1) - \phi_i'\left(L_1 + L_p\right)\right) \tag{4.65}$$

All coefficients being vectors and matrices can be calculated in (4.51), and considering first harmonic only modal coordinates can be expressed below for steady state response;

$$q_i = q_{is}\sin(\omega t) + q_{ic}\cos(\omega t) \tag{4.66}$$

Similarly, considering first harmonic for steady state electrical charge can be expressed as below;

$$Q = Q_s\sin(\omega t) + Q_c\cos(\omega t) \tag{4.67}$$

Under harmonic excitation $f = f_0\sin(wt)$ (4.51) becomes;

$$\left(\begin{bmatrix} K_{11} & K_{12} & \cdots \\ \vdots & \ddots & \vdots \\ K_{n1} & \cdots & K_{nn} \end{bmatrix} - \omega^2 \begin{bmatrix} M_{11} & M_{12} & \cdots \\ \vdots & \ddots & \vdots \\ M_{n1} & \cdots & M_{nn} \end{bmatrix}\right) \begin{Bmatrix} q_{1s}\sin(\omega t) + q_{1c}\cos(\omega t) \\ \vdots \\ q_{ns}\sin(\omega t) + q_{nc}\cos(\omega t) \end{Bmatrix} + \begin{Bmatrix} C_1 \\ \vdots \\ C_n \end{Bmatrix} Q_s \sin(\omega t) + Q_c \cos(\omega t) = \begin{Bmatrix} F_1 \\ \vdots \\ F_n \end{Bmatrix} \sin(\omega t) \tag{4.68}$$

Parsing equations in (4.68) for sines and cosines results in 2n number equations and equation pairs are given below for $1 \leq i < n$. n is the number of eigen functions used.

$$(K_{i1} - \omega^2 M_{i1})q_{1s} + (K_{i2} - \omega^2 M_{i2})q_{2s} + \cdots + (K_{in} - \omega^2 M_{in})q_{ns} + C_i Q_s - F_i = 0 \tag{4.69}$$

$$(K_{i1} - \omega^2 M_{i1})q_{1c} + (K_{i2} - \omega^2 M_{i2})q_{2c} + \cdots + (K_{in} - \omega^2 M_{in})q_{nc} + C_i Q_c = 0 \tag{4.70}$$

Equations (4.69) and (4.70) are for mechanical domain. If piezoelectric patch terminals are connected in parallel electrical equations can be derived as below;

Voltage on the terminals of both piezoelectric elements is;

$$V = \int_{\frac{h_{st}}{2}}^{\frac{h_{st}}{2}+h_p} E dz = \int_{\frac{h_{st}}{2}}^{\frac{h_{st}}{2}+h_p} h_{31} w'' z + \beta^s D dz = \frac{h_{31} J_{2p} w''}{2b_p} + \beta^s D h_p \tag{4.71}$$

(4.71) is independent of the x coordinate, and hence below equation can be written;

$$\int_{L_1}^{L_1+L_p} \frac{V}{\left(\left(L_1 + L_p\right) - L_1\right)} dx = \int_0^L \frac{V}{\left(\left(L_1 + L_p\right) - L_1\right)} \bar{X} dx \tag{4.72}$$

Evaluating (4.72) for (4.71) yields;

$$V = \frac{h_{31} J_{2p} w'}{2 b_p L_p} \Big|_0^L + \beta^s D h_p \tag{4.73}$$

By substituting (4.49) into (4.73) and considering Figure 4-3 for shunt circuit, the equation below can be written;

$$\begin{aligned} V &= \frac{h_{31} J_{2p}}{2 b_p L_p} \sum_n \left(\phi_i'(L_1 + L_p) - \phi_i'(L_1) \right) q_i + \frac{\beta^s Q h_p}{2 b_p L_p} \\ &= -\left(L_{ind} \ddot{Q} + R \dot{Q} + a Q^3 + b Q \right) \end{aligned} \tag{4.74}$$

For the case of piezoelectric terminals connected in series thickness in the electrical equations can be considered as doubled;

$$\begin{aligned} V &= 2 \int_{\frac{h_{st}}{2}}^{\frac{h_{st}}{2} + h_p} E dz \\ &= \frac{h_{31} J_{2p}}{b_p L_p} \sum_n \left(\phi_i'(L_1 + L_p) - \phi_i'(L_1) \right) q_i + \frac{2 \beta^s Q h_p}{b_p L_p} \\ &= -\left(L_{ind} \ddot{Q} + R \dot{Q} + a Q^3 + b Q \right) \end{aligned} \tag{4.75}$$

Using (4.74) for parallel electrical connection in cantilever system and substituting (4.67) yields;

$$\begin{aligned} & -L_{ind} \omega^2 (Q_s \sin(\omega t) + Q_c \cos(\omega t)) \\ & + R\omega (Q_s \sin(\omega t) - Q_c \cos(\omega t)) \\ & + b (Q_s \sin(\omega t) + Q_c \cos(\omega t)) \\ & + a (Q_s \sin(\omega t) + Q_c \cos(\omega t))^3 \\ & + \frac{h_{31} J_{2p}}{2 b_p L_p} \sum_n \left(\phi_i'(L_1 + L_p) - \phi_i'(L_1) \right) (q_{is} \sin(\omega t) \\ & + q_{ic} \cos(\omega t)) = 0 \end{aligned} \tag{4.76}$$

Considering only first harmonics and parsing the equations regarding sine and cosine terms gives;

$$bQ_s - R\omega Q_c - L_{ind}\omega^2 Q_s + \frac{3}{4}a(Q_s^2 + Q_c^2)Q_s + \frac{h_{31}J_{2p}}{2b_pL_p}\sum_n \left(\phi_i'(L_1 + L_p) - \phi_i'(L_1)\right) q_{is} + \frac{\beta^s h_p}{2h_pL_p} Q_s = 0 \tag{4.77}$$

$$bQ_c + R\omega Q_s - L_{ind}\omega^2 Q_c + \frac{3}{4}a(Q_s^2 + Q_c^2)Q_c + \frac{h_{31}J_{2p}}{2b_pL_p}\sum_n \left(\phi_i'(L_1 + L_p) - \phi_i'(L_1)\right) q_{ic} + \frac{\beta^s h_p}{2h_pL_p} Q_c = 0 \tag{4.78}$$

Equations derived up to now are in agreement with [66] and [45]

Equations giving the response of the system derived above do not consider damping. This results in infinite amplitude at resonance. Therefore, introducing proportional structural damping into the system can be useful in preventing the response from going to infinity. Calculation of elements of structural damping is given below.

$$H_{i,j} = \gamma_p c_{31}^D J_{3p} \int_0^L \left(\phi_i^{(4)}\bar{X} + 2\phi_i{}^{(3)}\bar{X}' + \phi_i{}''\bar{X}''\right)\phi_j dx + \gamma_{st}Y_{st}J_{3st}\int_0^L \phi_i^{(4)}\phi_j dx \tag{4.79}$$

Including structural damping (4.51) can be modified to give;

$$[M]\ddot{q} + [K]q + [H]iq + \{C\}Q = F \tag{4.80}$$

Equation sets (4.69) and (4.70) also can be modified as;

$$(K_{i1} - \omega^2 M_{i1})q_{1s} + H_{i1}q_{1c} + (K_{i2} - \omega^2 M_{i2})q_{2s} + H_{i2}q_{2c} + \cdots + (K_{in} - \omega^2 M_{in})q_{ns} + H_{in}q_{nc} + C_i Q_s - F_i = 0 \tag{4.81}$$

$$(K_{i1} - \omega^2 M_{i1})q_{1c} - H_{i1}q_{1s} + (K_{i2} - \omega^2 M_{i2})q_{2c} - H_{i2}q_{2s} + \cdots + (K_{in} - \omega^2 M_{in})q_{nc} - H_{in}q_{ns} + C_i Q_c = 0 \tag{4.82}$$

4.3 Deriving Equations for Response of Bimorph Composite Piezoelectric Integrated Cantilever Beam in 3-3 Mode with Linear Piezoelectric Material Assumption

In the previous heading, the cantilever beam system was considered to be polarized vertically to operate 3-1 mode. Even though 3-3 mode piezoelectric patch with two electrodes attached to cantilever beam structure is not practical, it can be analyzed theoretically. Nevertheless, 3-3 mode patches are commercially available with interdigitated electrodes. Piezoelectric patches with interdigitated electrodes will not be studied in this section but the next one.

In Figure 4-5, piezoelectric patches poled in different directions are depicted. In the z-direction, poled piezoelectric patch voltage on electrodes is independent of the x coordinate since electrodes are in contact with piezoelectric patch along the x direction. For the case of x direction poled piezoelectric patch voltage difference between electrodes is a function of x since in vertical displacement w at each x coordinate is a function of the coordinate. Moreover, the strain also varies along the z-direction at each x coordinate for the x direction poled piezoelectric material. By looking at Figure 4-6, it can be observed that even if strain changes along the z direction, it changes linearly, and strain can be taken into account as nominal strain when considering electrical displacement. The main idea behind the assumption is that excessive strain over the nominal strain generates electrical displacement, which compensates for deficient electrical displacement due to less strain.

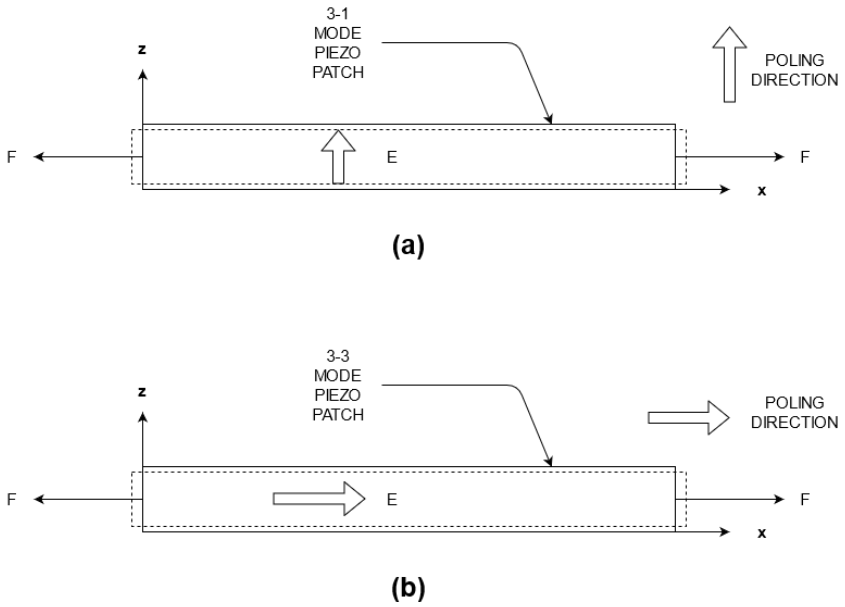

Figure 4-5 Piezoelectric Patch Poled in the z-direction (a) and in the x-direction (b)

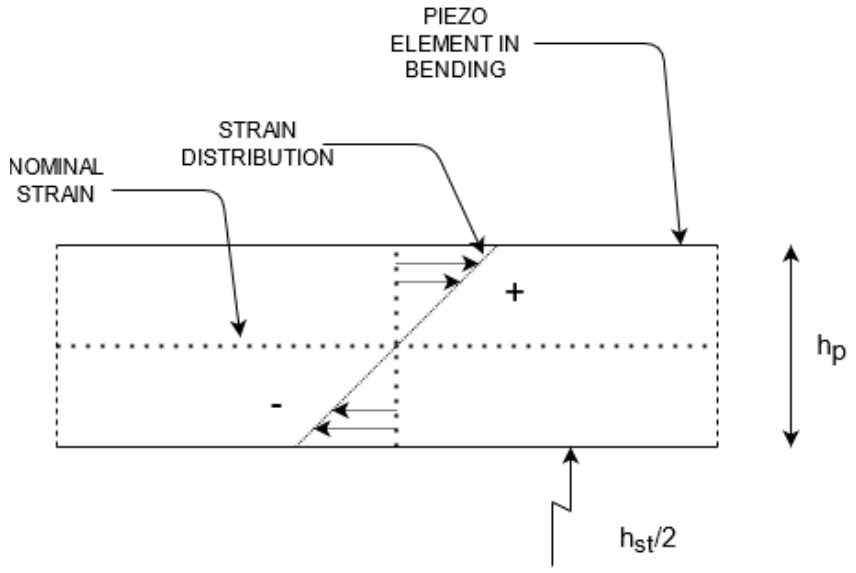

Figure 4-6 Piezoelectric Element on Bimorph Cantilever Beam. $h_{st}/2$ is Distance from Neutral Axis and h_p is Height of the Piezoelectric Patch

Under this assumption, (4.71) can be modified for 3-3 mode to give the equation below;

$$V = \int_0^L E dx = \int_0^L (h_{33} w'' z + \beta^s D)\bar{X} dx$$
$$= h_{33} z_{eq} (w'\bar{X}) \Big|_0^L + \beta^s D L_p \tag{4.83}$$

Where z_{eq} is the z location where average strain occurs and can be expressed as;

$$z_{eq} = \frac{h_{st} + h_p}{2}$$

For parallel connected piezoelectric patches (4.83) voltage difference between two electrodes can be expressed as below;

$$V = h_{33} z_{eq} (w'\bar{X}) \Big|_0^L + \frac{\beta^s Q L_p}{2 h_p b_p} \tag{4.84}$$

In addition to the voltage equation, mechanical equations also should be modified for 3-3 operating piezoelectric patch. In this case, C_i coefficient appearing in the mechanical domain is the only element related to electrical domain. For parallel connected terminals case, it can be written as;

$$C_i = h_{33} z_{eq} h_p 2 b_p D \int_0^L (\bar{X}'') \phi_i dx$$
$$= h_{33} z_{eq} Q \left(\phi_i'(L_1 + L_p) - \phi_i'(L_1) \right) \tag{4.85}$$

$K_{i,j}$ and $H_{i,j}$ are modified by replacing c_{31}^D with c_{33}^D for 3-3 mode case. After the modifications (4.80) and its expanded versions (4.81) and (4.82) can be used for calculations.

4.4 Deriving Equations for Response of Bimorph Composite Piezoelectric Integrated Cantilever Beam in 3-3 Mode with Interdigitated Electrodes Including Softening Effect

As mentioned in the previous section, 3-3 mode operating patches shown in Figure 4-5 (b) are available with interdigitated electrodes. In the literature, it is possible to find their modelling [67][68][69]. Moreover, 3-3 mode operating piezoelectric patches are found to have better performance in energy harvesting applications when compared to 3-1 mode operating piezoelectric patches [70][71][72][73][74].

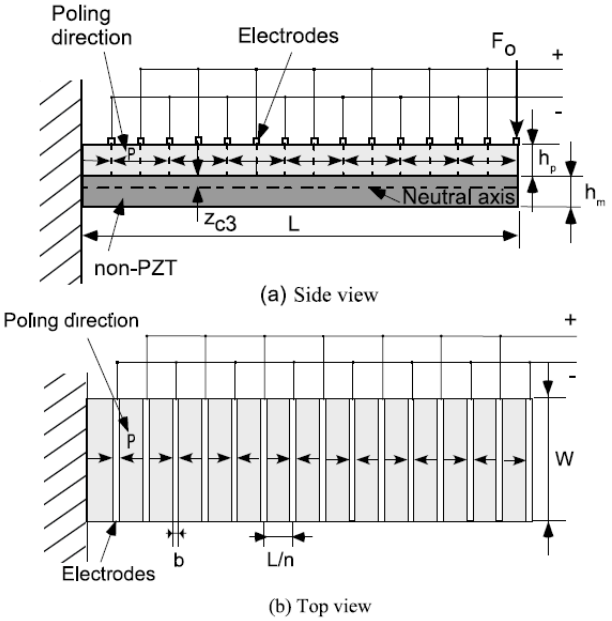

Figure 4-7 Piezoelectric Patch with Interdigitated Electrodes Integrated to Unimorph Cantilever Beam [73]

As can be seen in Figure 4-7, interdigitated electrodes are comb-like structures dividing the piezoelectric element into several pieces. Each piece is serially connected with opposite polarity, which is determined by the polarity of the electrodes themselves. Oppositely, in the electrical domain, each positive or negative electrode is connected to a single common node which is the case for parallel connection. In other words, combination of serial connection in mechanical domain

and parallel connection in electrical domain results in 3-3 mode operating piezoelectric patch mentioned in 4.3 with increased capacitance. Moreover, it can be intuitively sensed that the interdigitated electrode structure may cause a loss of electromechanical conversion efficiency due to unpolarized regions in the piezoelectric elements.

3-3 mode operating piezoelectric patches are commercially available as macrofiber composites (MFC) produced by Smart-Material company [75]. MFC's are made of piezoelectric fibers with dimensions of 0.35mm in width x 0.18mm in height, embedded in an epoxy layer. On the top and bottom of the piezoelectric structure, embedded copper electrodes are placed. In [76], MFC structure and dimensions for a specific product type are given.

Because of the interdigitated electrodes, capacitance calculation of the MFCs is not straightforward. Although equivalent electrode area is not given in the datasheets, it can be approximated as follows.

Assuming interdigitated electrodes divide piezoelectric patch into N many cells, each cell's capacitance can be approximated by considering (2.2) as follows;

$$C_{cell} = \frac{\varepsilon^{S}{}_{33} b_p h_p}{\left(L_p/N\right)} \tag{4.86}$$

The total capacitance of MFC is parallel connected N many cell capacitors as shown in Figure 4-8, and it can be expressed as;

$$C_{MFC} = NC_{cell} = \frac{\varepsilon^{S}{}_{33} b_p h_p}{L_p} N^2 \tag{4.87}$$

Parallel connection of cell capacitors can be interpreted as area increase of capacitor electrodes. The total area can be utilized to calculate electrical charge from electrical displacement.

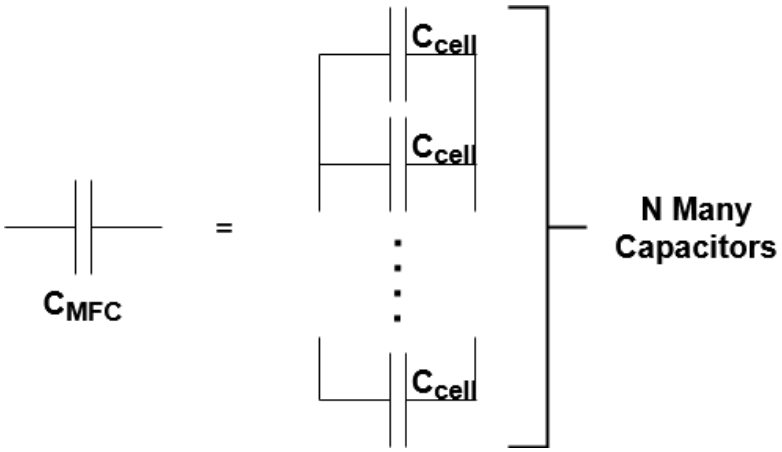

Figure 4-8 Cell Approximation of MFC

Value of C_{MFC} is measured to be 3.4nF for two parallel connected MFC4010 P1; thus, total electrode area can be approximated as $N(b_p h_p)$. Piezoelectric fiber width is given as 0.35mm on the invoice of its purchase order. Twenty-five fibers can be counted on MFC4010 P1. As a result, the width of the active area of the piezoelectric patch can be determined as 8.75mm, which is 87.5% of the active width b_p. The remaining with is filled with epoxy, and its effect on stiffness is neglected since its elastic modulus and thickness are much less than piezoelectric material or aluminum. Therefore, N can be calculated as;

$$N = \sqrt{\frac{0.875\varepsilon^S{}_{33} b_p h_p}{L_p C_{MFC}}} \tag{4.88}$$

Using N for total electrode area, electrical charge can be obtained using electrical displacement as;

$$Q = D(N b_p h_p) \tag{4.89}$$

(4.80) can be rewritten for MFC as;

$$V = h_{33} z_{eq} (w' \bar{X}) \Big|_0^L + \frac{\beta^s Q L_p}{2 h_p b_p N^2} \tag{4.90}$$

Also, (4.85) can be rewritten as;

$$C_i = \frac{h_{33} z_{eq} Q}{N} \left(\phi_i'(L_1 + L_p) - \phi_i'(L_1) \right) \tag{4.91}$$

Replacing the terms given in this section with the ones given in 4.3 can be used to calculate frequency response for linear piezoelectric material. Since calculation results obtained for the MFC case will be compared with tests instead of FEM software, softening effects should be included in the model. To do this, c_{33}^D should be replaced by $\left(c_{33}^D - k_q|S|\right)$ where k_q is quadratic softening constant referring to [59] as mentioned in Section 2.3. Hence, the strain energy of piezoelectric material U_p will include additional softening term as follows;

$$U_{NL} = \iiint \int k_q |S| S dS \bar{X} \, dxdydz = \iiint \frac{k_q |S| S^2 \bar{X}}{3} dxdydz \tag{4.92}$$

Replacing strain value S with zw'' and noting that the equation can be rewritten as;

$$\begin{aligned} U_{NL} &= \int_0^L \int_0^{b_p} \int_{\frac{h_{st}}{2}+h_{kapton}}^{h_p+\frac{h_{st}}{2}+h_{kapton}} \frac{k_q |zw''| (zw'')^2}{3} \bar{X} dzdydx \\ &+ \int_0^L \int_0^{b_p} \int_{-\left(h_p+\frac{h_{st}}{2}+h_{kapton}\right)}^{-\frac{h_{st}}{2}-h_{kapton}} \frac{k_q |zw''| (zw'')^2}{3} \bar{X} dzdydx \end{aligned} \tag{4.93}$$

Where h_{kapton} is the kapton layer thickness of one side embodying piezoelectric fibers. It is also important to note that moment due to kapton layer is negligible since its elastic modulus and thickness are much less than ceramic or aluminum. Evaluating the above integral for the y axis results in double integral of x and z axes multiplied by b_p. Evaluating remaining integral on z yields;

$$U_{NL} = \frac{1}{6} b_p k_q \left(\left(\frac{h_{st}}{2} + h_p + h_{kapton} \right)^4 - \left(\frac{h_{st}}{2} + h_{kapton} \right)^4 \right) \int_0^L (w'')^3 \bar{X} dx = \overline{J_{4p}} \int_0^L (w'')^3 \bar{X} dx \tag{4.94}$$

Taking variance of U_{NL} gives;

$$\int_{t_1}^{t_2} \delta U_{NL} dt = \int_{t_1}^{t_2} 3\overline{J_{4p}} k_q \int_0^L (w'')^2 \bar{X} \delta w'' dx\, dt \tag{4.95}$$

Applying IBP and substituting J_{4p} instead of $3\overline{J_{4p}}$ gives;

$$\int_{t_1}^{t_2} \delta U_{NL} dt = J_{4p} k_q \int_{t_1}^{t_2} \left((w'')^2 \bar{X} \delta w' \Big|_0^L - \int_0^L ((w'')^2 \bar{X})' \delta w' dx \right) dt \tag{4.96}$$

The first term in (4.96) is zero since $\bar{X}$ is zero at the boundaries. Substituting zero and applying one more IBP gives;

$$\int_{t_1}^{t_2} \delta U_{NL} dt = J_{4p} k_q \int_{t_1}^{t_2} \left((w'')^2 \bar{X} \delta w \Big|_0^L - \int_0^L ((w'')^2 \bar{X})'' \delta w dx \right) dt \tag{4.97}$$

Again since $\bar{X}$ is zero at the boundaries, the first term is zero, and the integral becomes;

$$\int_{t_1}^{t_2} \delta U_{NL} dt = J_{4p} k_q \int_{t_1}^{t_2} \int_0^L ((w'')^2 \bar{X})'' \delta w dx\, dt \tag{4.98}$$

Therefore, nonlinear mechanical term in the equation of motion, which is given in (4.48), will be as follows;

$$J_{4p}k_q((w'')^2\bar{X})'' \tag{4.99}$$

Applying transformation done in (4.50) to the nonlinear mechanical term gives $K_{nl_{i,j}}$ terms as;

$$K_{nl_{i,j}} = J_{4p}k_q\int_0^L \phi_i''^2\bar{X}\phi_j''dx \tag{4.100}$$

As a result, the matrix equation set becomes;

$$[M]\ddot{q} + [K]q + [H]iq + \{C\}Q - [K_{nl}]q^2 = F \tag{4.101}$$

Matrix terms in the equation above calculated as described in 4.3 but for elements of $[K]$ polymer layer thickness should be accounted for in J_{3p} as below;

$$J_{3p} = \frac{\left(\left(\frac{h_{st}}{2} + h_p + h_{kapton}\right)^3 - \left(\frac{h_{st}}{2} + h_{kapton}\right)^3\right)}{3} \tag{4.102}$$

Assuming steady state response and considering only first order contribution, the equation can be rewritten as;

$$\begin{aligned}
&\left(\begin{bmatrix} K_{11} & K_{12} & \cdots \\ \vdots & \ddots & \vdots \\ K_{n1} & \cdots & K_{nn} \end{bmatrix}\right.\\
&\left.-\omega^2\begin{bmatrix} M_{11} & M_{12} & \cdots \\ \vdots & \ddots & \vdots \\ M_{n1} & \cdots & M_{nn} \end{bmatrix}\right)\begin{Bmatrix} q_{1s}\sin(\omega t) + q_{1c}\cos(\omega t) \\ \vdots \\ q_{ns}\sin(\omega t) + q_{nc}\cos(\omega t) \end{Bmatrix}\\
&-\begin{bmatrix} K_{nl_{11}} & K_{nl_{12}} & \cdots \\ \vdots & \ddots & \vdots \\ K_{nl_{n1}} & \cdots & K_{nl_{nn}} \end{bmatrix}\begin{Bmatrix} (q_{1s}\sin(\omega t) + q_{1c}\cos(\omega t))\sqrt{q_{1s}^2 + q_{1c}^2} \\ \vdots \\ (q_{ns}\sin(\omega t) + q_{nc}\cos(\omega t))\sqrt{q_{1s}^2 + q_{1c}^2} \end{Bmatrix}\\
&+\begin{Bmatrix} C_1 \\ \vdots \\ C_n \end{Bmatrix}Q_s\sin(\omega t) + Q_c\cos(\omega t) = \begin{Bmatrix} F_1 \\ \vdots \\ F_n \end{Bmatrix}\sin(\omega t)
\end{aligned} \tag{4.103}$$

Describing function for the nonlinearity in the equation is given in [77] as;

$$\frac{8}{3\pi}\sqrt{q_{1s}^2+q_{1c}^2} \tag{4.104}$$

Therefore, mechanical equation set can be written by inserting nonlinear terms into (4.69) (4.70) as below;

$$\begin{aligned}&\left(K_{i1}-\omega^2M_{i1}-\frac{8}{3\pi}K_{nl_{i1}}\sqrt{q_{1s}^2+q_{1c}^2}\right)q_{1s}+H_{i1}q_{1c}\\&\quad+\left(K_{i2}-\omega^2M_{i2}-\frac{8}{3\pi}K_{nl_{i2}}\sqrt{q_{2s}^2+q_{2c}^2}\right)q_{2s}\\&\quad+H_{i2}q_{2c}+\cdots\\&\quad+\left(K_{in}-\omega^2M_{in}-\frac{8}{3\pi}K_{nl_{in}}\sqrt{q_{ns}^2+q_{nc}^2}\right)q_{ns}\\&\quad+H_{in}q_{nc}+C_iQ_s-F_i=0\end{aligned} \tag{4.105}$$

$$\begin{aligned}&\left(K_{i1}-\omega^2M_{i1}-\frac{8}{3\pi}K_{nl_{i1}}\sqrt{q_{1s}^2+q_{1c}^2}\right)q_{1c}-H_{i1}q_{1s}\\&\quad+\left(K_{i2}-\omega^2M_{i2}-\frac{8}{3\pi}K_{nl_{i2}}\sqrt{q_{2s}^2+q_{2c}^2}\right)q_{2c}\\&\quad-H_{i2}q_{2s}+\cdots\\&\quad+\left(K_{in}-\omega^2M_{in}-\frac{8}{3\pi}K_{nl_{in}}\sqrt{q_{ns}^2+q_{nc}^2}\right)q_{nc}\\&\quad-H_{in}q_{ns}+C_iQ_c=0\end{aligned} \tag{4.106}$$

The mechanical nonlinear equation set derived above can be used with the electrical equations described in Section 4.3

4.5 Matlab and Comsol Simulation Results

Using equations derived in sections from 4.2 to 4.4 response of a bimorph cantilever beam can be obtained. In this section, results obtained from analytically derived equations and FEM analyses are presented. At first, a plain cantilever beam is considered, and frequency responses are given. After, frequency response of a

cantilever beam with discontinuity in which piezoelectric material has no electromechanical coupling taken into account. This is followed by results of responses of bimorph cantilevers with 3-1 and 3-3 operation modes for open and short circuit conditions. Lastly, the calculated frequency responses of the system with nonlinear circuit and simulated time response of the system are given for the aforementioned operation modes.

4.5.1 Matlab and Comsol Simulation Results for Plain Cantilever Beam

By employing the equations derived in sections from 4.2 to 4.4 with zero piezoelectric material thickness, the response of a plain cantilever for the first mode of the beam can be obtained by using only one mode contribution. The parameters used are given in Table 4.1. Eigen function for undamped fixed-free transverse vibration is which is given below, is utilized.

$$\phi_i = \frac{\left(\cosh\left(\frac{\lambda_i}{Lx}\right) - \cos\left(\frac{\lambda_i}{Lx}\right) - \sigma_i\left(\sinh\left(\frac{\lambda_i}{Lx}\right) - \sin\left(\frac{\lambda_i}{Lx}\right)\right)\right)}{\sqrt{m_{st}L}}$$

Where,

$$\sigma_i = \frac{(-\sin(\lambda_i) + \sinh(\lambda_i))}{\cos(\lambda_i) + \cosh(\lambda_i)}$$

and,

$$\omega_i = \lambda_i^2 \sqrt{\frac{Y_{st}J_{3st}}{mL^4}}$$

Table 4.1 Parameters Used for Frequency Response of Plain Cantilever Beam

Parameter	Value
Length (L) (mm)	118.8
Height (h_{st}) (mm)	1

Table 4.1 cont'd

Width (b_{st}) (mm)	30
Elastic modulus (Y_{st}) (GPa)	70
Mass per unit length (m_{st}) (kg/m)	0.081
Damping constant (γ_{st})	0

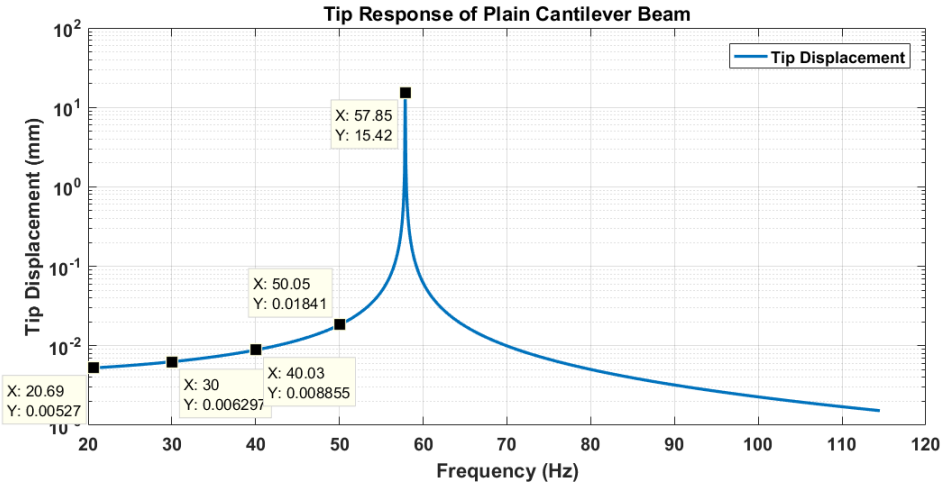

Figure 4-9 Matlab Result for Tip Response of Plain Cantilever Beam

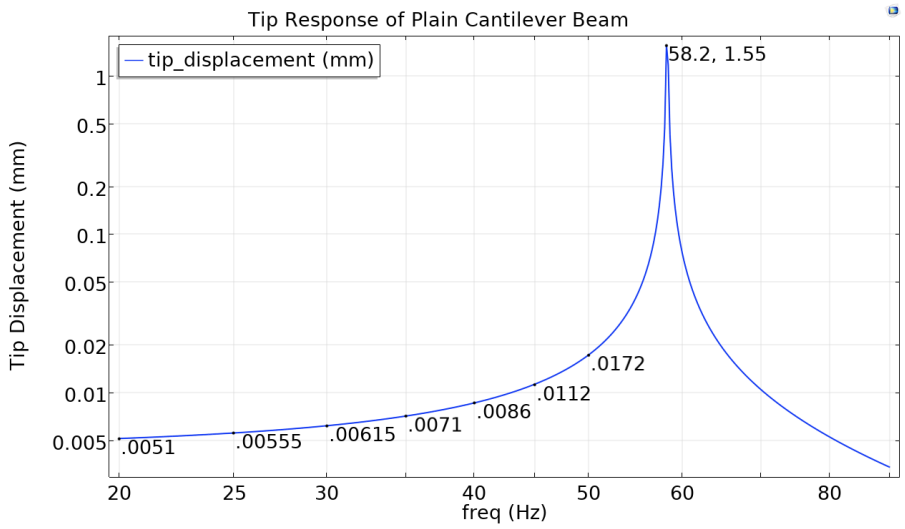

Figure 4-10 FEM Result for Tip Response of Plain Cantilever Beam

Resonant frequency results for both results were found to be not varying more than 1%, and amplitude values are close within 6% range.

4.5.2 Matlab and Comsol Simulation Results for Cantilever Beam with Plain Discontinuity

In order to observe the difference between FEM results and calculations for discontinuity and the effect of number of modes used, setting electromechanical coupling coefficient can be set to zero. For the calculations, eigen functions given in 4.5.1 are used. The parameters used are given in Table 4.2.

Table 4.2 Parameters Used for Frequency Response of Cantilever Beam with Plain Discontinuity

Parameter	**Value**
Length of the host structure (L) (mm)	118.8
Height of the host structure (h_{st}) (mm)	1
Width of the host structure (b_{st}) (mm)	30
Elastic modulus of the host structure (Y_{st}) (GPa)	70
Mass per unit length of the host structure (m_{st}) (kg/m)	0.081
Length of the piezoelectric material (L_p) (mm)	39.3
Piezoelectric material starting coordinate (L_1) (mm)	0.1
Height of the piezoelectric material (h_p) (mm)	0.24
Width of the piezoelectric material (b_p) (mm)	30
Elastic modulus of the piezoelectric material (Y_p) (GPa)	70
Mass per unit length of the host structure (m_{st}) (kg/m)	0.081
Damping constant (γ_{st})	$2\text{x}10^{-3}$
Damping constant (γ_p)	$2\text{x}10^{-3}$
Excitation amplitude (g)	0.1

In Figure 4-11, it can be noticed that the change in resonant frequency gets smaller as the number of eigen functions used in calculations increases. This is an indication of convergence which is mentioned in the expansion theorem. In addition to this, the comparison of calculation with ten eigen functions and FEM results shows less than 1% resonant frequency error. However, the difference in amplitude values gets higher and higher as frequency reaches to resonance value.

Damping effect on the structure is demonstrated in Figure 4-13 and Figure 4-14. By looking at the figures, it can be said that a small amount of structural trims the amplitude at the resonance frequency, and it does not change the frequency itself considerably.

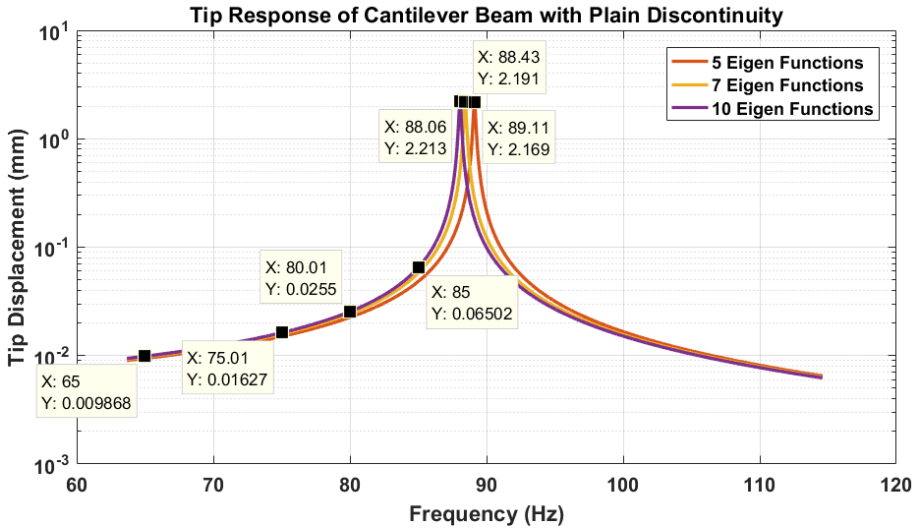

Figure 4-11 Matlab Response Tip Response of Cantilever Beam with Plain Discontinuity with Damping Constant of γ=2e-3

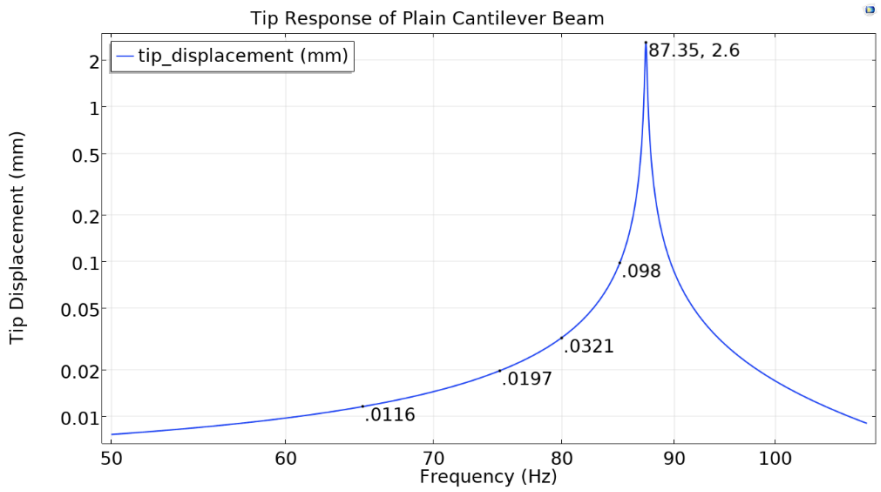

Figure 4-12 FEM Result for Tip Response of Cantilever Beam with Plain Discontinuity with Damping Constant of γ=2e-3

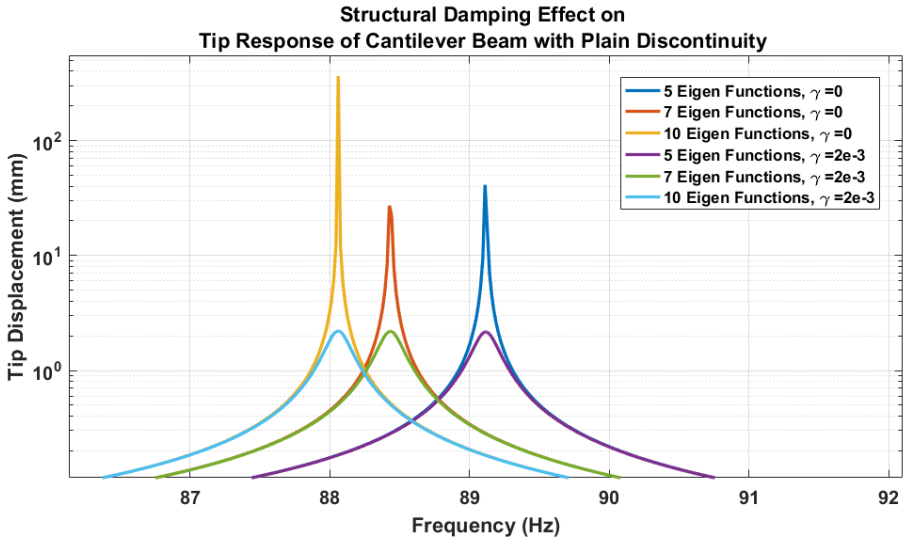

Figure 4-13 Damped and Undamped Response Comparison of Calculated Tip Response of Cantilever Beam with Plain Discontinuity

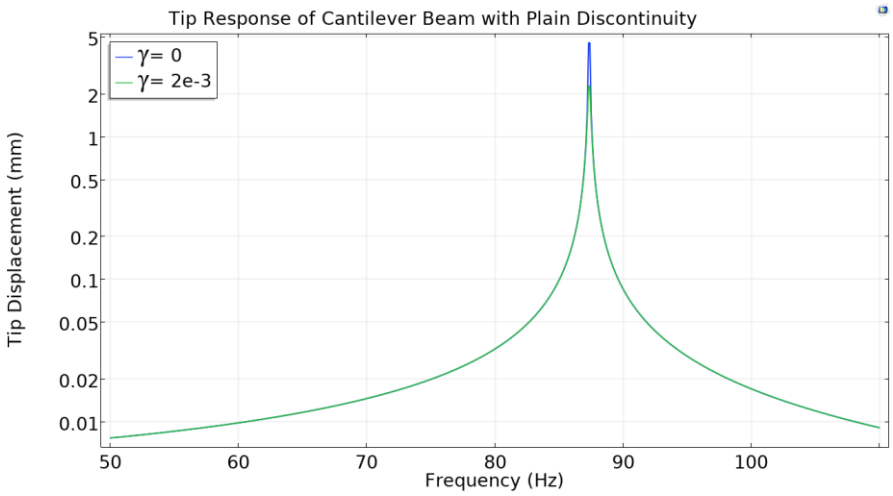

Figure 4-14 Damped and Undamped FEM Response Comparison of Tip Response of Cantilever Beam with Plain Discontinuity

4.5.3 Matlab and Comsol Simulation Results for Cantilever Beam with 3-1 Mode Piezoelectric Effect with Open and Short Circuit Conditions with Linear Piezoelectric Material Assumption

Taking piezoelectric effects into account results below can be obtained. Parameters used are given in Table 4.3, whose piezoelectric material parameters are taken from Comsol for PZT-5H material. By comparing Figure 4-15 and Figure 4-16, it can be observed that resonant frequencies of calculations and FEM analysis are close for piezoelectric material integrated cantilever beam for open and short circuit conditions. In the previous section, it was showed that increasing eigenfunctions used in calculations decrease the difference between FEM and calculation results. Relying on this, using more eigenfunctions in calculations decreases the error to a value of 1.7%.

Table 4.3 Parameters Used for Frequency Response of Cantilever Beam with Plain Discontinuity

Parameter	**Value**
Number of eigenfunctions used	7
Length of the host structure (L) (mm)	118.8
Height of the host structure (h_{st}) (mm)	1
Width of the host structure (b_{st}) (mm)	30
Elastic modulus of the host structure (Y_{st}) (GPa)	70
Mass per unit length of the host structure (m_{st}) (kg/m)	0.081
Length of the piezoelectric material (L_p) (mm)	39.3
Piezoelectric material starting coordinate (L_1) (mm)	0.1
Height of the piezoelectric material (h_p) (mm)	0.24
Width of the piezoelectric material (b_p) (mm)	30
Constant electric field mechanical compliance (${s^E}_{31}$) (1/Pa)	1.65×10^{-11}
Mass per unit length of the host structure (m_p) (kg/m)	0.03888
Damping constant (γ_{st})	2×10^{-3}
Damping constant (γ_p)	2×10^{-3}
Constant stress dielectric permittivity (${\varepsilon^T}_{33}$) (F/m)	3.01036×10^{-8}
Piezoelectric Strain Coefficient (d_{31}) (C/N)	2.74×10^{-10}

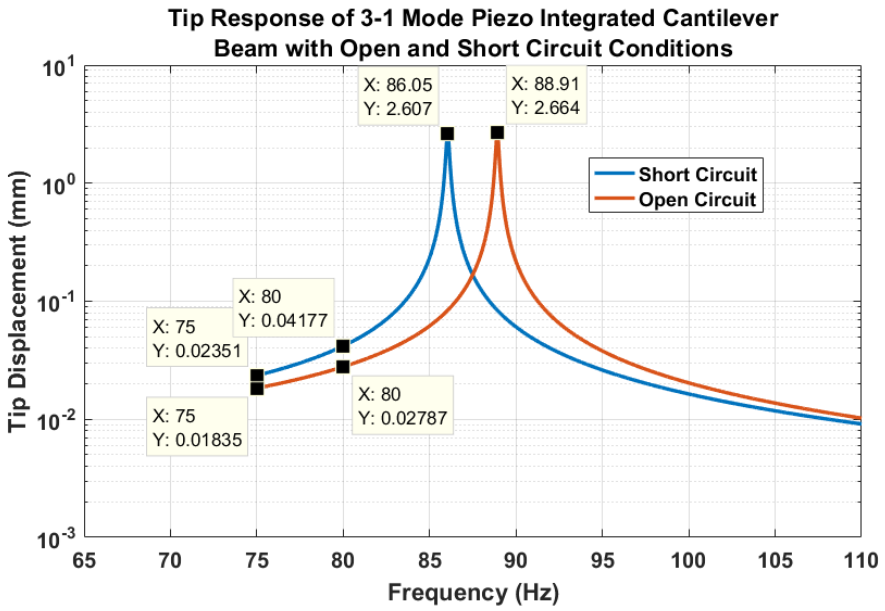

Figure 4-15 Matlab Result for Tip Response of 3-1 Mode Piezoelectric Material Integrated Cantilever Beam with Open and Short Circuit Conditions

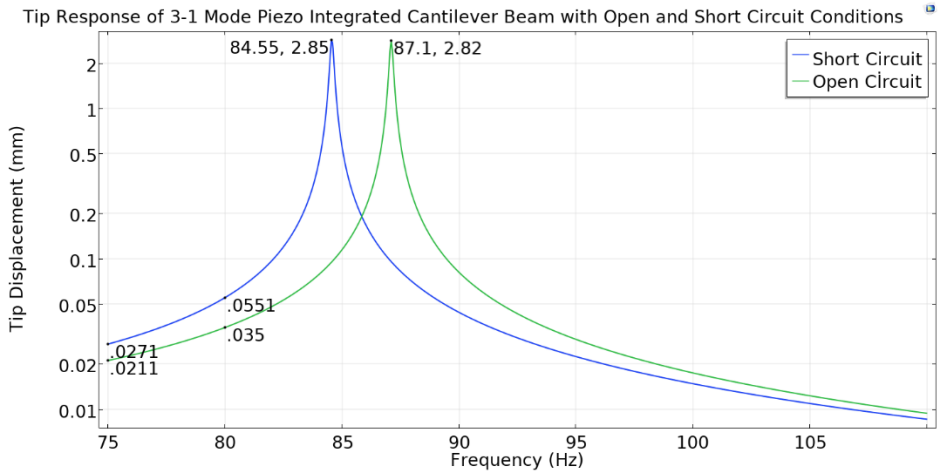

Figure 4-16 FEM Result for Tip Response of 3-1 Mode Piezoelectric Material Integrated Cantilever Beam with Open and Short Circuit Conditions

4.5.4 Matlab and Comsol Simulation Results for Cantilever Beam with 3-3 Mode Piezoelectric Effect with Open and Short Circuit Conditions Disregarding Softening Nonlinear Effect

Although it is difficult to find piezoelectric patches poled in lengthwise as depicted in Figure 4-5, they can be modelled and simulated. Calculation and FEM results are given below. Parameters used in this section different from Table 4.3 are listed in Table 4.5.

Table 4.4 Parameters Used for Frequency Response of Cantilever Beam with Plain Discontinuity

Parameter	Value
Constant electric field mechanical compliance ($s^E{}_{33}$) (1/Pa)	$2.07\text{x}10^{-11}$
Constant stress dielectric permittivity ($\varepsilon^T{}_{33}$) (F/m)	$3.01036\text{x}10^{-8}$
Piezoelectric Strain Coefficient (d_{33}) (C/N)	5.9310^{-10}

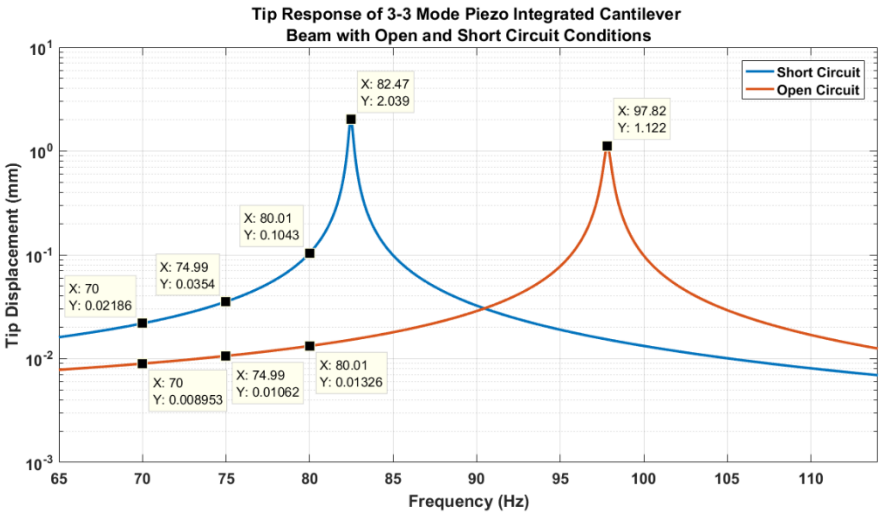

Figure 4-17 Matlab Results for Tip Response of 3-3 Mode Piezoelectric Material Integrated Cantilever Beam with Open and Short Circuit Conditions

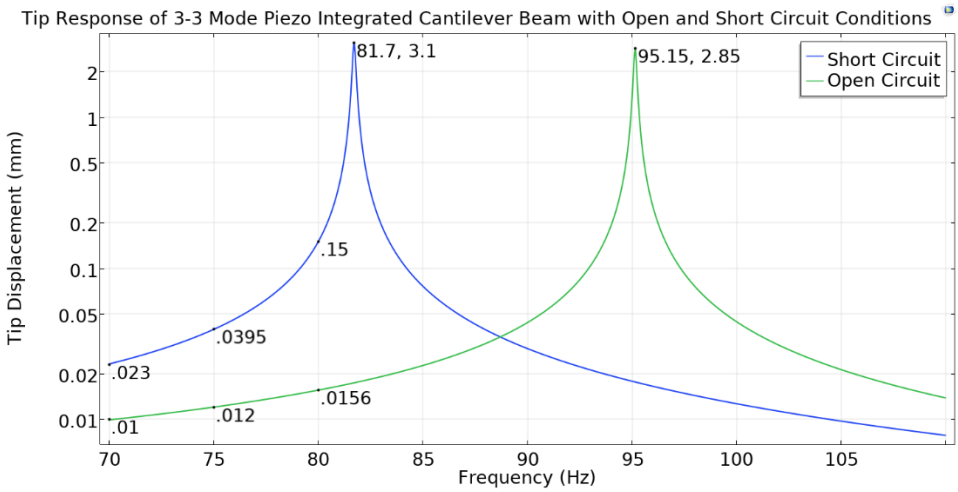

Figure 4-18 FEM Result for Tip Response of 3-3 Mode Piezoelectric Patch Integrated Cantilever Beam with Open and Short Circuit Conditions

Similar to the previous section, the resonant frequency difference between Figure 4-17 and Figure 4-18 is small, which is not more than 2.8%, and amplitude difference increase as resonant frequency is approached because of frequency shift.

4.5.5 Matlab and Comsol Simulation Results for Cantilever Beam with 3-1 Mode Piezoelectric Effect with Nonlinear Varactor Circuit Disregarding Softening Effect

In this section piezoelectric cantilever system having nonlinear shunt circuit is investigated using analytical modelling and FEM. GeneSic GB2X100MPS12-227 can be considered as the nonlinear capacitor, and as done in [2][8] and [5] Q-V relation of the product can be approximated as combination of linear and cubic capacitors. In order to demonstrate the nonlinearity, using fictitious piezoelectric material and diode, which are obtained by multiplying certain parameters of the components with constants, seems beneficial. Therefore, the piezoelectric parameter d_{31} of PZT5-H is considered to be doubled, and the linear portion of the nonlinear capacitor is disregarded.

The original Q-V curve of GeneSic GB2X100MPS12-227 is given in Figure 4-19. A cubic and linear curve can be fit for 22 parallel connected diodes using the data from the figure. Read data and fit curve are given in Figure 4-20. From the figure, it can be observed that curve fit contains small errors similar to curves obtained in [2][8] and [5].

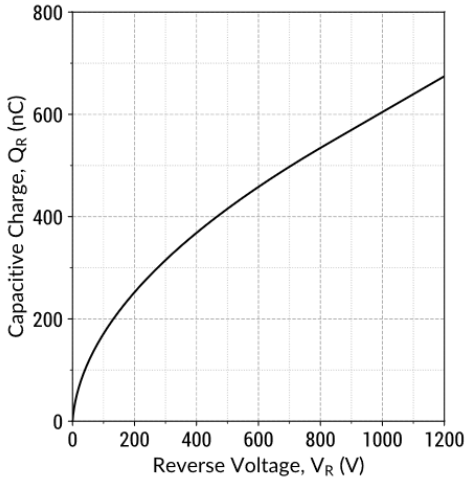

Figure 4-19 Q-V Curve of GeneSic GB2X100MPS12-227 [78]

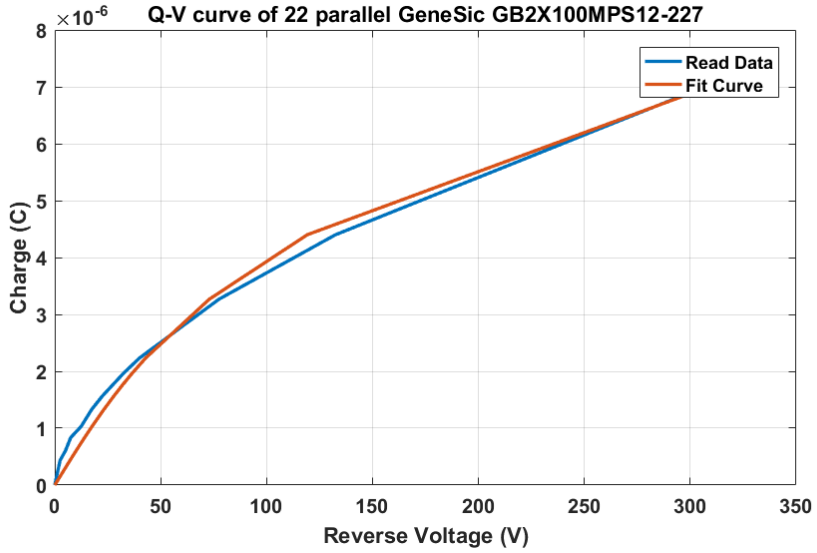

Figure 4-20 Read Data and Fit Curve for 22 Parallel Connected GeneSic GB2X100MPS12-227

By using cubic capacitance only, tip displacement of the cantilever beam can be simulated with Comsol and Matlab. Calculations of Matlab are straightforward, but Comsol simulations in time domain can be conducted by employing continuous sine sweep or employing discrete sine sweep.

Discrete sine sweep can be done by exciting cantilever beam at a certain frequency and amplitude. When steady state is reached, peak amplitude can be read from the results. In the case of continuous sine sweep, sine frequency incremented with time. Taking FFT of the tip displacement data can indicate the frequency where the jump occurs. For Comsol simulations, both methods are used; six constant frequency simulations are run to observe low frequency jump, and one continuous sine sweep is run to observe high frequency jump. Nevertheless, parameters used in Matlab and Comsol simulations are given in Table 4.5.

In Figure 4-21, Matlab results for open, short, and nonlinear circuit results are depicted with six constant frequency excitation response amplitudes. It can be seen from the figure that the pattern drawn by response amplitude of Comsol simulations is similar to Matlab simulations. Moreover, frequencies where jumps occur are similar; namely, the frequency difference is about 2.6%.

Table 4.5 Simulation Parameters Used for Cantilever Beam with 3-1 Mode Piezoelectric Effect with Nonlinear Varactor Circuit Disregarding Softening Effect

Parameter	**Value**
Number of eigenfunctions used	7
Length of the host structure (L) (mm)	120
Height of the host structure (h_{st}) (mm)	1
Width of the host structure (b_{st}) (mm)	30
Elastic modulus of the host structure (Y_{st}) (GPa)	70
Mass per unit length of the host structure (m_{st}) (kg/m)	0.081
Length of the piezoelectric material (L_p) (mm)	39.3
Piezoelectric material starting coordinate (L_1) (mm)	0.1

Table 4.5 (cont'd)

Height of the piezoelectric material (h_p) (mm)	0.24
Width of the piezoelectric material (b_p) (mm)	30
Constant electric field mechanical compliance ($s^E{}_{33}$) (1/Pa)	1.65×10^{-11}
Mass per unit length of the host structure (m_p) (kg/m)	0.03888
Damping constant (γ_{st})	2×10^{-3}
Damping constant (γ_p)	2×10^{-3}
Constant stress dielectric permittivity ($\varepsilon^T{}_{33}$) (F/m)	3.01036×10^{-8}
Piezoelectric Strain Coefficient (d_{31}) (C/N)	$2 \times (2.74 \times 10^{-10})$
Cubic Coefficient of Nonlinear Capacitance (a)	5.4774×10^{17}
Linear Coefficient of Nonlinear Capacitance (b)	0

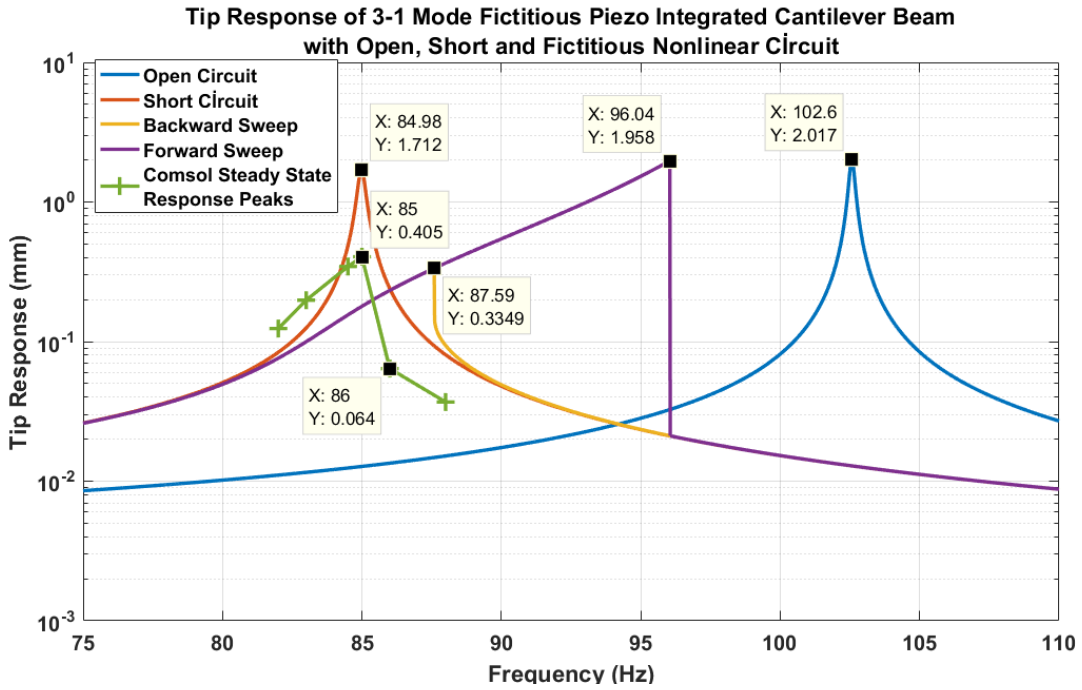

Figure 4-21 Matlab Results for Tip Response of 3-1 Mode Fictitious Piezoelectric Patch Integrated Cantilever Beam and Comsol Steady State Simulation Results for Low Frequency Jump

Time domain continuous forward sweep is given in Figure 4-22. From the figure, it is hard to interpret if there is any jump or not, but taking FFT of the data, which is given in Figure 4-23, tells that there is a jump at 94 Hz. Further, the curve before the jump resembles the Matlab simulation curve. Thus, it can be said that the jump frequency error for forward sweep between time domain simulations and the Matlab simulations is about 2.2%. Moreover, nonlinear effect on the mechanical response due to the third harmonic of the fictitious cubic capacitor can be observed in Figure 4-23.

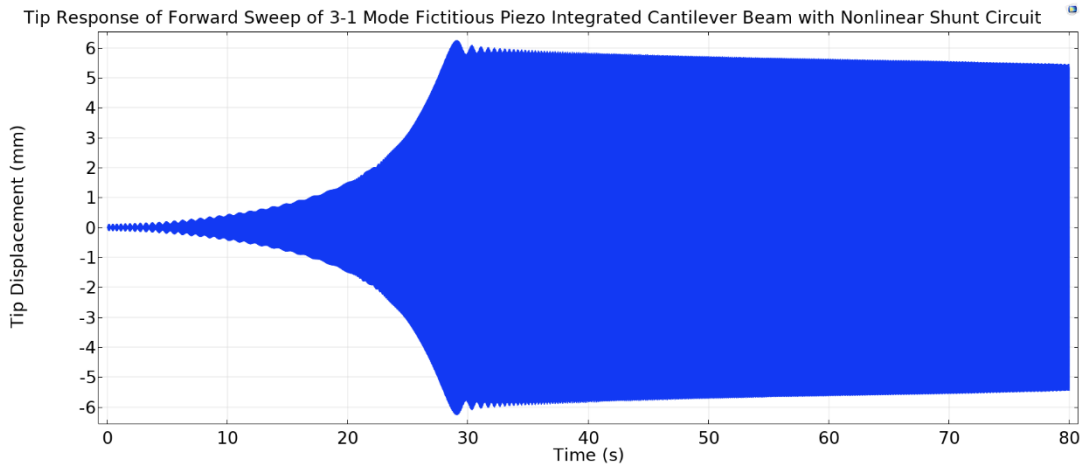

Figure 4-22 Time Domain Simulation of Forward Sweep of 3-1 Mode Fictitious Piezoelectric Patch Integrated Cantilever Beam with Nonlinear Shunt Circuit

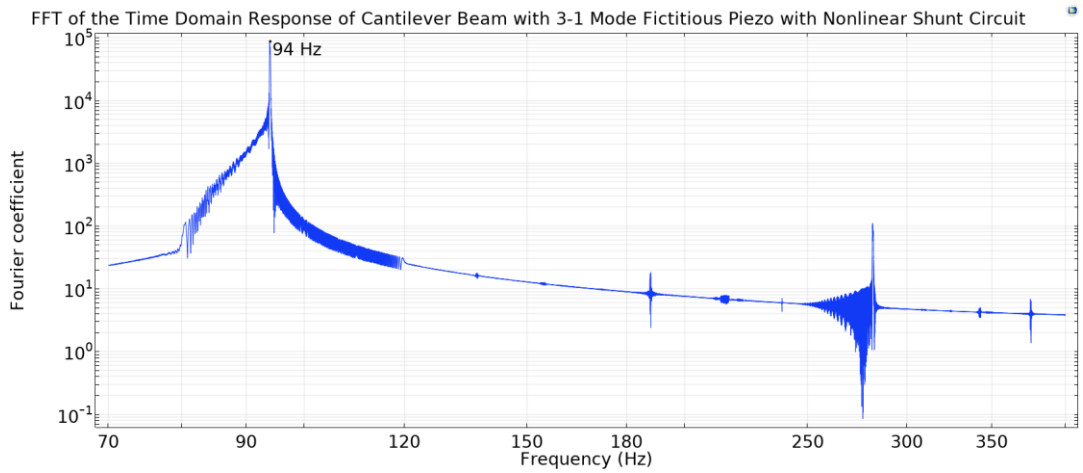

Figure 4-23 FFT of the Time Domain Response of Cantilever Beam with 3-1 Mode Fictitious Piezoelectric Patch with Nonlinear Shunt Circuit

4.5.6 Matlab Simulations for Cantilever Beam with Piezoelectric Patch Having Interdigitated Electrodes with Open and Short Circuits Shunted and Commercially Available Nonlinear Capacitor Shunted Including Softening Effect

In this section mathematical model of piezoelectric cantilever bimorph with interdigitated electrodes is simulated. In the simulations, GB2X100MPS12-227 diode shown in Figure 5-5 is modelled as nonlinear capacitor, and MFC4010 P1 shown in Figure 5-1 is modelled as piezoelectric patch with interdigitated electrodes. Since in the previous sections, it is shown that mathematical model results are in agreement with the FEM results, results in this section will be compared with tests instead of FEM software.

In the modelling of GB2X100MPS12-227, a curve fitting procedure is done for different voltage ranges considering operating voltage ranges for different amplitudes. For the case of MFC4010 P1, PZT-5A piezoceramic fibers are used. Properties of the fibers are taken from [79]. The parameters used for simulations are given in Table 4.6.

Table 4.6 Simulation Parameters Used for Cantilever Beam with Interdigitated Electrodes Piezoelectric Patch Including Softening Effect

Parameter	Value
Number of eigenfunctions used	7
Length of the host structure (L) (mm)	118
Height of the host structure (h_{st}) (mm)	1
Width of the host structure (b_{st}) (mm)	10
Elastic modulus of the host structure (Y_{st}) (GPa)	69
Mass per unit length of the host structure (m_{st}) (kg/m)	0.081
Length of the piezoelectric material (L_p) (mm)	40
Piezoelectric material starting coordinate (L_1) (mm)	0.4

Table 4.6 (cont'd)

Width of the piezoelectric material (b_p) (mm)	8.75
Height of the piezoelectric material (h_p) (mm)	0.18
Constant charge elastic stiffness mechanical compliance ($c^D{}_{33}$) (1/Pa)	$14.7\text{x}10^{10}$
Mass per unit length of the host structure (m_p) (kg/m)	0.02441
Damping constant (γ_{st}) at 0.05g, 0.2g, 1g and 4g respectively	$1.5\text{x}10^{-2}$, $2\text{x}10^{-2}$, $3\text{x}10^{-2}$, $5.5\text{x}10^{-2}$
Damping constant (γ_p)	$5\text{x}10^{-3}$
Constant strain dielectric impermittivity ($\beta^S{}_{33}$) (m/F)	$15.751\text{x}10^{7}$
Piezoelectric Constant (h_{33}) (C/N)	$21.5\text{x}10^{8}$
C_{MFC} (F)	$1.73\text{x}10^{-9}$
Cubic Coefficient of Nonlinear Capacitance (a) at 0.05g, 0.2g, 1g and 4g respectively	$1.657\text{x}10^{22}$, $1.657\text{x}10^{22}$, $1.063\text{x}10^{22}$, $7.413\text{x}10^{21}$
Linear Coefficient of Nonlinear Capacitance (b) at 0.05g, 0.2g, 1g and 4g respectively	2.192e8, 2.192e8, 2.726e8, 3.261e8
Kapton layer thickness (h_{kapton}) (mm)	$60\text{x}10^{-3}$
Distance of displacement measuring point from the base (mm)	105

Unlike previous ones, results of different shunt circuits are given separately in this section; since softening effect is included in the model, the results interfere with each other when plotted together.

Results for open circuit condition are given in Figure 4-24. By looking at the figure, it can be perceived that softening effect is not so potent between 0.05g and 0.2g amplitudes since frequency response curve seems linear and frequency shift is not much. However, increasing amplitude introduces significant softening nonlinearity.

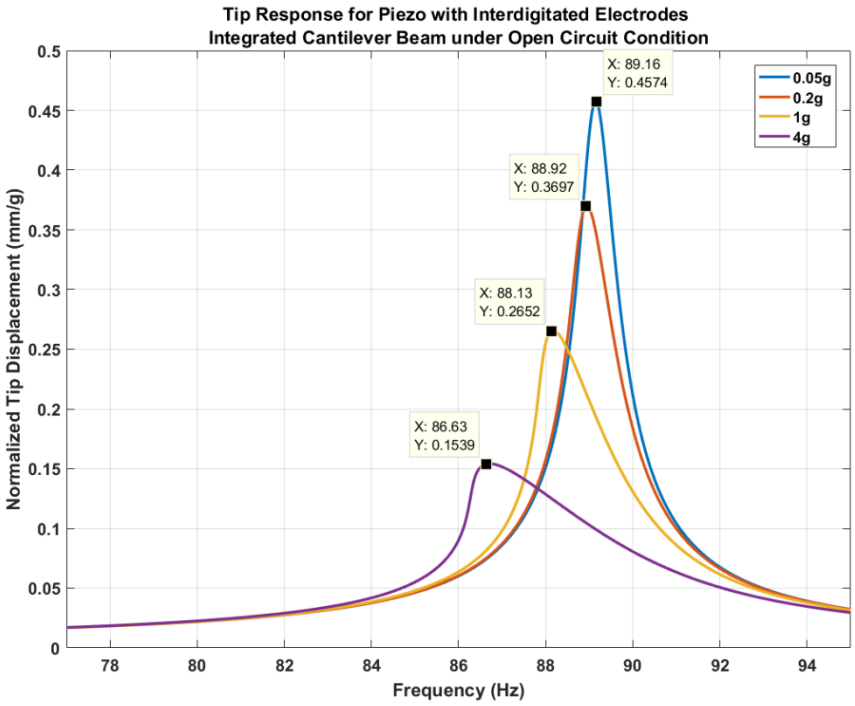

Figure 4-24 Matlab Result for Piezoelectric Patch with Interdigitated Electrodes Integrated Cantilever Beam under Open Circuit Condition

For the nonlinear shunt case, results are given in Figure 4-25. The figure illustrates that hardening nonlinearity exists in the system since resonance frequency is shifted to the right on the frequency axis. Moreover, softening nonlinear response curves did not shift to the left as much as the ones in Figure 4-24. In other words, even though the softening effects are dominant for higher amplitudes, hardening effect is present.

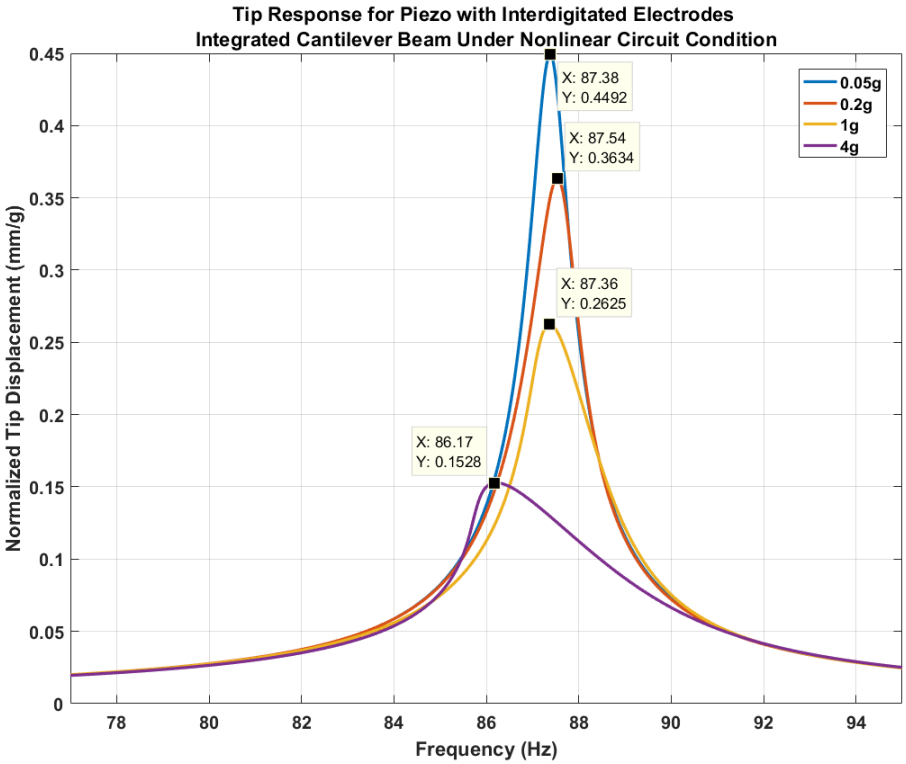

Figure 4-25 Matlab Result for Piezoelectric Patch with Interdigitated Electrodes Integrated Cantilever Beam under Nonlinear Capacitor Shunt Circuit Condition

Matlab results for the short circuit case are presented in Figure 4-26. As expected, the curves are very similar to open circuit condition, but they have a certain offset. The offset is about 3.36 Hz.

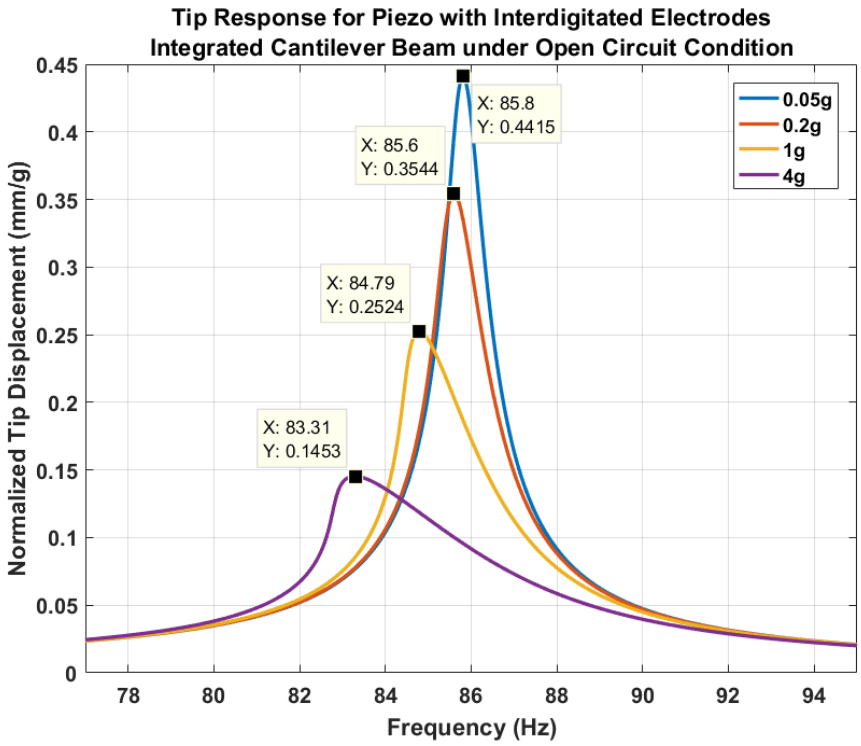

Figure 4-26 Matlab Result for Piezoelectric Patch with Interdigitated Electrodes Integrated Cantilever Beam under Short Circuit Condition

4.5.7 Matlab Simulations for Cantilever Beam with Piezoelectric Patch Having Interdigitated Electrodes with Open and Short Circuits Shunted and Fictitious Aggressive Hardening Nonlinear Capacitor Shunted Including Softening Effect

In the previous section, a realizable system was studied. Simulation results showed that hardening stiffness could be achievable even for diode, which is designed for electrical power transmission. In this section, 1000 parallel connected SD199E6327 varactor diode is used as nonlinear capacitor with the assumption that it can withstand high voltages and low leakage currents. Particularly, the diode is commercially available, but it has high leakage currents, and it cannot operate at high voltage, but due to its aggressive hardening capacitance, it can provide a greater nonlinear response for the cantilever system.

In order to demonstrate what happens with more aggressive hardening capacitance it is sufficient to fit a single curve to Q-V characteristics. The parameters for nonlinear capacitor are given in Table 4.7. The remaining parameter set is given in Table 4.6.

Table 4.7 Simulation Parameters Used for Cantilever Beam with Interdigitated Electrodes Piezoelectric Patch Including Softening Effect

Parameter	**Value**
Cubic Coefficient of Nonlinear Capacitance (a)	5.335×10^{22}
Linear Coefficient of Nonlinear Capacitance (b)	7.619×10^{7}
Damping constant (γ_{st}) at 0.05g, 0.1g, 0.2g, 0.5g and 1g respectively	1.5×10^{-2}, 1.75×10^{-2} 2×10^{-2}, 2.5×10^{-2}, 3×10^{-2}

Simulation results are given in Figure 4-27. It can be observed that the hardening effect dominates frequency shift; however, as the excitation amplitude increases, frequency response curves start to indicate softening effect existence.

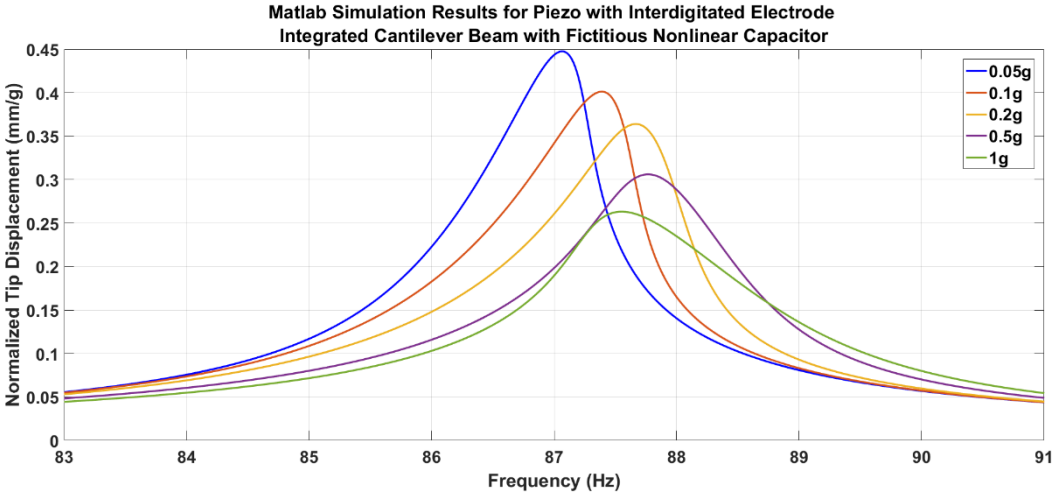

Figure 4-27 Matlab Result for Piezoelectric Patch with Interdigitated Electrodes Integrated Cantilever Beam under Fictitious Nonlinear Capacitor Shunt Circuit Condition

4.6 Summary of the Chapter

This chapter is devoted to modelling of piezoelectric patch integrated fixed-free cantilever beam with shunt circuits.

The chapter starts with derivation of equation of motion with two different methods; Hamiltonian Principle and Newton's second law. Two methods are utilized in order to prevent any miscalculation. Same mechanical equations are obtained with both methods, and therefore they validate each other.

In the following subsections 4.2, 4.3, and 4.4 equations for piezoelectric patches operating in 3-1 mode, 3-3 mode, and 3-3 mode with interdigitated electrodes are derived. Then the equations are used in Matlab simulations which are reported in Section 4.5.

Being the last subsection of this Chapter, 4.5 includes Matlab and Comsol simulation results. Initially, mechanical system is simulated in Matlab and Comsol for plain cantilever beam and for Cantilever beam with discontinuity. It was shown that the results of the simulations are similar for the linear continuous body case. For the discontinuous body case, as eigenfunction number is increased, the resonance frequencies come closer, but Matlab results give higher resonance frequency than Comsol results. Including piezoelectric effects, as expected, in 4.5.3 and 4.5.4, it is presented that open and short circuit case both simulation methods gave closer resonance frequencies. Moreover, including nonlinear circuits, in 4.5.5 frequencies where jumps occurred are found to be close. In 4.5.6, piezoelectric patch with interdigitated electrodes is simulated, and its results can be compared with the experimental results presented in 5.1.3. The subsection is finished with a simulation of piezoelectric patch with interdigitated electrodes and fictitious aggressive hardening nonlinear capacitance in order to demonstrate what could happen with a P-N junction designed for vibration isolation purposes.

CHAPTER 5

EXPERIMENTAL WORK

In this chapter, the experimental setup and results are presented. The chapter starts with a detailed description of the setup and a discussion of the reasons for the decision of the components used in experiments. The chapter continues with the experimental results and ends with the comparison of experimental and simulation results.

5.1 Experimental Setup

5.1.1 Piezoelectric Cantilever Beam Assembly and Nonlinear Capacitor

The main structural element of the experiments is the piezoelectric patch, which is chosen to be MFC because of two reasons. One reason is that MFC's can operate in 3-3 mode with use of interdigitated electrodes. Due to this, electromechanical coupling of the system is higher when compared to 3-1 mode operation. Another reason is that use of interdigitated electrodes in the MFC's inherently results in much less capacitance when compared to well-known 3-1 mode operating piezoelectric patches. This gives a wider band for finding commercial nonlinear capacitors.

MFC's with 3-3 mode operation can be found in several sizes. Among the sizes, MFC4010 P1 is a good candidate since it is not too small to work with, and its capacitance is only about a nano farad.

Since MFC's can operate voltages up to 1500V, they are connected in parallel in order to avoid very high voltages that might damage the capacitor or cause unexpected sparks. MFC4010 P1 used in the experiments is given in Figure 5-1.

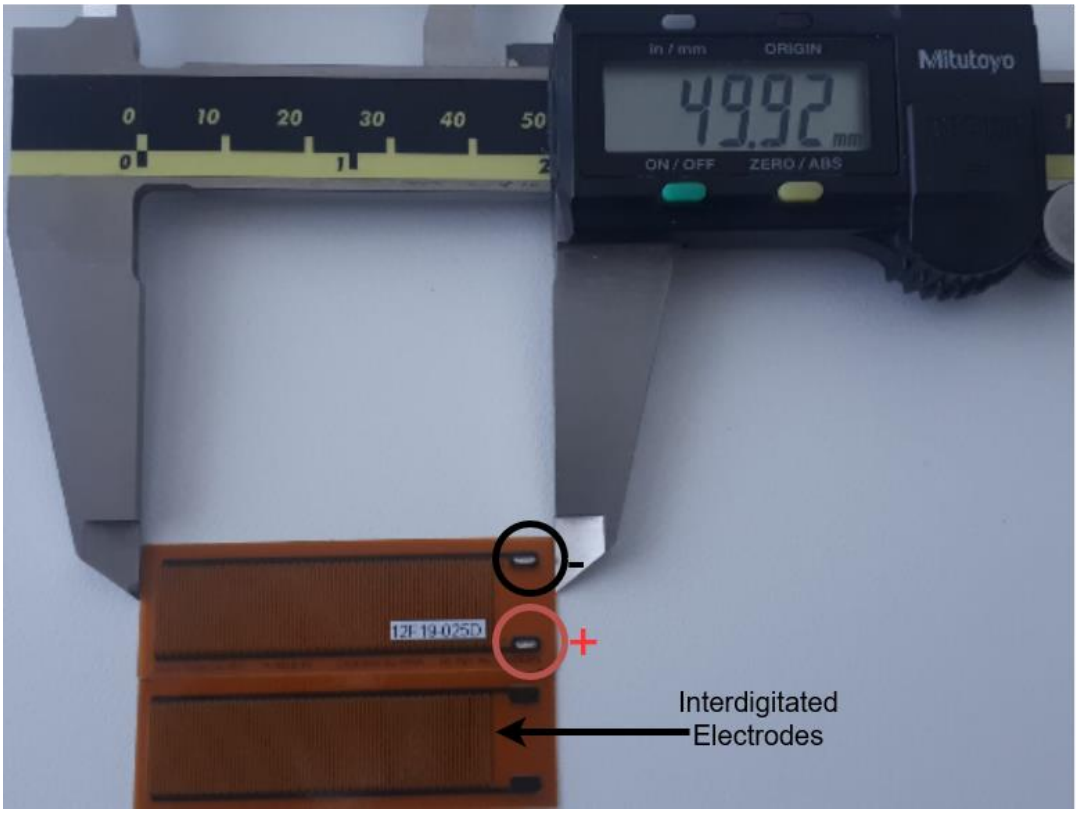

Figure 5-1 MFC4010 P1

The piezoelectric patches used are composite structures that consist of piezoelectric fibers in rectangular cross-section (180μm in height and 350μm in width) with a length of 40mm for MFC4010, epoxy, and kapton films. To increase piezoelectric patches' effectiveness, MFC's are attached to a cantilever beam so that their distance from the neutral axis is raised. Moreover, a longer cantilever beam results in a higher stiffness contribution of the piezoelectric materials to the system so that every piezoelectric material section contributing to unwanted inherent capacitance can convert mechanical energy to electrical energy. The resulting bimorph is then clamped with two clamps; Kapton clamp and cantilever clamp. The clamps had 0.4x45 chamfer, which is included in simulations, in order to avoid sharp edges contacting to piezoelectric patches. Constructed assembly is given in Figure 5-2 and Figure 5-3 with total length and clamp length, respectively. The reason behind using kapton clamp in addition to the cantilever clamp is that fixed end boundary condition

is moved closer to the piezoelectric fibers. Consequently, piezoelectric patches' effectiveness is enhanced since the fibers experience higher mechanical stresses and, therefore, strains.

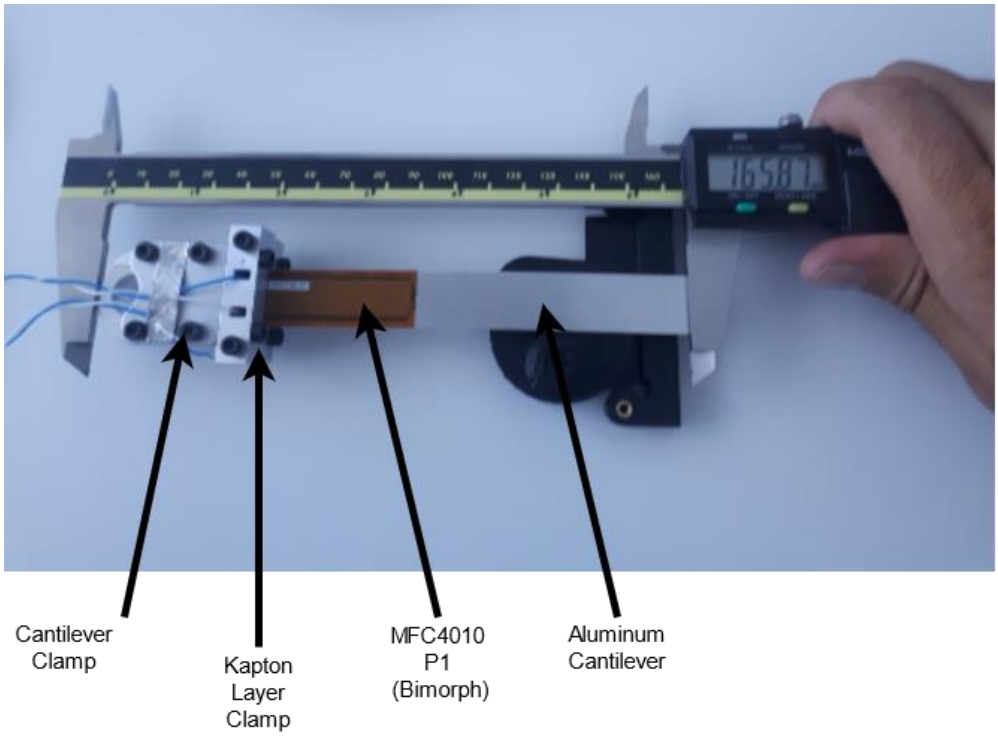

Figure 5-2 Cantilever Beam Assembly with Total Length

Figure 5-3 Cantilever Beam Assembly with Clamp Length

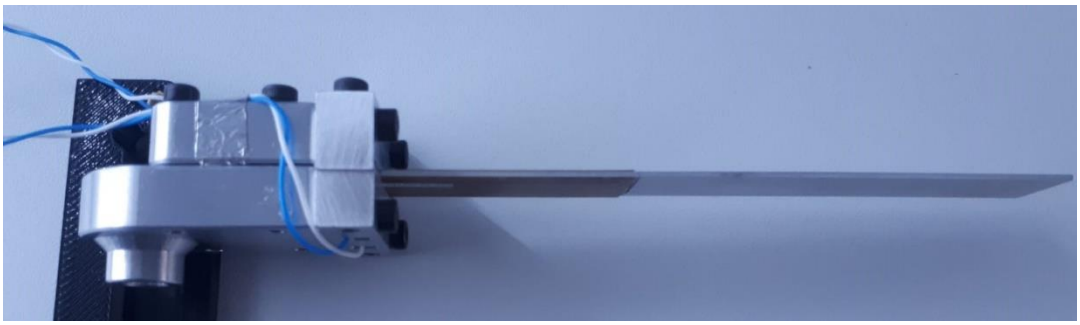

Figure 5-4 Side View of the Cantilever Assembly

The mechanical assembly is shunted to a nonlinear capacitor, which is depicted in Figure 5-5. The capacitor is nothing but a Schottky diode (GB2X100MPS12-227) containing two diodes. As shown in the figure, diode cathodes are shunted to obtain nonlinear capacitor. The capacitance of the component is given in Figure 5-6 for various reverse voltage values. As can be observed from the figure capacitance of each diode is about 8nF. When compared to the inherent capacitance of the parallel connected piezoelectric patches, which is measured to be 3.4nF, nonlinear capacitor's capacitance is higher, and as reverse voltage increases, its capacitance drops below the inherent capacitance.

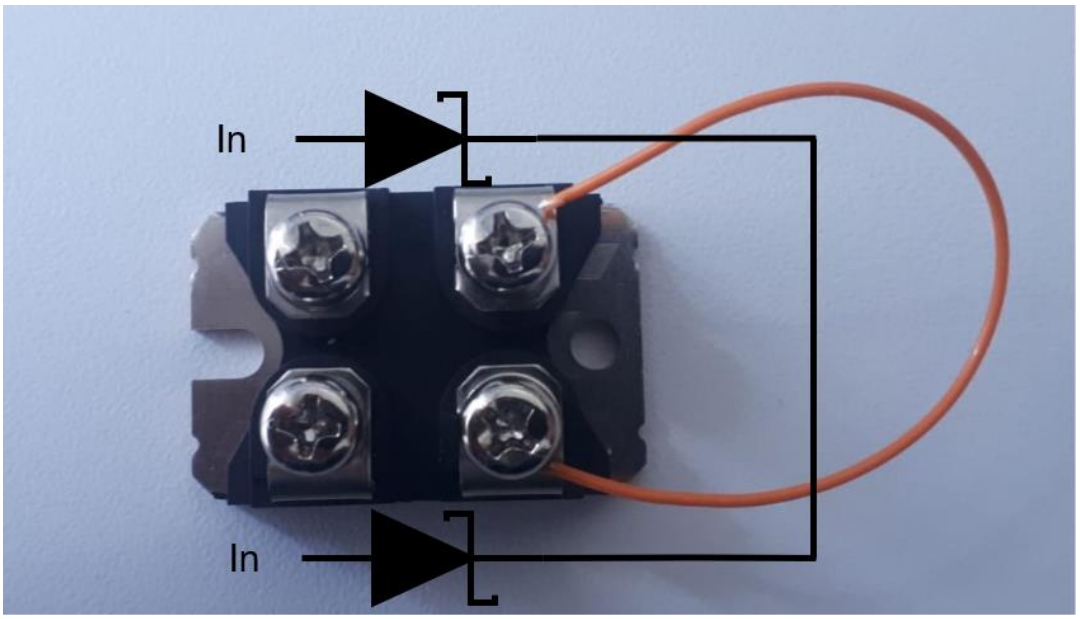

Figure 5-5 Nonlinear Capacitor

The diode is advantageous due to the fact that it accommodates two diodes in a single casing. On top of that, since the component is made of SiC material, it has very low leakage currents. Since the MFC used in experiments generates very low amount of electrical charge, leakage currents become an issue.

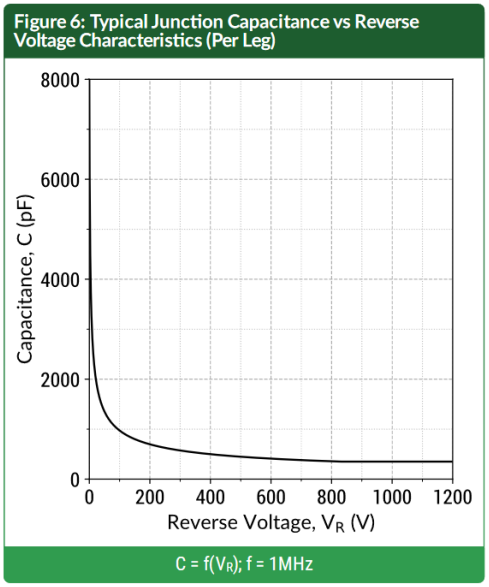

Figure 5-6 V-C Curve for Nonlinear Capacitor [78]

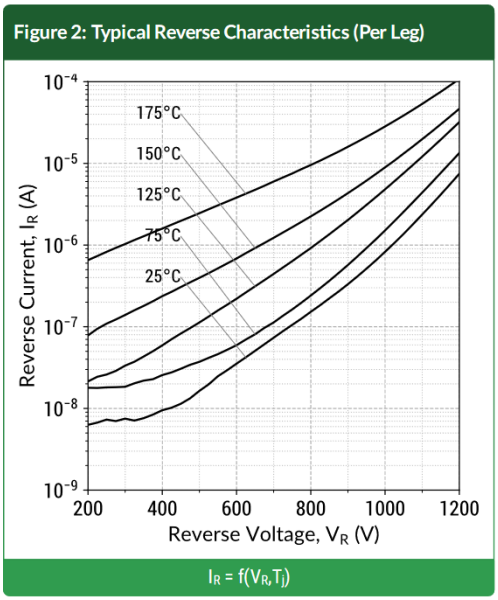

Figure 5-7 Leakage Current vs. Reverse Voltage Graph of the Nonlinear Capacitor [78]

In Figure 5-7, leakage currents at various reverse voltages are given for the nonlinear electrical component. Unlike Si Schottky diodes, from the figure, it can be observed that even for about 800V reverse voltage, it has leakage currents of about several hundreds of nano Amperes.

5.1.2 Experimental Equipment and Software

In the experiments, the following instruments are used

- Siemens SCADAS mobile data acquisition
- Dynalabs DYN-MS-250 modal shaker
- Dynalabs DYN-SA-350 amplifier
- PCB 288D01 force sensor/accelerometer
- Polytec Vibrogo VGO-200 laser vibrometer.
- Siemens LMS Test Lab 19.1 software

The modal shaker is driven using the amplifier without feedback. Frequency sweep is done in one minute on 70-90Hz frequency range, which contains the first mode of the cantilever beam tested. The sweep is repeated four times, and average is taken for FRF data which is given by the software. At each sweep, quasi-steady state behavior is observed. Sampling rate was designated to be 2048Hz. Time domain displacement data of the point about 15mm away from the tip of the beam are recorded. Setup is depicted in Figure 5-8

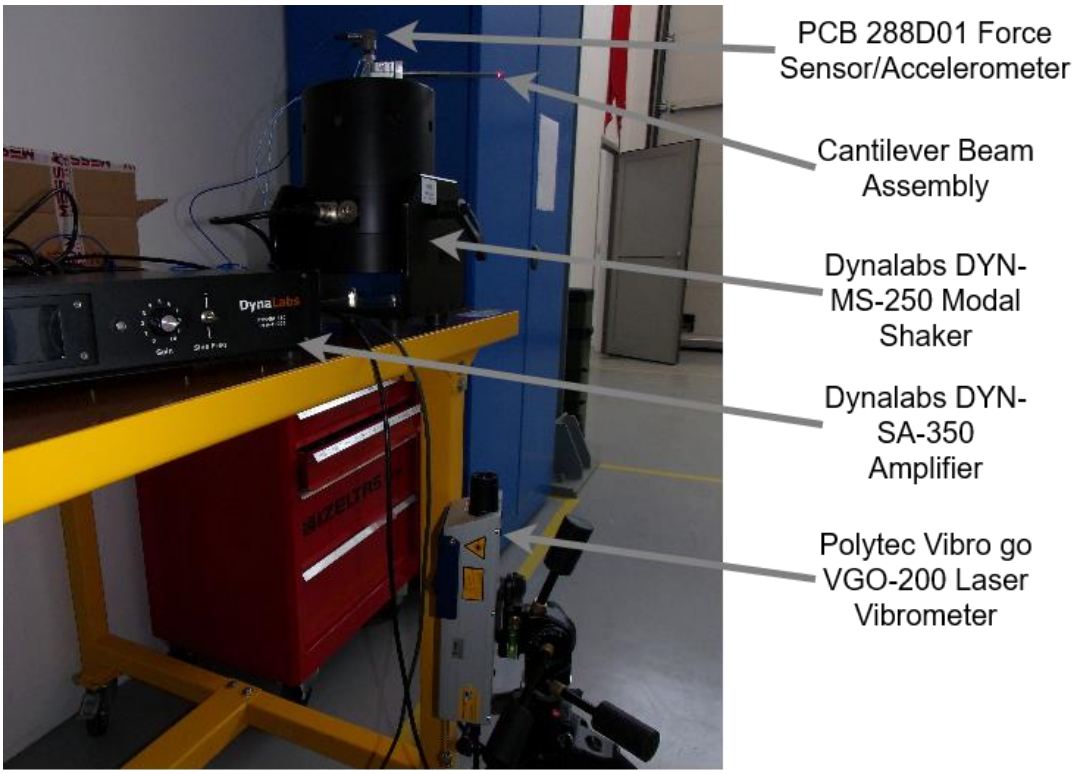

Figure 5-8 Test Setup

5.1.3 Experimental Results

Experiments are conducted for open, short, and nonlinear capacitance shunt circuits. In this section, frequency response plots of the conducted experiments are presented. The plots are constructed by frequency response data obtained from Siemens LMS Test Lab 19.1 software. In order to create reliable data, it is required to satisfy quasi-steady state condition in time domain, and looking at Figure 5-9, it can be stated that the condition is satisfied.

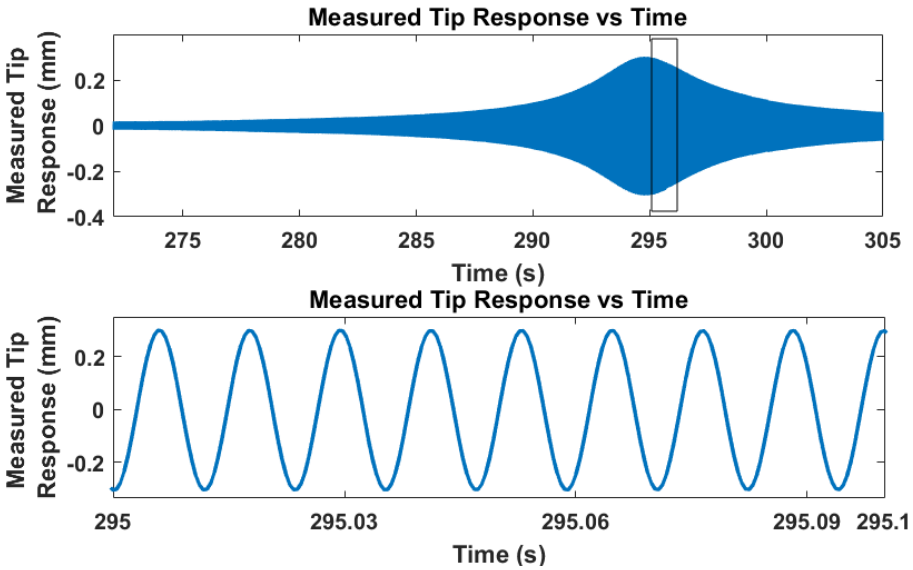

Figure 5-9 Sample Time Domain Data of Nonlinear Shunt Circuit condition Excited at 0.2g

Frequency response results for open circuit conditions are given in Figure 5-10. The figure shows that as the amplitude increases, structural damping and softening nonlinearity also increases. It can also be observed that a slight resonance frequency difference occurred for quadruple amplitude rise. Therefore, it can be said that linear resonance frequency is close to 85Hz.

In Figure 5-11, experiment frequency response results with nonlinear capacitor circuit are given. Looking at the results hardening effect can be observed as frequency shift for small amplitudes; however, for high amplitudes softening nonlinearity seems to be dominant. Despite the softening dominance, the overall hardening effect can be monitored for every frequency as frequency shifts.

In Figure 5-12, results for short circuit condition are presented. The results are similar to the ones with open circuit condition in terms of frequency and amplitude when 4g amplitude is disregarded. At 4g amplitude, the resonant response of the short circuit condition seems to be heavily damped.

By comparing open and short circuit responses, it can be detected that each resonant frequency has about 1.85Hz offset. Being an important parameter, this indicates the effectiveness of the piezoelectric material in the system. When open circuit and short circuit responses are compared, for 0.2g amplitude excitation nonlinear circuit resonant frequency remarkably passes beyond resonant frequency 0.05g excitation of open circuit condition. This implies that even for 0.05g amplitude, slight softening nonlinearity occurs.

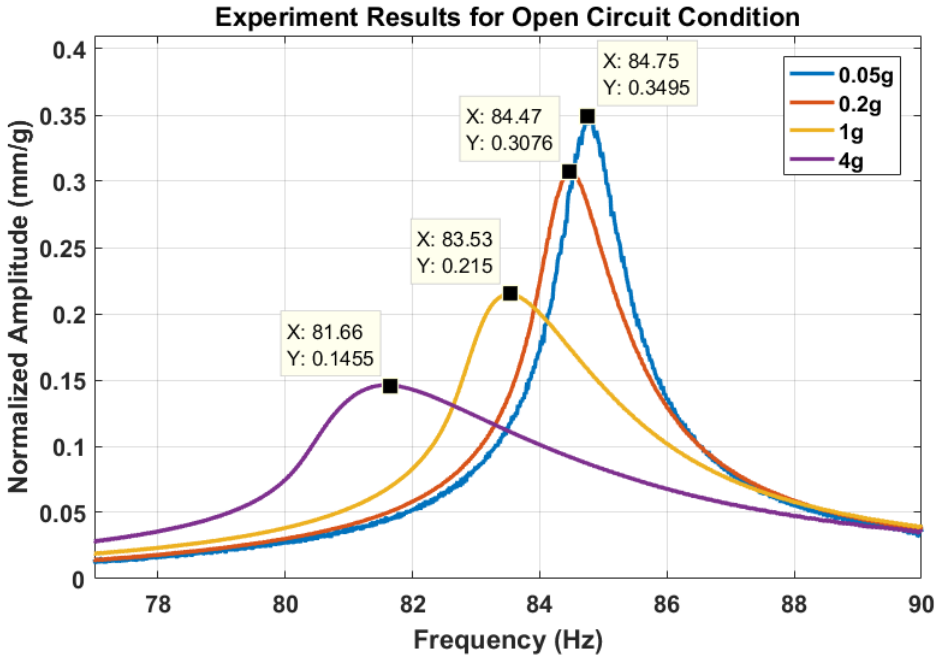

Figure 5-10 Open Circuit Condition Experiment Frequency Response Results

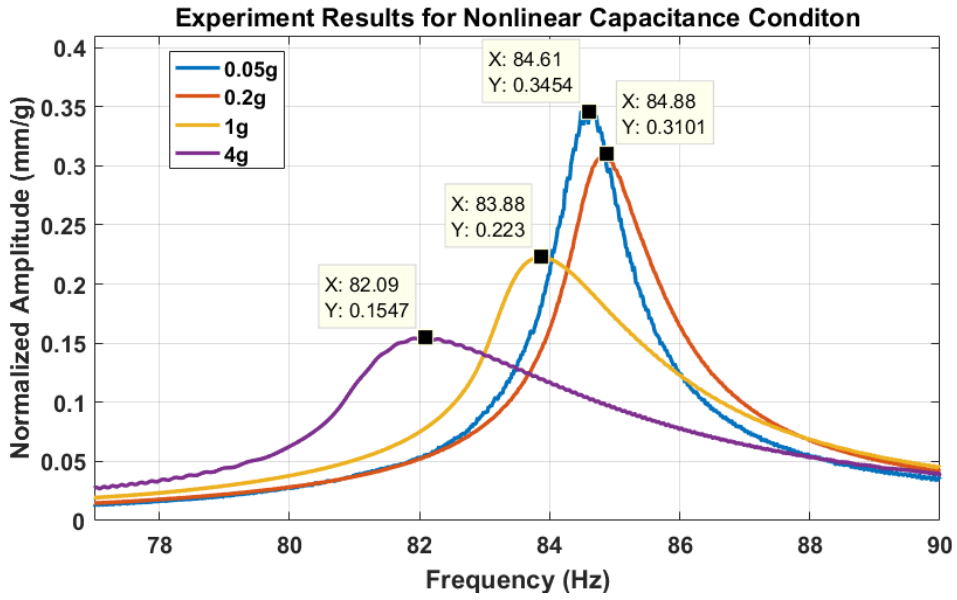

Figure 5-11 Nonlinear Capacitor Circuit Condition Experiment Frequency Response Results

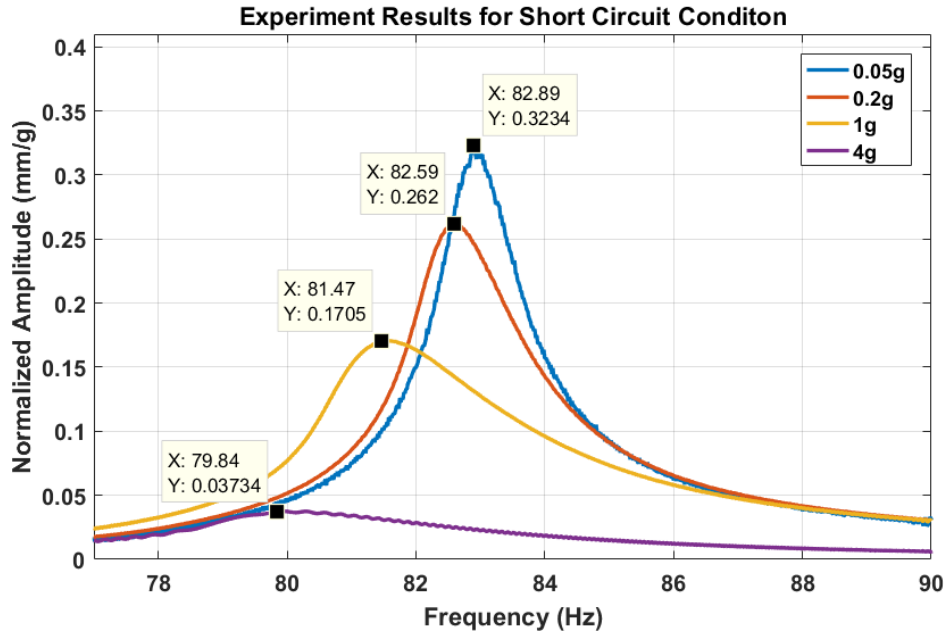

Figure 5-12 Short Circuit Condition Experiment Frequency Response Results

5.1.4 Comparison of Experimental Results and Matlab Simulations

Matlab simulation results for MFC4010 P1 piezoelectric patch and GB2X100MPS12-227 diode are presented in 4.5.6, whose equations are derived in 4.4. Comparing simulation results with the experiment results, patterns for open and short circuit conditions resemble each other. Nevertheless, there are differences in peak responses. This may be mainly because of the damping coefficient. Fine tuning of structural damping and softening coefficient can give closer results, but the scope of this work is to illustrate hardening stiffness could be achieved with a P-N junction.

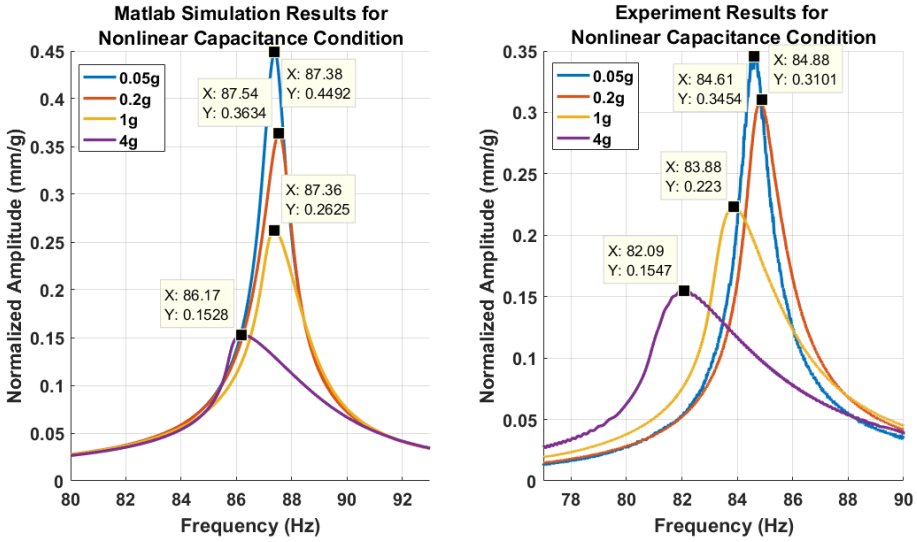

Figure 5-13 Comparison of Matlab Simulation Results and Experiment Results for Nonlinear Capacitance Condition

Matlab simulation resonance frequency differs 5.2% from test resonance frequency for open circuit condition. For short circuit condition the difference is 3.5%. Considering that Comsol simulation results differ about 2.5% from the Matlab ones, variations between test results and simulation results are a little higher than expected. This may be primarily because of unideal test set setup. That is to say, bonding of piezoelectric patches may not be ideal, and fixed free boundary condition could not be achieved accurately. Since two clamps are used, and the kapton layer clamp may not be tightened sufficiently in order not to harm piezoelectric patches' electrodes,

fixed boundary condition may not be provided. Regarding that most of the stiffness is contributed by the cantilever beam's portion closer to the fixed boundary, lack of stiffness in the tests can be explained by unideal clamping and bonding.

The hardening and softening patterns of the tests and Matlab results are in agreement, but again fine tuning of softening and damping parameters can be performed to attain closer results.

CHAPTER 6

SUMMARY, DISCUSSION, CONCLUSION, AND FUTURE WORK

6.1 Summary, Discussion, and Conclusion

The main purpose of this thesis is to show that passive nonlinear capacitors can be utilized for nonlinear mechanical behavior through use of piezoelectric materials. In the literature, P-N junctions are utilized as nonlinear capacitors for electromagnetic vibrations, which is discussed in 2.1. Since frequencies of electromechanical vibrations are very high, hard capacitors having low capacitances are commercially available as varactor diodes.

Varactor diodes could be employed as nonlinear stiffness providing elements in electromechanical vibrations. This idea is investigated in Chapter 3. The chapter started with conceptual proof that use of hardening capacitance results in hardening stiffness in mechanical domain. Then quasi static loading of a simple single DOF piezoelectric patch with 10000 parallel manufactured varactors is demonstrated. Finally, time domain and frequency domain response of the piezoelectric patches under harmonic excitation is investigated. Frequency responses of the piezoelectric actuators have illustrated that nonlinearity can be achieved with varactors. Even though varactor diode modelling is not elaborative and accurate, it was pointed out that nonlinearity could be obtained.

After showing that nonlinearity can be attained by varactors, in Chapter 4 nonlinear piezoelectric model is extended for the cantilever beam case. In the chapter, different modes of operations and shunt circuit conditions of piezoelectric materials attached to cantilever beam is studied. Nevertheless, in 4.5.6 realistic case in which commercially available components are used is simulated. Commercially available piezoelectric patch is chosen to be MFC4010 P1 MFC and GB2X100MPS12-227 diode. MFC piezoelectric patch is chosen since it operates in 3-3 mode, and it has

much lower capacitance when compared to piezoelectric materials having conventional electrodes. This low capacitance allows the use of the piezoelectric actuator in conjunction with commercially available diodes, which results in hardening stiffness. GB2X100MPS12-227 diode is chosen for its high capacitance, high reverse voltages, and low leakage currents. Even though the diode is designed for power electrics applications and is not named as varactor, it has a P-N junction and capacitance associated with the junction. As a result, tests and simulations have proved that P-N junctions can serve as a nonlinear capacitor and provide a hardening effect even if it is not designed for hardening capacitance. Results of piezoelectric material with fictitious harder capacitance are given in 4.5.7 to illustrate how response could be when a diode is designed for aggressive hardening capacitance.

Making use of hardening capacitors to obtain hardening stiffness is shown but if it is possible to manufacture of appropriate diode that would result in aggressive nonlinear mechanical behavior is a question mark. To touch briefly on the possibility of manufacturing textbooks related to semiconductors can be consulted. In [80], junction capacitance is defined by a function including doping density, reverse voltage, built in potential, doping profile, depletion region area, and dielectric permittivity of substrate. Proper design can be achieved by manipulating the available ones among those parameters. In order to design a highly nonlinear capacitor, hyper abrupt junction profile should be adopted. An intricate surface profile could be created to dope in order to have greater capacitance. Moreover, considering typical doping depths mentioned in the textbook is about a micron, a diode can be produced by layers, each having its own junctions. Therefore, a hardening capacitor that takes up a small volume can be designed. GaAs or SiC substrate material can be chosen to provide low leakage current and high voltage resistance.

The method introduced in this thesis can be used for vibration isolation or energy harvesting applications due to the fact that the nonlinearity could broaden useful frequency range.

6.2 Future Work

In this thesis, it is demonstrated that hardening stiffness can be introduced in electrical domain via piezoelectric material as an electromechanical transducer. However, limits and effectiveness of the nonlinearity are yet to be explored. For future work, a study on capacitance limits, volume occupation, cost, and effectiveness of the nonlinear P-N junction capacitor can be investigated for vibration isolation and energy harvesting applications. Besides the possible studies, suitability of the suggested method on the real engineering cases where additional constraints are introduced can be investigated for piezoelectric patches and amplified piezoelectric stacks. Regarding that piezoelectric patches are commonly used for continuous systems, and amplified piezoelectric stacks are commonly used for lumped systems, the suggested method could be utilized for wing or gimbal vibration suppression or energy harvesting.

REFERENCES

[1] R. A. Ibrahim, “Recent advances in nonlinear passive vibration isolators,” *J. Sound Vib.*, vol. 314, no. 3–5, pp. 371–452, 2008.

[2] X. Wang and A. Mortazawi, “Duffing resonator circuits for performance enhancement of wireless power harvesters,” *2015 IEEE MTT-S Int. Microw. Symp. IMS 2015*, pp. 1–4, 2015.

[3] A. Rydberg, H. Grönqvist, and E. Kollberg, “Millimeter- and Submillimeter-Wave Multipliers Using Quantum-Barrier-Varactor (QBV) Diodes,” *IEEE Electron Device Lett.*, vol. 11, no. 9, pp. 373–375, 1990.

[4] E. Gluskin, “The use of non-linear capacitors,” *Int. J. Electron.*, vol. 58, no. 1, pp. 63–81, 1985.

[5] M. Li, K. Krishnamurthi, and R. G. Harrison, “A fully distributed heterostructure-barrier varactor nonlinear transmission-line frequency multiplier and pulse sharpener,” *IEEE Trans. Microw. Theory Tech.*, vol. 46, no. 12 PART 2, pp. 2295–2301, 1998.

[6] T. Bryllert, A. Malko, J. Vukusic, and J. Stake, “A 175 GHz HBV frequency quintupler with 60 mW output power,” *IEEE Microw. Wirel. Components Lett.*, vol. 22, no. 2, pp. 76–78, 2012.

[7] J. Stake, A. Malko, T. Bryllert, and J. Vukusic, “Status and prospects of high-power heterostructure barrier varactor frequency multipliers,” *Proc. IEEE*, vol. 105, no. 6, pp. 1008–1019, 2017.

[8] K. Krishnamurthi and R. G. Harrison, “Analysis of symmetric-varactor frequency triplers,” *IEEE MTT-S Int. Microw. Symp. Dig.*, vol. 2, pp. 649–652, 1993.

[9] J. T. Evans and R. Womack, “An Experimental 512-Bit Nonvolatile Memory with Ferroelectric Storage Cell,” *IEEE J. Solid-State Circuits*, vol. 23, no. 5,

pp. 1171–1175, 1988.

[10] S. L. Miller, J. R. Schwank, R. D. Nasby, and M. S. Rodgers, “Modeling ferroelectric capacitor switching with asymmetric nonperiodic input signals and arbitrary initial conditions,” *J. Appl. Phys.*, vol. 70, no. 5, pp. 2849–2860, 1991.

[11] V. I. Cojocaru and T. J. Brazil, “Large-signal equivalent circuit model for hyperabrupt p-n junction varactor diodes,” *Conf. Proc. - Eur. Microw. Conf.*, vol. 2, no. 22, pp. 1115–1121, 1992.

[12] B. G. Streetman and S. K. Banerjee, “SOLID STATE ELECTRONIC DEVICES, 6th Edition,” pp. 64–70, 2006.

[13] R. G. Meyer and M. L. Stephens, “Distortion in Variable-Capacitance Diodes,” *IEEE J. Solid-State Circuits*, vol. 10, no. 1, pp. 47–54, 1975.

[14] X. Wang and A. Mortazawi, “Bandwidth Enhancement of RF Resonators Using Duffing Nonlinear Resonance for Wireless Power Applications,” *IEEE Trans. Microw. Theory Tech.*, vol. 64, no. 11, pp. 3695–3702, 2016.

[15] E. M. Qureshi, X. Shen, and J. J. Chen, “Vibration control laws via shunted piezoelectric transducers: A review,” *Int. J. Aeronaut. Sp. Sci.*, vol. 15, no. 1, pp. 1–19, 2014.

[16] B. Yan, K. Wang, Z. Hu, C. Wu, and X. Zhang, “Shunt Damping Vibration Control Technology: A Review,” *Appl. Sci.*, vol. 7, no. 5, 2017.

[17] A. V. F. N. W. Hagood, “Damping Of Structural Vibrations With Piezoelectric Materials And Passive Electrical Networks,” *J. Sound Vib.*, vol. 146, no. 2, pp. 243–268, 1991.

[18] K. Yamada, H. Matsuhisa, H. Utsuno, and K. Sawada, “Optimum tuning of series and parallel LR circuits for passive vibration suppression using piezoelectric elements,” *J. Sound Vib.*, vol. 329, no. 24, pp. 5036–5057, 2010.

[19] P. Soltani, G. Kerschen, G. Tondreau, and A. Deraemaeker, “Piezoelectric vibration damping using resonant shunt circuits: An exact solution,” *Smart Mater. Struct.*, vol. 23, no. 12, 2014.

[20] C. H. Park and D. J. Inman, “Enhanced piezoelectric shunt design,” *Shock Vib.*, vol. 10, no. 2, pp. 127–133, 2003.

[21] A. J. Fleming, S. Behrens, and S. O. R. Moheimani, “Reducing the inductance requirements of piezoelectric shunt damping systems,” *Smart Mater. Struct.*, vol. 12, no. 1, pp. 57–64, 2003.

[22] J. J. Hollkamp, “Multimodal Passive Vibration Suppression with Piezoelectric Materials and Resonant Shunts,” *J. Intell. Mater. Syst. Struct.*, vol. 5, no. 1, pp. 49–57, 1994.

[23] C. G. S. Agnes and D. J. Inman, “Nonlinear Piezoelectric Vibration Absorbers,” *Smart Mater. Struct.*, vol. 2720, pp. 247–258, 1992.

[24] B. Zhou, F. Thouverez, and D. Lenoir, “Essentially nonlinear piezoelectric shunt circuits applied to mistuned bladed disks,” *J. Sound Vib.*, vol. 333, no. 9, pp. 2520–2542, 2014.

[25] P. S. Soltani and G. Kerschen, “The nonlinear piezoelectric tuned vibration absorber,” *Smart Mater. Struct.*, vol. 24, no. 7, p. 75015, 2015.

[26] B. Lossouarn, J. F. Deü, and G. Kerschen, “A fully passive nonlinear piezoelectric vibration absorber,” *Philos. Trans. R. Soc. A Math. Phys. Eng. Sci.*, vol. 376, no. 2127, 2018.

[27] D. Niederberger and M. Morari, “An autonomous shunt circuit for vibration damping,” *Smart Mater. Struct.*, vol. 15, no. 2, pp. 359–364, 2006.

[28] H. Shen, H. Ji, J. Qiu, and K. Zhu, “A semi-passive vibration damping system powered by harvested energy,” *Int. J. Appl. Electromagn. Mech.*, vol. 31, no. 4, pp. 219–233, 2009.

[29] W. W. Clark, “Vibration control with state-switched piezoelectric materials,” *J. Intell. Mater. Syst. Struct.*, vol. 11, no. 4, pp. 263–271, 2000.

[30] A. Ramaratnam and N. Jalili, “A switched stiffness approach for structural vibration control: Theory and real-time implementation,” *J. Sound Vib.*, vol. 291, no. 1–2, pp. 258–274, 2006.

[31] C. Richard, D. Guyomar, D. Audigier, and H. Bassaler, “<title>Enhanced semi-passive damping using continuous switching of a piezoelectric device on an inductor</title>,” *Smart Struct. Mater. 2000 Damping Isol.*, vol. 3989, pp. 288–299, 2000.

[32] L. R. Corr and W. W. Clark, “Comparison of low-frequency piezoelectric switching shunt techniques for structural damping,” *Smart Mater. Struct.*, vol. 11, no. 3, pp. 370–376, 2002.

[33] J. Ducarne, O. Thomas, and J. F. Deü, “Structural vibration reduction optimization by switch shunting of piezoelectric elements,” *ASME Int. Mech. Eng. Congr. Expo. Proc.*, vol. 10 PART A, pp. 339–348, 2008.

[34] C. L. Davis and G. A. Lesieutre, “Actively tuned solid-state vibration absorber using capacitive shunting of piezoelectric stiffness,” *J. Sound Vib.*, vol. 232, no. 3, pp. 601–617, 2000.

[35] M. Lallart *et al.*, “Blind switch damping (BSD): A self-adaptive semi-active damping technique,” *J. Sound Vib.*, vol. 328, no. 1–2, pp. 29–41, 2009.

[36] L. Petit, E. Lefeuvre, C. Richard, and D. Guyomar, “A broadband semi passive piezoelectric technique for structural damping,” *Smart Struct. Mater. 2004 Damping Isol.*, vol. 5386, p. 414, 2004.

[37] A. Badel *et al.*, “Piezoelectric vibration control by synchronized switching on adaptive voltage sources: Towards wideband semi-active damping,” *J. Acoust. Soc. Am.*, vol. 119, no. 5, pp. 2815–2825, 2006.

[38] K. Makihara, J. Onoda, and K. Minesugi, “Using tuned electrical resonance

to enhance bang-bang vibration control," *AIAA J.*, vol. 45, no. 2, pp. 497–504, 2007.

[39] X. Han, M. Neubauer, and J. Wallaschek, "Improved piezoelectric switch shunt damping technique using negative capacitance," *J. Sound Vib.*, vol. 332, no. 1, pp. 7–16, 2013.

[40] H. Ji, J. Qiu, J. Cheng, and D. Inman, "Application of a negative capacitance circuit in synchronized switch damping techniques for vibration suppression," *J. Vib. Acoust. Trans. ASME*, vol. 133, no. 4, pp. 1–10, 2011.

[41] M. Kodejška, J. Václavík, and P. Mokrý, "A system for the vibration suppression in the broad frequency range using a single piezoelectric actuator shunted by a negative capacitor," *Proc. 2010 IEEE Int. Symp. Appl. Ferroelectr. ISAF 2010, Co-located with 10th Eur. Conf. Appl. Polar Dielectr. ECAPD 2010*, 2010.

[42] R. A. Morgan and K. W. Wang, "An active-passive piezoelectric absorber for structural vibration control under harmonic excitations with time-varying frequency, part 1: Algorithm development and analysis," *J. Vib. Acoust. Trans. ASME*, vol. 124, no. 1, pp. 77–83, 2002.

[43] R. A. Morgan and K. W. Wang, "An active-passive piezoelectric absorber for structural vibration control under harmonic excitations with time-varying frequency, part 2: Experimental validation and parametric study," *J. Vib. Acoust. Trans. ASME*, vol. 124, no. 1, pp. 84–89, 2002.

[44] D. Niederberger, M. Morari, and S. J. Pietrzko, "Adaptive resonant shunted piezoelectric devices for vibration suppression," *Smart Struct. Mater. 2003 Smart Struct. Integr. Syst.*, vol. 5056, p. 213, 2003.

[45] M. S. Tsai and K. W. Wang, "On the structural damping characteristics of active piezoelectric actuators with passive shunt," *J. Sound Vib.*, vol. 221, no. 1, pp. 1–22, 1999.

[46] J. J. Dosch, D. J. Inman, and E. Garcia, “A Self-Sensing Piezoelectric Actuator for Collocated Control,” *J. Intell. Mater. Syst. Struct.*, vol. 3, no. 1, pp. 166–185, 1992.

[47] S. Nima Mahmoodi and M. Ahmadian, “Active vibration control with modified positive position feedback,” *J. Dyn. Syst. Meas. Control. Trans. ASME*, vol. 131, no. 4, pp. 1–8, 2009.

[48] T. Bailey and J. E. Ubbard, “Distributed piezoelectric-polymer active vibration control of a cantilever beam,” *J. Guid. Control. Dyn.*, vol. 8, no. 5, pp. 605–611, 1985.

[49] C. M. A. Vasques and J. Dias Rodrigues, “Active vibration control of smart piezoelectric beams: Comparison of classical and optimal feedback control strategies,” *Comput. Struct.*, vol. 84, no. 22–23, pp. 1402–1414, 2006.

[50] G. M. De Freitas Otsubo, T. M. P. Silva, D. D’Assunção, and C. De Marqui, “Effects of nonlinear energy sink on the aeroelastic behavior of an electromechanically coupled typical section,” *31st Congr. Int. Counc. Aeronaut. Sci. ICAS 2018*, pp. 1–7, 2018.

[51] T. M. P. Silva, M. A. Clementino, C. De Marqui, and A. Erturk, “An experimentally validated piezoelectric nonlinear energy sink for wideband vibration attenuation,” *J. Sound Vib.*, vol. 437, pp. 68–78, 2018.

[52] D. J. Leo, *Engineering Analysis of Smart Material Systems*. John Wiley & Sons, 2008.

[53] A. Erturk and D. J. Inman, *Piezoelectric Energy Harvesting*, First Edit. John Wiley & Sons, Ltd, 2011.

[54] K. H. Mak, A. A. Popov, and S. McWilliam, “Experimental model validation for a nonlinear energy harvester incorporating a bump stop,” *J. Sound Vib.*, vol. 331, no. 11, pp. 2602–2623, 2012.

[55] F. Goldschmidtboeing, C. Eichhorn, M. Wischke, M. Kroener, and P. Woias,

"The influence of ferroelastic hysteresis on mechanically excited PZT cantilever beams," *PowerMEMS*, no. 1, pp. 114–117, 2011.

[56] U. Von Wagner and P. Hagedorn, "Piezo-beam systems subjected to weak electric field: Experiments and modelling of non-linearities," *J. Sound Vib.*, vol. 256, no. 5, pp. 861–872, 2002.

[57] D. Tan, P. Yavarow, and A. Erturk, "Resonant nonlinearities of piezoelectric macro-fiber composite cantilevers with interdigitated electrodes in energy harvesting," *Nonlinear Dyn.*, vol. 92, no. 4, pp. 1935–1945, 2018.

[58] D. Tan, P. Yavarow, and A. Erturk, "Nonlinear elastodynamics of piezoelectric macro-fiber composites with interdigitated electrodes for resonant actuation," *Compos. Struct.*, vol. 187, pp. 137–143, 2018.

[59] S. Leadenham and A. Erturk, "Unified nonlinear electroelastic dynamics of a bimorph piezoelectric cantilever for energy harvesting, sensing, and actuation," *Nonlinear Dyn.*, vol. 79, no. 3, pp. 1727–1743, 2015.

[60] F. Lemmermeyer, "SOLVING POLYNOMIAL EQUATIONS." [Online]. Available: http://www.fen.bilkent.edu.tr/~franz/M300/solv.pdf. [Accessed: 22-Nov-2020].

[61] A. Erturk and D. J. Inman, "A distributed parameter electromechanical model for cantilevered piezoelectric energy harvesters," *J. Vib. Acoust. Trans. ASME*, vol. 130, no. 4, pp. 1–15, 2008.

[62] N. G. Elvin and A. A. Elvin, "A general equivalent circuit model for piezoelectric generators," *J. Intell. Mater. Syst. Struct.*, vol. 20, no. 1, pp. 3–9, 2009.

[63] A. Erturk and D. J. Inman, "Mechanical considerations for modeling of vibration-based energy harvesters," *2007 Proc. ASME Int. Des. Eng. Tech. Conf. Comput. Inf. Eng. Conf. DETC2007*, vol. 1 PART B, no. 540, pp. 769–778, 2008.

[64] Leonard Meirovitch, “Fundamentals of Vibration,” John Wiley & Sons, 2001, p. 408.

[65] A. D. Peter Hagedorn, “Vibrations and Waves in Continuous Mechanical Systems,” McGraw-Hill, 2007, p. 247.

[66] M. B. Özer, “New Techniques in the Design, Analysis and Optimization of Tuned Dynamic Vibration Absorbers,” THE UNIVERSITY OF ILLINOIS AT CHICAGO Graduate College, 2004.

[67] A. A. Bent and N. W. Hagood, “Piezoelectric fiber composites with interdigitated electrodes,” *J. Intell. Mater. Syst. Struct.*, vol. 8, no. 11, pp. 903–919, 1997.

[68] R. Igreja and C. J. Dias, “Analytical evaluation of the interdigital electrodes capacitance for a multi-layered structure,” *Sensors Actuators, A Phys.*, vol. 112, no. 2–3, pp. 291–301, 2004.

[69] S. B. Kim, J. H. Park, S. H. Kim, H. Ahn, H. C. Wikle, and D. J. Kim, “Modeling and evaluation of d 33mode piezoelectric energy harvesters,” *J. Micromechanics Microengineering*, vol. 22, no. 10, 2012.

[70] H. Liu, J. Zhong, C. Lee, S. W. Lee, and L. Lin, “A comprehensive review on piezoelectric energy harvesting technology: Materials, mechanisms, and applications,” *Appl. Phys. Rev.*, vol. 5, no. 4, 2018.

[71] S. B. Kim, H. Park, S. H. Kim, H. C. Wikle, J. H. Park, and D. J. Kim, “Comparison of MEMS PZT cantilevers based on d31 and d 33 modes for vibration energy harvesting,” *J. Microelectromechanical Syst.*, vol. 22, no. 1, pp. 26–33, 2013.

[72] N. Chidambaram, A. Mazzalai, and P. Muralt, “Measurement of effective piezoelectric coefficients of PZT thin films for energy harvesting application with interdigitated electrodes,” *IEEE Trans. Ultrason. Ferroelectr. Freq. Control*, vol. 59, no. 8, pp. 1624–1631, 2012.

[73] C. Mo, S. Kim, and W. W. Clark, “Theoretical analysis of energy harvesting performance for unimorph piezoelectric benders with interdigitated electrodes,” vol. 055017.

[74] H. A. Sodano, J. M. Lloyd, and D. J. Inman, “An experimental comparison between several active composite actuators for power generation,” *Smart Struct. Mater. 2004 Smart Struct. Integr. Syst.*, vol. 5390, p. 370, 2004.

[75] “MFC P1 Type.” [Online]. Available: https://www.smart-material.com/MFC-product-P1.html. [Accessed: 26-Dec-2020].

[76] S. Shahab and A. Erturk, “Coupling of experimentally validated electroelastic dynamics and mixing rules formulation for macro-fiber composite piezoelectric structures,” *J. Intell. Mater. Syst. Struct.*, vol. 28, no. 12, pp. 1575–1588, 2017.

[77] A. Gelb and W. E. Vander Velde, *Multiple-Input Describing Functions and Nonlinear System Design*. McGraw-Hill Book Company, 1968.

[78] “GB2X100MPS12-227 1200V 100A SiC Schottky MPS Diode - Silicon Carbide Schottky Diode - GeneSiC Semiconductor | Enhanced Reader.” [Online]. Available: https://www.genesicsemi.com/sic-schottky-mps/GB2X100MPS12-227/GB2X100MPS12-227.pdf. [Accessed: 29-Mar-2021].

[79] D. Berlincourt and H. H. A. Krueger, “Properties of Morgan electro ceramic ceramics.” Technical Publication TP-226, Morgan Electro Ceramics., 2000.

[80] D. A. Neamen, *Semiconductor Physics and Devices Basic Principles*, 4th ed. 2006.